TRANSIENT EVOLUTION OF PASSIVE MODELOCKING--

THEORY AND EXPERIMENT

by

Christopher Perry Ausschnitt

B. S., Princeton University
(1968)

M. S., University of Pennsylvania
(1970)

SUBMITTED IN PARTIAL FULFILLMENT OF THE

REQUIREMENTS FOR THE DEGREE OF

DOCTOR OF SCIENCE

at the

MASSACHUSETTS INSTITUTE OF TECHNOLOGY

January, 1976

Signature of Author...
    Department of Electrical Engineering and Computer Science

Certified by..
                                            Thesis Supervisor

Accepted by...
        Chairman, Departmental Committee on Graduate Studies

TRANSIENT EVOLUTION OF PASSIVE MODELOCKING--

THEORY AND EXPERIMENT

by

Christopher Perry Ausschnitt

Submitted to the Department of Electrical Engineering
and Computer Science on January 14, 1976, in partial
fulfillment of the requirements for the Degree of
Doctor of Science

ABSTRACT

We present the first deterministic theory of the
transient evolution of passive modelocking which gives
a closed form expression for the pulse on each transit
through the system. Included are studies of the buildup
from noise, the modelocking threshold, the steady state
operating point and the stability of the steady state.
Simple criteria are established which enable the design
of passively modelocked systems to generate pulses of
prespecified width and amplitude.

Experimental verification of the theory is carried
out on the TEA CO_2 laser modelocked by an SF_6 satur-
able absorber. The match of pulse shape and relative
amplitude is found to be excellent. The passive mode-
locking results are compared to forced modelocking
experiments conducted on the same laser system using a
Ge acousto-optic intracavity modulator.

An experimental and theoretical study of the short
pulse saturation properties of the SF_6 absorber is also
conducted. The mechanism which induces modelocking is
shown to be the fast rotational bleaching of the ab-
sorbing transition.

THESIS SUPERVISOR: Hermann A. Haus
TITLE: Elihu Thomson Professor of Electrical
                   Engineering

To the unknown Haitian sorceress who said:

"He who would find buried treasure,
must dig alone, in the dark of night,
and leave a little of his own blood behind."

ACKNOWLEDGEMENTS

First and foremost, I wish to thank my advisor, Professor Hermann A. Haus, "... teacher in every art, who brought the fire that hath proved to mortals a means to mighty ends."* Our frequent discussions illuminated, not only the path my thesis was to take, but the course of my maturation as a scientist as well.

To Professor Abraham Szőke I also owe a great debt of gratitude for his good humored and conscientious guidance and advice.

My daily interaction with present and former members of the Gas Laser Research Group, notably Peter Hagelstein, John Miller, Terry Holcomb, and Yongyut Manichaikul, stimulated many fruitful ideas and investigations.

The technical assistance of Frank Barrows was invaluable in all phases of the experimental work.

The unsurpassable secretarial skill of Cindy Kopf was essential to the completion of this thesis and many interim reports.

---

* Aeschylus, Prometheus Unbound

TABLE OF CONTENTS

LIST OF FIGURES

LIST OF TABLES

I. Introduction

Recent interest in the generation of short optical pulses has been stimulated by the promise of communications and radar applications, the possibility of laser induced fusion, and fundamental phenomena of short pulse propagation and scattering. Modelocking has proved a reliable means of obtaining a train of short pulses from laser oscillators. Pulses of sub-picosecond duration have been achieved.[1] As a consequence, modelocking has been an area of intense research activity.

Modelocking is common to every variety of laser-- gaseous, liquid and solid state, homogeneous and inhomogeneous, continuous, Q-switched and gain switched. Experimental techniques of modelocking lasers can be divided into three major categories:

1. Spontaneous- or self-,[2-4] in which the laser modelocks in the absence of any intracavity perturbation.

2. Passive-,[5-13] in which the introduction of a saturable absorber or nonlinear refractive index material into the laser cavity induces modelocking.

3. Active- or forced-,[14-20] in which intracavity modulation at the cavity mode spacing or multiples thereof, induces

modelocking.

More complete reference lists may be found in review articles.[21-23] Spontaneous modelocking is plagued by inconsistency while active modelocking, though consistent, is burdened by the electronics and device problems, and power level constraints which accompany intracavity modulation. To date, therefore, passive modelocking holds forth the greatest promise of consistently producing bandwidth limited pulses in the simplest manner and with the widest operating range.

Its promise and the vast literature notwithstanding, many aspects of passive modelocking are not well understood. In particular, prior to the recent work by Haus,[24-25] most theories have consisted of either computer studies[26-29] or qualitative analytic studies of pulse shaping without prediction of a pulse shape.[30-32] Haus developed a new formalism which enabled him to obtain closed form expressions for the steady state pulse produced by passive modelocking in the two limiting cases where (1) the absorber relaxation time is short compared to the pulse width, and (2) the absorber relaxation time is much longer than the pulsewidth.

Here we focus our attention on the transient evolution of passive modelocking with a fast saturable absorber. The transient problem is important not merely because it is of interest to know how modelocking builds up to the steady state,

but because many modelocked systems, e.g. gain or Q switched lasers, never reach a steady state and, hence, can only be fully explained by a transient theory. Furthermore, we find that an understanding of the transient problem yields deeper insight into the steady state.

The ultimate objective of the present study is to create a design handbook for passively modelocked systems. Toward that objective we present:

1. A closed form deterministic theory of the transient evolution of passive modelocking.

2. Experimental verification of the theory on the TEA CO_2 laser using SF_6 as a saturable absorber.

3. A study of the short pulse saturation of SF_6.

The body of the thesis is divided into three chapters corresponding to each of the above topics.

A major stumbling block to the development of simple design criteria for passive modelocking has been the assertion by previous authors that the buildup of modelocking is a statistical process.[31,33-36] Thus, a significant contribution of the present study is to show that the conditions for which consistent modelocking is observed experimentally are those very conditions for which the buildup is, in fact, deterministic. The closed form theory then enables the quantitative specification of design criteria for the generation of stable

pulses of prespecified shape, amplitude, and repetition time.

The chief contribution of the experimental work is the matching of the shape and amplitude of pulses generated by the TEA CO_2 laser modelocked by an SF_6 saturable absorber to those predicted by theory over a range of system parameters. A detailed study of short pulse SF_6 saturation is also conducted to demonstrate that the modelocking mechanism is the saturation of the absorber within a cavity transit time rather than the nonlinear dielectric coupling proposed by previous authors.[5,37,38]

Both theory and experiment point the way to the improved design of passively modelocked systems. The promised design criteria and possible system configurations for the generation of shorter, more reproducible pulses are presented in the final chapter.

II. Theory

Previous authors have taken a statistical approach to
the study of the buildup of passive modelocking, stating
that the occurrence of modelocking relies on the selective
bleaching of the absorber by the highest intensity spike in
a cavity transit time. Justification of the statistical model
depends upon the nature of the field in the cavity at the
time at which the absorber saturation becomes significant.
The number of oscillating cavity modes determines the structure
of the field, i.e. the number of intensity fluctuations in a
cavity transit time. If many modes are present the field is
rapidly fluctuating and the statistical model, in which the
absorber selects the highest spike, applies. If, on the other
hand, only a few modes are present, the field is slowly varying
over a cavity transit so that the buildup of modelocking can-
not be due to the selective bleaching of the absorber by a
noise spike.

The number of oscillating modes present can be controlled
by the degree to which the saturated gain exceeds the loss. For
operation near threshold, the parabolic frequency dependence
of the gain profile near line center, and the saturation of
the gain medium as power builds up in the cavity, can ensure
that the field is comprised of only a few modes. Thus, the

well-known experimental observation that shot-to-shot con-
sistent modelocking requires near threshold operation[31,39,40]
precludes the validity of the statistical model in most cases
of interest.

Indeed, we show here that the ideal case for the buildup
of passive modelocking is one in which the gain rises suf-
ficiently slowly and saturates sufficiently easily that lasing
is initially confined to the single mode (SM) nearest line
center. Modelocking results from the fact that at a definite
power level in the cavity the SM state to which the initial
noise evolves becomes unstable with respect to a sinusoidal
perturbation. An expression for the modelocking threshold,
defined as the point at which the SM acquires a sinusoidal
modulation, is found. The subsequent evolution of the system
from SM to steady state modelocked operation is determinis-
tic and is treated as a succession of quasi steady state so-
lutions to the modelocking equation.

For each set of system parameters--characterizing the
cavity, saturable absorber and gain medium--a unique stable
steady state solution is reached. A straightforward technique
for determining the evolution to and characteristics of the
steady state from the given system parameters, is presented.
Depending upon the system parameters the steady state can be
either SM operation, single pulse per transit operation or
multi-pulse per transit operation.

We begin the analysis with a derivation of the basic
modelocking equation and an enumeration of the steady state
solutions in sections 2.1 and 2.2. A separate section, 2.3,
is devoted to the modelocking threshold since it is pivotal
to the deterministic theory. The subsequent transient evolu-
tion of the system is treated in 2.4. The stability of the
various possible steady state solutions is analyzed in 2.5.
In section 2.6 the theory is extended to include more complex
laser and absorber media than first considered. Modifications
and constraints applied to the theory by strong absorber sa-
turation are determined in 2.7. The physical significance of
the antisymmetric pulse solution to the modelocking equation
is discussed in 2.8.

2.1 Assumptions and Basic Equation

The passively modelocked laser system consists of three elements (see Figure 1)--the laser cavity, the active gain medium (amplifier) and the saturable absorber. The basic equation describing the system was derived by Haus.[24] The notation and method of derivation employed here parallels that of Haus, and is extended to justify the application of the equation to the transient problem.

The field in the nth transit through the cavity can be described by

$$E(t, n) = v(t, n) \, e^{j\omega_0 t} \tag{2.1}$$

where t is the time local to a single round trip transit, ω_0 is the frequency at line center of the laser medium and v is the envelope on the field within a single transit. The optical carrier $\exp j\omega_0 t$ plays no role in the modelocking analysis so that we need only concern ourselves with the evolution of the envelope v from one pass to the next. A waveform v(t, n) starting at the reference plane (see Figure 1) on the nth pass, is modified after making a round trip transit through the cavity such that

$$v(t, n + 1) = e^{-L_C} e^{G} e^{-2L_A} e^{G} v(t, n) \tag{2.2}$$
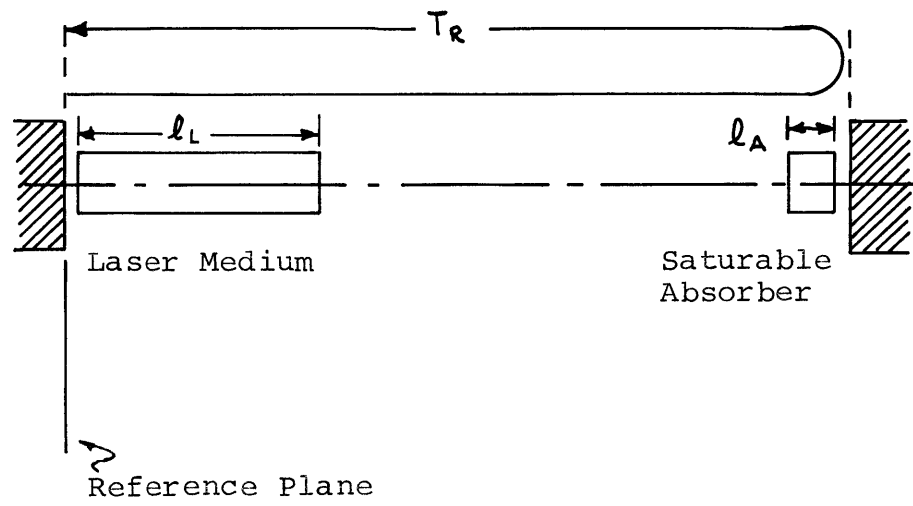
Figure 1: Modelocked Oscillator

where:

L_C = cavity loss

G = amplifier gain

L_A = absorber loss.

We assume that the net change of the waveform over a single pass is small enough that the exponential in (2.2) can be expanded to first order. Treating the integer n, which counts the transits through the cavity, as a continuum variable, we obtain the differential equation describing the transient evolution of the waveform v(t, n)

$$\frac{\partial v(t, n)}{\partial n} = [2G - (L_C + 2L_A)] \, v(t, n). \tag{2.3}$$

On first glance equation (2.3) is merely an expression of growth or decay of the waveform v(t, n) due to the existence of net gain or loss in the cavity. The first term on the right is the gain of the active medium. The second term is the total loss--cavity plus absorber. However, the gain dispersion and absorber nonlinearity provide shaping of the waveform with each cavity transit. In solving (2.3) we must account for the shaping as well as the growth or decay.

In order to give a more detailed description of the changes

of the waveform over each transit we characterize the components of the modelocking system as follows:

1. The cavity loss is constant in time and the cavity modes are uniformly spaced in frequency.

2. The gain medium is homogeneously broadened and its relaxation time is much longer than the cavity transit time, i.e. the gain is constant over a single transit time.

3. The absorber is homogeneously broadened, has a relaxation time which is much shorter than the cavity transit time and is located against one of the cavity mirrors.

Both the amplifier and the absorber are described as two level quantum systems. The difference in the relaxation times of the two media, however, enables us to obtain simple expressions for their response to the field in the cavity. Because the laser medium relaxation time is much longer than the cavity transit time, the laser population difference responds only to the time average power within one transit. Thus, its rate equation becomes[41]

$$\frac{1}{T_R} \frac{dN_L(n)}{dn} = - \frac{N_L(n) - N_L^{\,e}(n)}{T_L} - \frac{\sigma_L \, P(n)}{\hbar \omega_o \, A_L} \, N_L(n) \qquad (2.4)$$

where T_R is the round trip cavity transit time, $N_L(n)$
is the difference in population density at the nth pass,
$N_L{}^e(n)$ is the equilibrium density which varies with the
pumping rate, T_L is the relaxation time, σ_L is the optical
cross section of the medium, A_L is the beam cross section in
the medium and $P(n)$ is the time average power in the field
given by

$$P(n) = \frac{1}{T_R} \int_{-T_R/2}^{T_R/2} |v(t, n)|^2 \, dt. \tag{2.5}$$

If the change of power and pumping rate is slow compared
to the medium relaxation time T_L, i.e.

$$\frac{1}{P}\left|\frac{dP}{dn}\right|, \quad \frac{1}{N_L{}^e}\left|\frac{dN_L{}^e}{dn}\right| << \frac{T_R}{T_L}, \tag{2.6}$$

then the population difference remains in equilibrium with the
time average power. The population difference at the nth
pass becomes

$$N_L(n) = \frac{N_L{}^e(n)}{1 + \frac{P(n)}{P_L}} \tag{2.7}$$

where we have defined the laser medium saturation power

$$P_L \equiv \frac{\hbar\omega_o \, A_L}{\sigma_L T_L} \, .$$

Equation (2.7) dictates the saturation behavior of the homogeneously broadened laser medium. The gain of the amplifier at line center is given by

$$G(\omega_o, \, n) = \sigma_L \ell_L A_L \, N_L(n) = \frac{G_o(n)}{1 + \dfrac{P(n)}{P_L}} \qquad (2.8)$$

where ℓ_L is the length of the gain medium and $G_o(n)$ is the small signal gain. The lineshape of the medium is Lorentzian:

$$G(\omega, \, n) = \frac{G(\omega_o, \, n)}{1 + \dfrac{(\omega - \omega_o)^2}{\omega_L^2}} \qquad (2.9)$$

where ω_L is the halfwidth of the lasing transition. The imaginary component of the gain dispersion is ignored here since it plays no role in modelocking with a fast absorber and has been discussed elsewhere.[24,42]

We wish to determine the effect of the gain medium on the waveform v. The waveform in the cavity has a discrete spectrum comprised of the axial modes, namely

$$v(n, t) = \sum_m V_m(n) \, e^{jm\Delta\omega} \qquad (2.10)$$

where $\Delta\omega = 2\pi/T_R$ is the mode spacing and V_m is the amplitude of the mth mode. The total bandwidth of the waveform is assumed small compared to ω_L so that the gain can be expanded to second order in frequency.

$$G(m\Delta\omega, n) \simeq G(\omega_O, n) \left[1 - \frac{\delta\omega_O^2}{\omega_L^2} - \frac{2\delta\omega_O \, m\Delta\omega}{\omega_L^2} - \frac{(m\Delta\omega)^2}{\omega_L^2} \right] \qquad (2.11)$$

where $\delta\omega_O$ is the shift of the discrete spectrum with respect to the center of the lasing transition. Transforming into the time domain, the frequency dependence becomes an operator on $v(n, t)$ by replacing $(jm\Delta\omega)^n$ by $(d/dt)^n$. Thus, the effect of the gain can be expressed as

$$G(d/dt, n) \, v(t, n) = G(\omega_O, n) \left[1 - \frac{\delta\omega_O^2}{\omega_L^2} - 2j \frac{\delta\omega_O}{\omega_L^2} \frac{d}{dt} \right.$$

$$\left. + \frac{1}{\omega_L^2} \frac{d^2}{dt^2} \right] v(t, n) \qquad (2.12)$$

when operating on a waveform of envelope $v(t, n)$. The only effect of a nonzero $\delta\omega_O$ is, as one might expect, to cause

a carrier frequency shift in the field. From the stand point
of the transient buildup, however, an interesting result arises
when two adjacent modes are equally spaced from line center,
i.e. $\delta\omega_O = \Delta\omega/2$. This will be discussed in section 2.8.
Until then we shall assume $\delta\omega_O = 0$, in which case

$$G(d/dt,\ n)\ v(t,\ n) = G(\omega_O,\ n)\left[1 + \frac{1}{\omega_L^2}\frac{d^2}{dt^2}\right]v(t,\ n). \qquad (2.13)$$

The saturable absorber, having a fast relaxation time,
responds to the instantaneous power in the field. Its popu-
lation difference obeys the rate equation

$$\frac{dN_A(t,\ n)}{dt} = -\frac{N_A(t,\ n) - N_A^e}{T_A} - \frac{\sigma_A\left|v(t,\ n)\right|^2}{\hbar\omega_O\ A_A}N_A(t,\ n) \qquad (2.14)$$

where the subscript A denotes the absorber parameters analo-
gous to the laser parameters used in (2.4). For the purposes
of the present study we assume that the relaxation time is
short compared to the time dependence of the waveform, i.e.

$$\frac{1}{v}\left|\frac{dv}{dt}\right| << \frac{1}{T_L}, \qquad (2.15)$$

so that the population difference remains in equilibrium with

the instantaneous power in the field $|v|^2$. The absorber can now be described by

$$L(t, n) = \frac{L^e}{1 + \dfrac{|v(t, n)|^2}{P_A}} \tag{2.16}$$

where we have defined the small signal absorber loss

$$L^e \equiv \sigma_A \, \ell_A \, A_A \, n^e$$

and the absorber saturation power

$$P_A \equiv \frac{\hbar \omega_o \, A_A}{\sigma_A T_A} \, .$$

Making use of (2.13) and (2.16), equation (2.3) for the transient evolution of the waveform $v(t, n)$ becomes a nonlinear partial differential equation:

$$\frac{\partial v(t, n)}{\partial n} = \Delta\omega_c T_R \left[\left(g(n) + \frac{1 + q}{\omega_L^2} \frac{\partial^2}{\partial t^2} \right) \right.$$

$$\left. - \left(1 + \frac{q}{1 + \dfrac{|v(t, n)|^2}{P_A}} \right) \right] v(t, n). \tag{2.17}$$

We have defined the same quantities normalized to the cavity

loss as were used by Haus, namely the saturated gain

$$g(n) \equiv \frac{2G(\omega_o, n)}{\Delta\omega_c T_R} \qquad (2.18)$$

and the small signal absorber loss

$$q \equiv \frac{2L^e}{\Delta\omega_c T_R} , \qquad (2.19)$$

and have made use of the fact that the constant cavity loss

per transit is expressible as

$$L_C = \Delta\omega_c T_R \qquad (2.20)$$

where $\Delta\omega_c$ is the cavity mode halfwidth.

Furthermore, in contrast to the fast absorber equation

used by Haus, we have neglected the linewidth broadening due

to gain saturation by making the substitution

$$\frac{g}{\omega_L^2} \simeq \frac{1 + q}{\omega_L^2} .$$

The approximation is justified by the fact that the analysis is only valid in the regime where the gain is near threshold. Thus, gain variation is negligible compared to the normalized cavity loss, but is significant compared to $1 + q - g$. Also, many systems are bandwidth limited by a dispersive element (e.g. etalon) inside the laser cavity, in which case the "diffusion" operator expressing pulse broadening in time is gain independent. Although the following analysis can be carried out without making this approximation, the inclusion of power broadening sacrifices simplicity for little additional insight into the problem.

In the limit of weak absorber saturation we can expand the absorber loss to first order in the instantaneous power in the field, namely

$$\frac{q}{1 + \frac{|v(t,\,n)|^2}{P_A}} \simeq q \left(1 - \frac{|v(t,\,n)|^2}{P_A} \right) . \tag{2.21}$$

Equation (2.17) now reduces to the modelocking equation derived by Haus[24]

$$\frac{\partial v}{\partial n} = \Delta\omega_c T_R \left[\left(g + \frac{1 + q}{\omega_L^2} \frac{\partial^2}{\partial t^2} \right) - \left(1 + q - q \frac{|v|^2}{P_A} \right) \right] v. \tag{2.22}$$

In order to treat the transient evolution of the waveform
$v(t, n)$ we must first find the steady state solutions to
(2.22) for which the waveform v experiences no change from
one transit through the cavity to the next.

2.2 The Steady State Modelocking Solutions

In the steady state $\partial v / \partial n = 0$ and the modelocking equation (2.22) becomes an ordinary differential equation:

$$\left[\left(g + \frac{1 + q}{\omega_L^2} \frac{d^2}{dt^2} \right) - \left(1 + q - q \frac{|v(t)|^2}{P_A} \right) \right] v(t) = 0. \quad (2.23)$$

Haus has shown that one stable solution to (2.23) is a solitary pulse

$$v(t) = \frac{v_o}{\cosh \dfrac{t}{\tau_p}} \quad (2.24)$$

where the pulse parameters v_o and τ_p are determined by the system parameters via the eigenvalue relations

$$1 + q - g = \frac{q}{2} \frac{v_o^2}{P_A} = \frac{1 + q}{\omega_L^2 \tau_p^2} \quad (2.25)$$

in conjunction with (2.9).

The secant hyperbolic steady state solution found by Haus, however, is only one solution to equation (2.23). The fact that it is a solitary pulse solution implies that it

corresponds to the case where the cavity transit time is much longer than the pulsewidth, $T_R \gg \tau_p$, so that the inherent periodicity of the system can be ignored. During the buildup of modelocking the periodicity of the system must be taken into account since the pulsewidth τ_p is initially comparable to T_R. As a first step toward understanding the transient buildup, we must find the periodic solutions to (2.23).

In general, equation (2.23) is the equation of motion of a particle in the potential well

$$U(v) = \frac{q|v|^4}{2P_A} - (1 + q - g) |v|^2 + C \qquad (2.26)$$

where C is a constant and v is in one-to-one correspondence with the particle displacement. If the particle is launched with zero velocity at the well height 0, corresponding to a maximum displacement v_o, it oscillates between the turning points defined by the roots of U(v). By definition one of the turning points is at $v = v_o$. Thus, the solution is periodic, with two possible time dependences which we label symmetric (S) and antisymmetric (AS) (see Appendix A)

$$S: \quad v(t) = v_o \ \text{dn} \ (t/\tau_p, \ \gamma) \qquad 0 \le \gamma \le 1 \qquad (2.27a)$$

$$AS: \quad v(t) = v_o \ \text{cn} \ (t/\tau_p, \ 1/\gamma) \qquad 1 \le \gamma \le \sqrt{2} \qquad (2.27b)$$

where dn and cn are Jacobian elliptic functions of t/τ_p and modulus γ.[42] γ is defined by the two roots of the potential

$$\gamma^2 = \frac{v_o{}^2 - v_1{}^2}{v_o{}^2} \qquad (2.28)$$

where v_1, the second root, can be real or imaginary. Equation (2.28) relates the modulus γ to the constant C as given by Equation (8) of Appendix A. Substitution of (2.27) in (2.23) gives the eigenvalue relations

$$\frac{1}{\omega_L{}^2 \tau_p{}^2} = \frac{q|v_o|^2}{2(1 + q)\ P_A} \begin{cases} 1 & S \qquad\qquad (2.29a) \\ \gamma^2 & AS \qquad\quad (2.29b) \end{cases}$$

and

$$1 + q - g = \frac{q|v_o|^2}{2P_A}(2 - \gamma^2) \qquad (2.30)$$

which determine the peak amplitude v_o and "pulsewidth" τ_p within each period. The periodicity of the solution, which we require to equal the cavity transit time T_R, determines the constant γ via the relations

$$\frac{T_R}{\tau_p} = \begin{cases} 2mK(\gamma) & \quad S & \quad (2.31a) \\ 4mK(1/\gamma) & \quad AS & \quad (2.31b) \end{cases}$$

where K is the complete elliptic integral of the first kind, and m is an integer which determines the number of solutions fitted in a transit time. In the limit $T_R \gg \tau_p$, equation (2.31) dictates that $\gamma \rightarrow 1$ and equations (2.27)-(2.30) become the secant hyperbolic solution and eigenvalue relations found by Haus (2.34)-(2.25). The potential well and steady state solutions for various values of γ are shown in Figures 2 and 3.

In treating the transient evolution of the modelocking solution we shall first concern ourselves with the S solution which exists in the range

$$0 \le \gamma \le 1 \qquad\qquad (2.32)$$

where periodic steady state solutions of the form given in (2.27a) exist. Equation (2.32) sets limits on the relative magnitude of T_R and τ_p via (2.31a) such that

$$m\pi < \frac{T_R}{\tau_p} < \infty. \qquad\qquad (2.33)$$

Potential Well   Waveform

(a) $\gamma^2 = 0$

(b) $\gamma^2 = \frac{1}{2}$

(c) $\gamma^2 = 1^-$
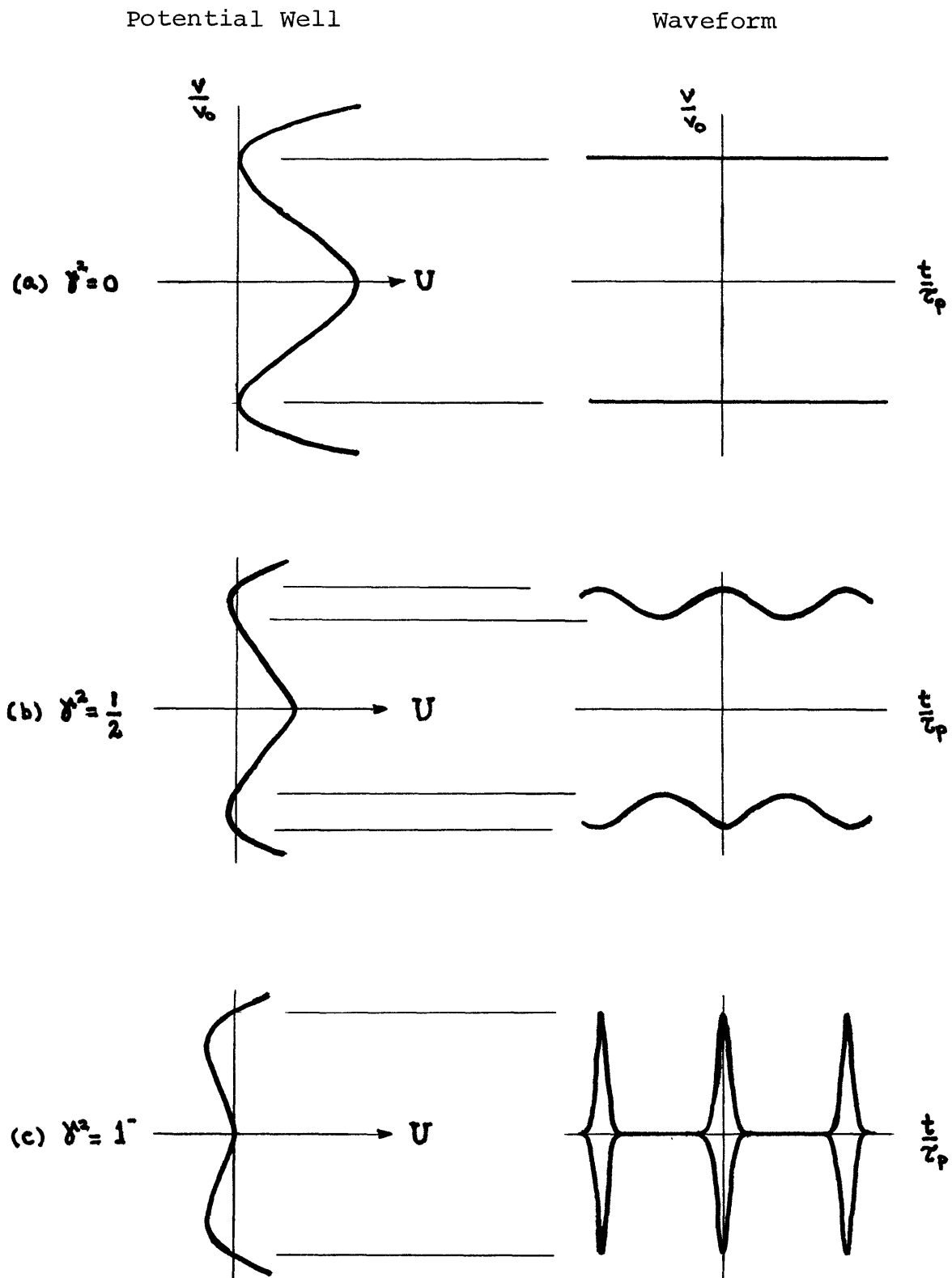
Figure 2: Symmetric Modelocking Solutions

Potential Well   Waveform

(a) $\gamma^2 = 2$

(b) $\gamma^2 = \frac{3}{2}$

(c) $\gamma^2 = 1^+$
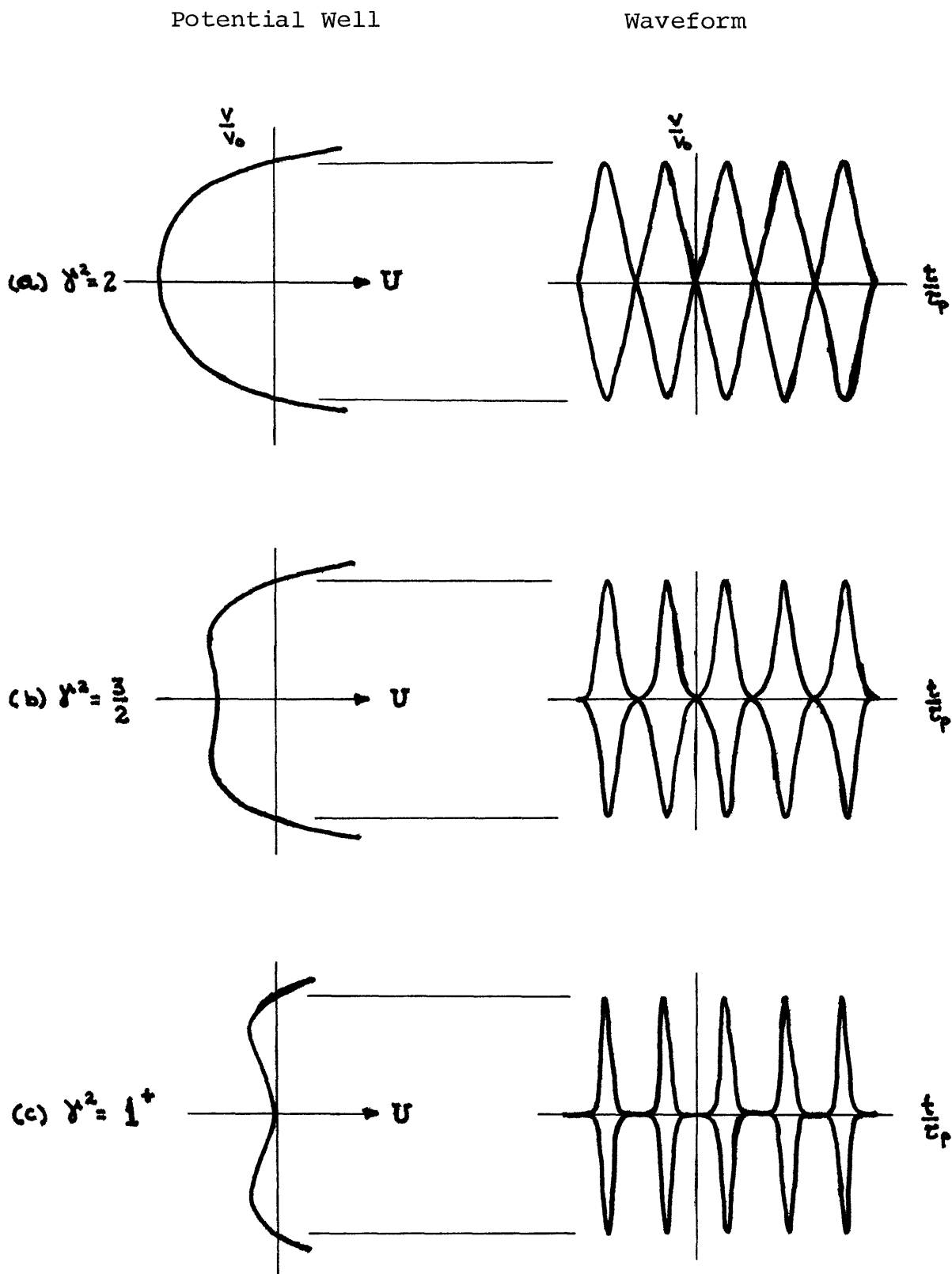
Figure 3: Antisymmetric Modelocking Solution

The lower limit of (2.33) corresponds to the case where the waveform v is SM with an infinitesimal sinusoidal ripple m one half wavelengths of which are fitted in a round trip transit. As noted earlier, the upper limit is the case where v is m secant hyperbolic pulses per transit time. Requiring the ratio T_R/τ_p to remain finite during the buildup of modelocking restricts the solution to the regime (2.32).

The time average power in a single transit time is determined by substituting the general solution (2.27a) in equation (2.5). The integral of $|v|^2$ over one period is expressible in terms of E, the complete elliptic integral of the second kind of argument γ, so that (2.5) gives

$$P = \frac{2|v_o|^2 \tau_p}{T_R} E(\gamma) = |v_o|^2 \frac{E(\gamma)}{K(\gamma)} . \tag{2.34}$$

Using (2.34) in (2.8) we can determine the saturated gain g for a particular solution. The requirement that the value of g be consistent with the eigenvalue relations (2.29a) and (2.30) places constraints on the system parameters for which modelocking solutions exist.

The parameters specified by the system are the round trip transit time in the cavity T_R, the small signal gain g_o, the saturation power of the laser P_L, the laser line-width ω_L, the small signal loading of the absorber q, and

the saturation power of the absorber P_A. In order to describe the regimes of successful modelocking we now determine the pulsewidth and power in one period of the general solution as a function of the system parameters. The five determining equations are listed in Table I.

Making use of (2.34) equations (2.9), (2.29a) and (2.30) can now be used to solve for P and τ_p in terms of the known system parameters.

$$\frac{P}{P_L} = \frac{1}{2} \left[\frac{2(1+q)}{q} \frac{P_A}{P_L} \frac{E}{K} \frac{1}{2-\gamma^2} - 1 \right]$$

$$\pm \frac{1}{2} \sqrt{ \left[\frac{2(1+q)}{q} \frac{P_A}{P_L} \frac{E}{K} \frac{1}{2-\gamma^2} + 1 \right]^2 - \frac{8g_o}{q} \frac{P_A}{P_L} \frac{E}{K} \frac{1}{2-\gamma^2} } \qquad (2.35)$$

$$\frac{1}{\omega_L^2 \tau_p^2} = \frac{q}{2(1+q)} \frac{K}{E} \frac{P}{P_A} \qquad (2.36)$$

As indicated in (2.35), two solutions exist for the time average power P. We shall show in section 2.5 that the higher power solution is always unstable and, hence, non-physical.

Table I

PARAMETER DETERMINING EQUATIONS

1. Eigenvalue Relations

$$\frac{q|v_0|^2}{2P_A} = \frac{1 + q}{\omega_L^2 \, \tau_p^2}$$

$$1 + q - g = \frac{1 + q}{\omega_L^2 \, \tau_p^2} \, (2 - \gamma^2)$$

2. Gain Saturation

$$g(n) = \frac{g_0(n)}{1 + \dfrac{P(n)}{P_L}}$$

$$P(n) = |v_0|^2 \, \frac{E(\gamma)}{K(\gamma)}$$

3. Periodicity

$$\frac{1}{m} \frac{T_R}{\tau_p} = 2K(\gamma)$$

Equation (2.35) also prescribes definite boundaries on γ for the existence of solutions. The fact that the power must be real sets the requirement that

$$\frac{E}{K}\frac{1}{2-\gamma^2} \geq \frac{q}{2(1+q)}\frac{P_L}{P_A}\left\{\frac{2g_0}{1+q} - 1 + 2\sqrt{\frac{g_0}{1+q}\left(\frac{g_0}{1+q} - 1\right)}\right\}.$$

(2.37)

If (2.37) is not satisfied, modelocking solutions of the form given in (2.27a) do not exist.

The possible steady state solutions for a fixed set of system parameters q, P_A/P_L and $\omega_L T_R$, and variable g_0, are illustrated in Figures 4-9. As an example, we have chosen the following values for the fixed parameters:

$q = 5$

$$\frac{P_A}{P_L} = 20$$

$\omega_L T_R = 150.$

The small signal absorber loading is five times greater than

the cavity loss. The absorber is twenty times harder to saturate than the laser. Approximately fifty cavity modes lie within the laser linewidth.

The time average power curves given by (2.44) and the corresponding inverse pulsewidth curves given by (2.36) are shown in Figures 4 and 5 respectively. The apices of the curves are defined by the value of γ for which the equal sign of (2.37) applies. By substitution in (2.35) we find the power at the apex of each curve to be

$$\frac{P_a}{P_L} = \frac{g_0}{1 + q} + \sqrt{\frac{g_0}{1 + q}\left[\frac{g_0}{1 + q} - 1\right]} - 1 \; . \qquad (2.38)$$

As g_0 increases we see that the curves of allowed modelocking solutions become confined to smaller values of γ and larger values of inverse pulsewidth and average power. Ultimately condition (2.37) cannot be satisfied for any value of γ and the solutions vanish altogether when at $\gamma = 0$

$$g_0 = \frac{q}{4}\frac{P_L}{P_A}\left[\frac{1 + q}{q}\frac{P_A}{P_L} + 1\right]^2 \qquad (2.39)$$

so that the maximum allowable time average power is
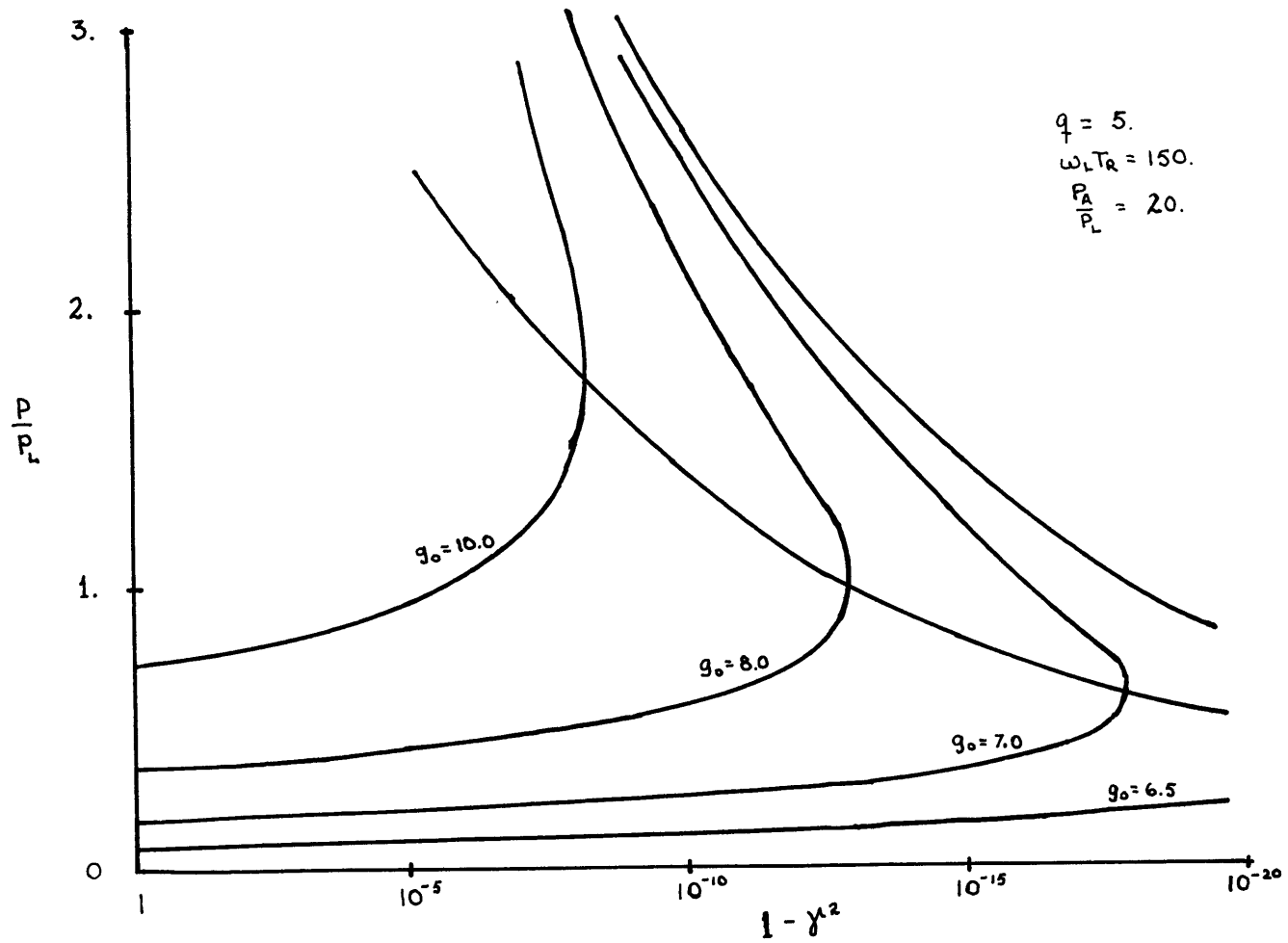
Figure 4: Time Average Power of Allowed Solutions
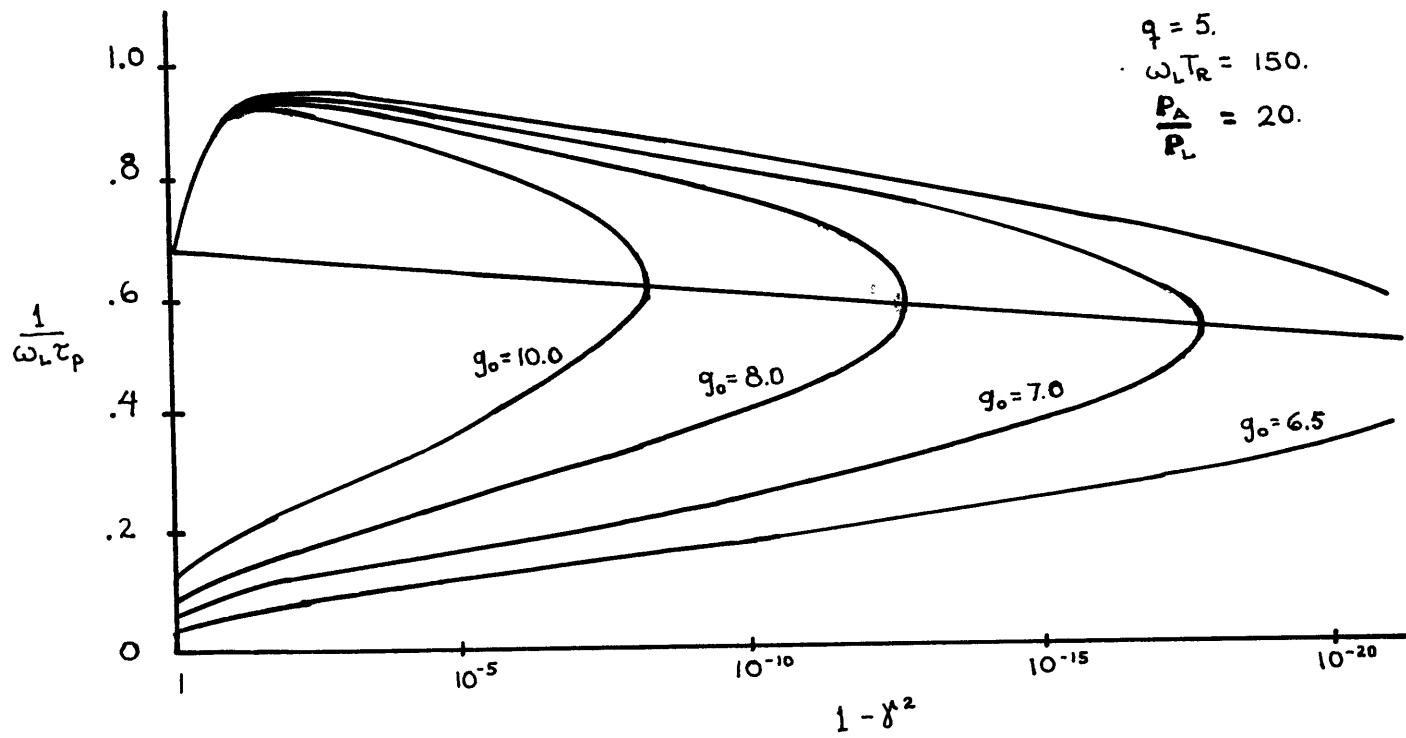
Figure 5:   Inverse Pulsewidth of Allowed Solutions

$$\frac{P}{P_A} = \frac{1}{2} \left(\frac{1 + q}{q} - \frac{P_L}{P_A} \right) \quad .$$

Equation (2.39) tells us that the loading q and saturation

power P_A of the absorber must be sufficient to accommodate

the average power required to saturate the gain to its steady

state value specified by the eigenvalue relation (2.30) of

the modelocking solution. The significance of the line con-

necting the apices in the Figures will be discussed in 2.5.

The steady state operating point for the system at a

given g_O is determined by searching for a value of the modu-

lus γ for which the periodicity condition (2.31a) and the

pulsewidth condition (2.36) are simultaneously satisfied. The

periodicity curves are characterized by m, the multiplicity

of the solution in a transit time. Figure 6 shows the inter-

cepts on the m = 1 curve. As g_O is increased from 1 + q,

we see from Figure 5 that initially no modelocking solutions

are possible since they cannot fit in a transit time through

the cavity. In this regime SM operation is the only stable

solution. Modelocking initiates when the first intercept with

the m = 1 curve is found. As the gain is increased further

the operating point of the system moves along the m = 1 locus.

The actual solutions for increasing values of g_O are shown

in Figure 7. We see that the SM field evolves rapidly to

well separated pulses with increasing g_O.
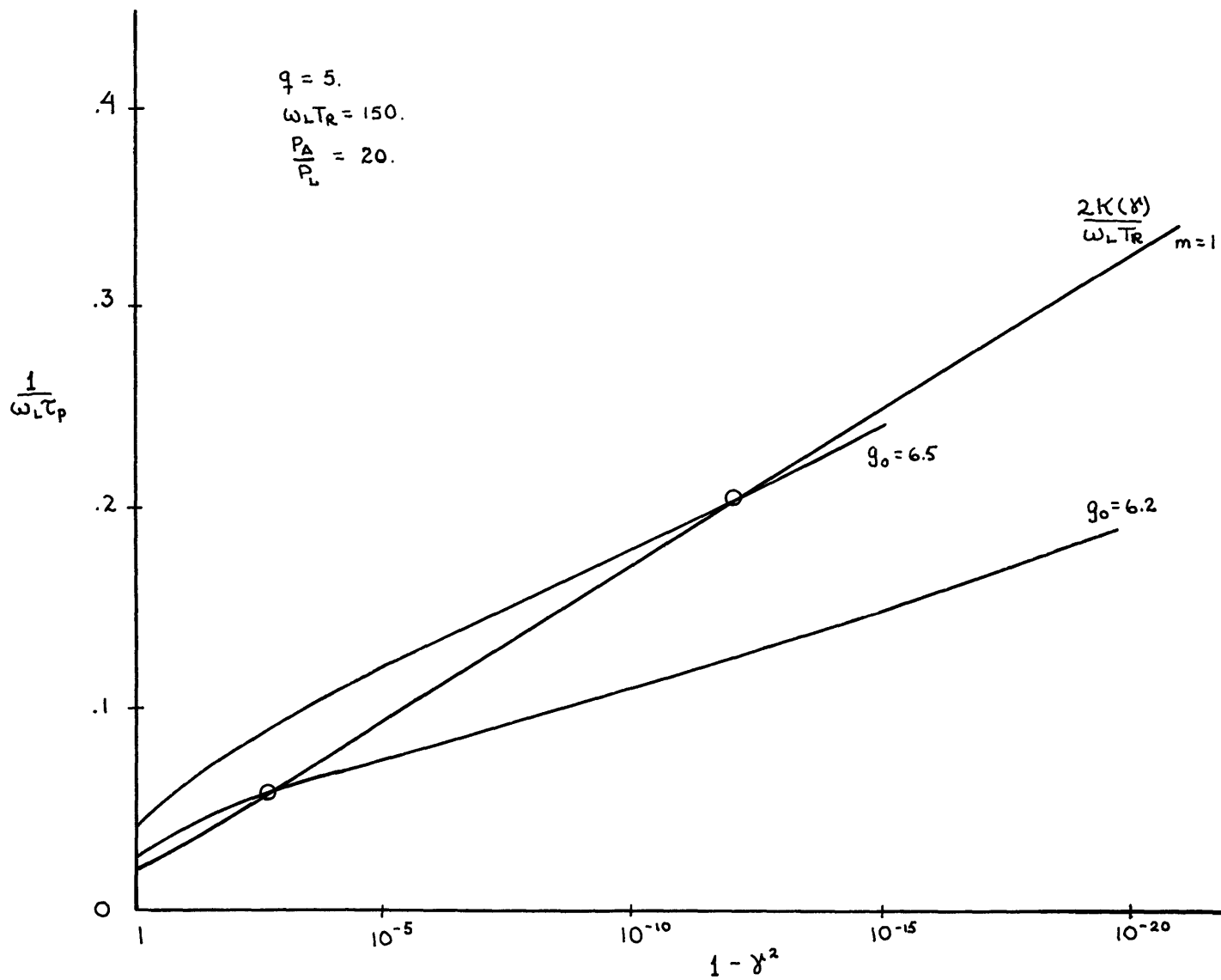
Figure 6: Steady State Operating Points for Single Pulse Solutions
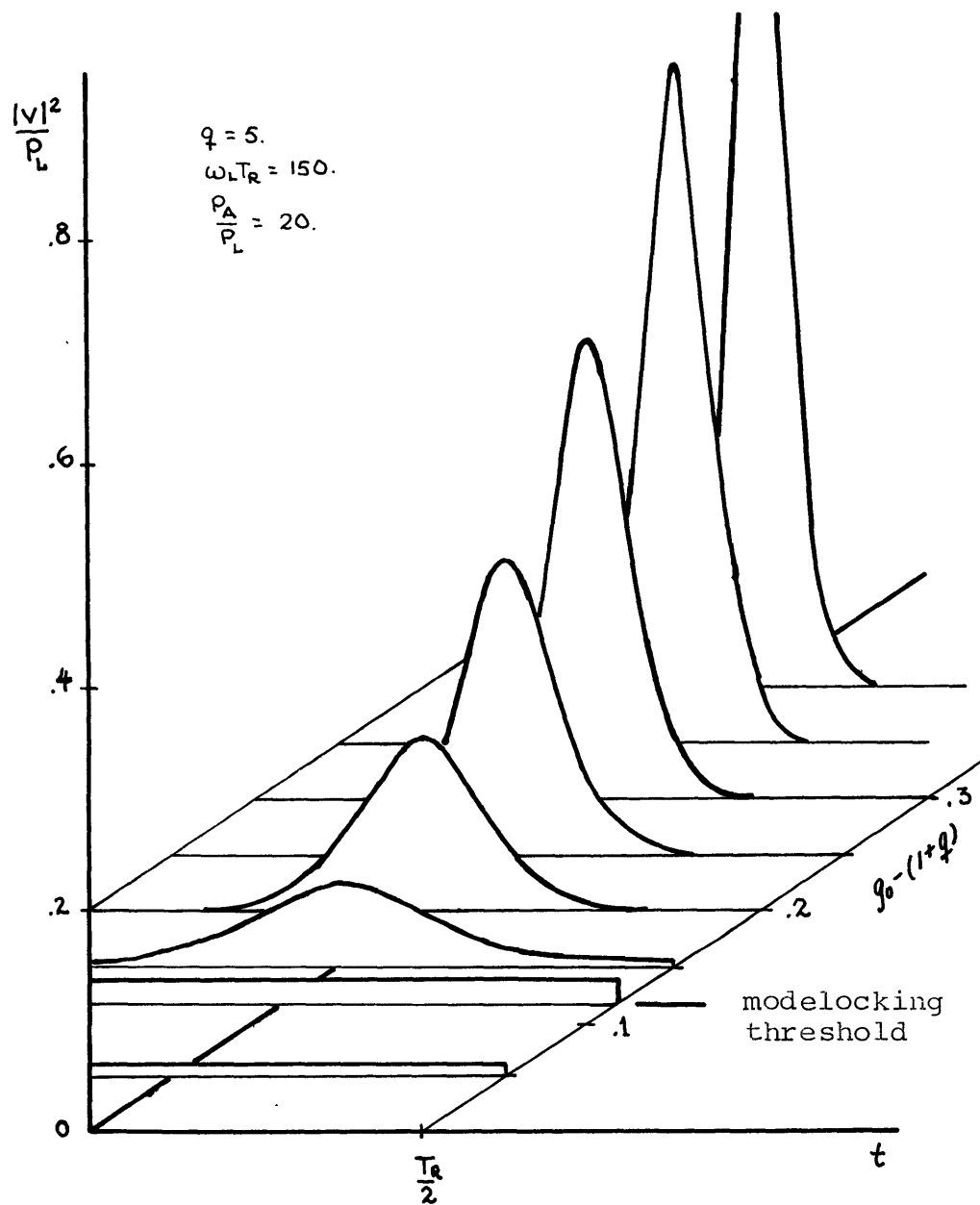
Figure 7: Symmetric Single Pulse Solutions for Increasing
Small Signal Gain

In fact, Figure 7 gives us a feeling for how the transient buildup occurs--the SM field acquires a sinusoidal ripple at a power level defined as the modelocking threshold, and builds up to a single pulse in a succession of steady state solutions. The axis here, however, is small signal excess gain and not n. The evolution of modelocking for a given g_o as a function of n is treated in Sections 2.3 and 2.4.

By looking at the wider range of pulsewidths shown in Figure 8, we see that as g_o continues to increase the intercept of the m = 1 curve with the allowed pulsewidth curve is lost. (Note that there is a regime in which two intercepts may be possible. We shall show in Section 2.5 that only the solution characterized by the lower value of γ is stable.) At this point the system must make the transition to the m = 2 locus, and the solution becomes two pulses per transit time. The system hops from single pulse to double pulse operation and so on up the ladder until g_o reaches the value given by (2.39) and modelocking solutions cease to be possible. The solutions at the various operating points indicated in Figure 8 are illustrated in Figure 9.

We now turn our attention to the AS solution defined in the range

$$1 < \gamma < \sqrt{2} \tag{2.40}$$
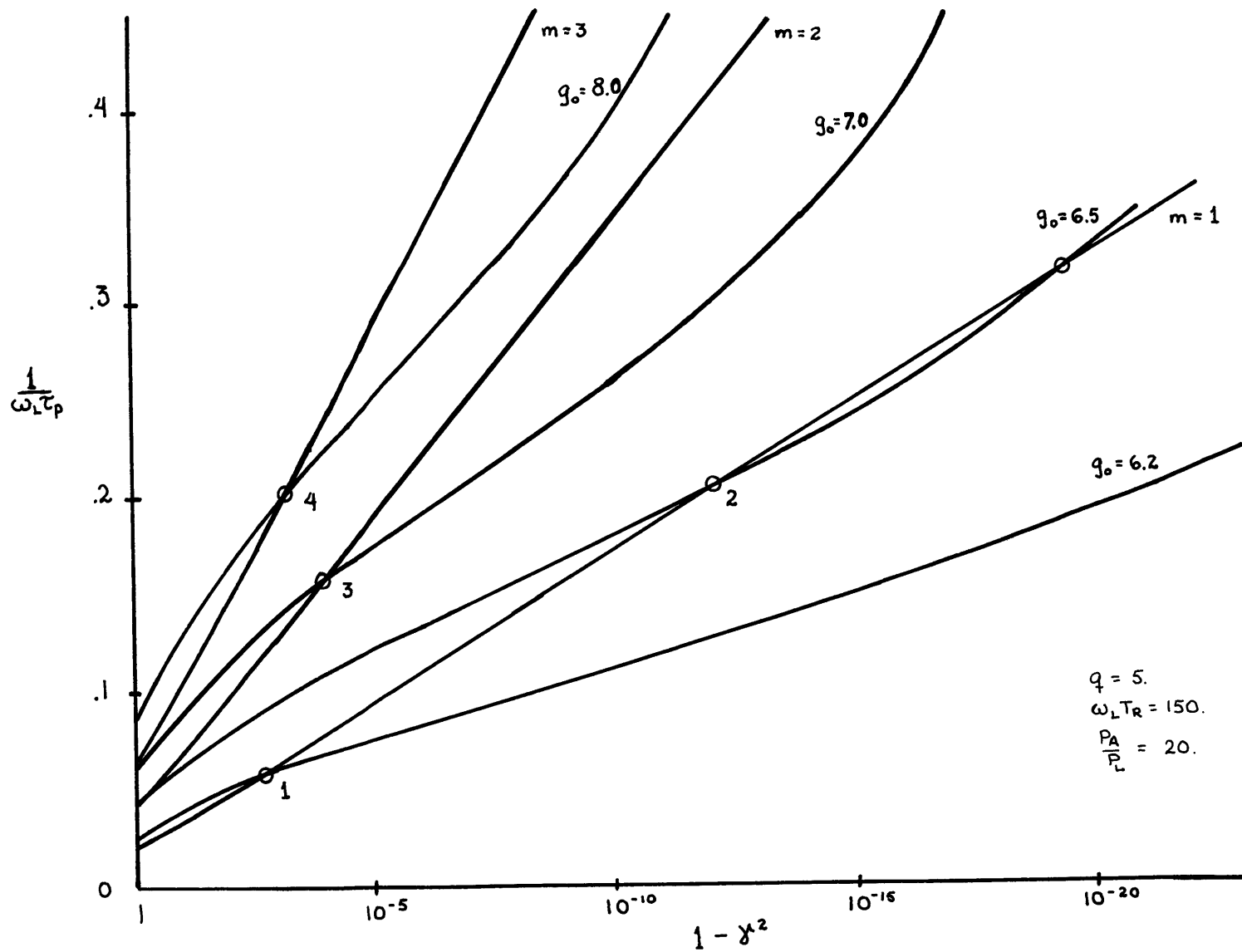
Figure 8: Single and Multi-Pulse Steady State Operating Points
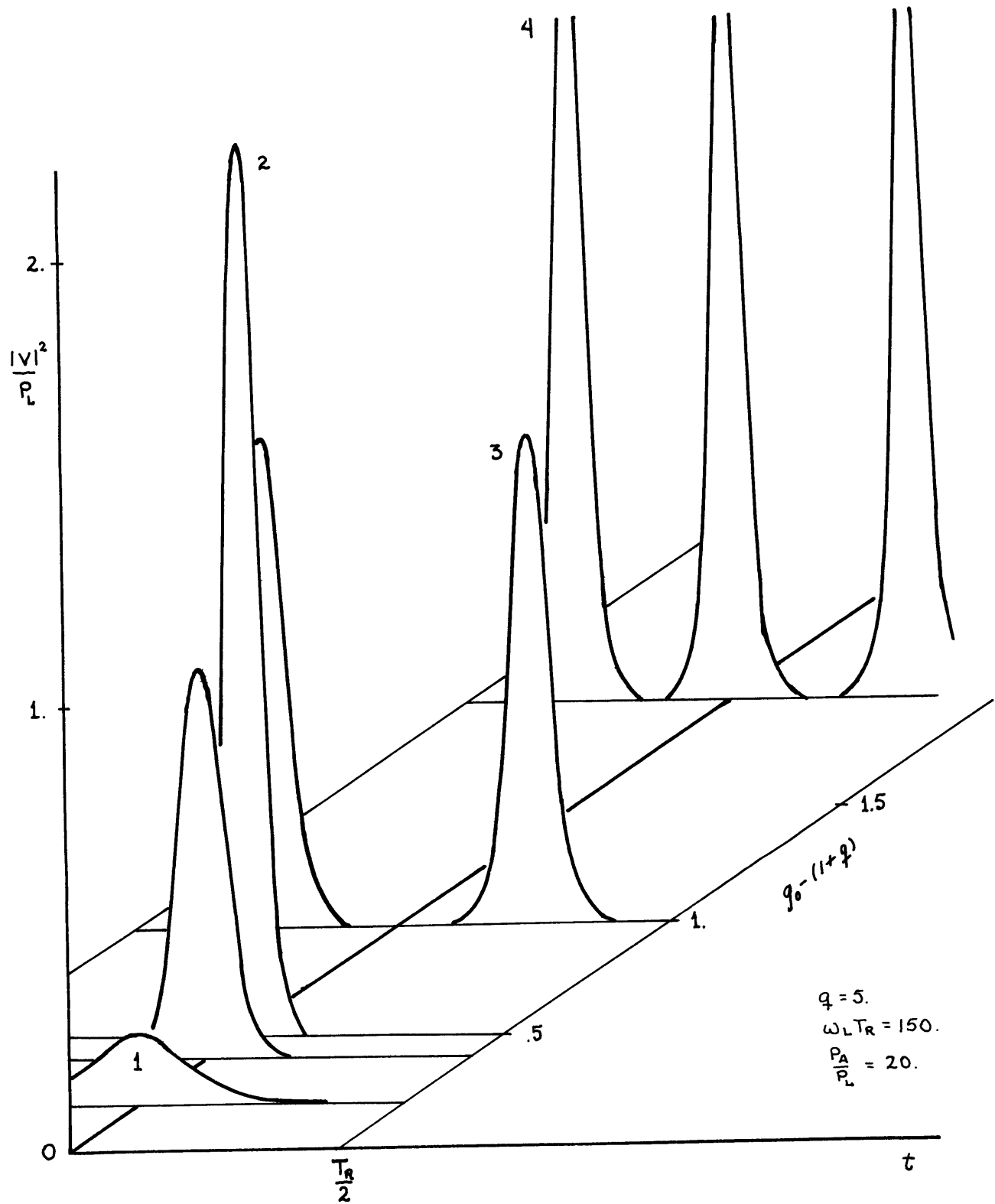
Figure 9: Variation of Pulse Multiplicity with Increasing
Small Signal Gain

by (2.27b). The limits on the relative magnitude of T_R and τ_p is given by (2.31b).

$$4mK \left(\frac{1}{\sqrt{2}} \right) < \frac{T_R}{\tau_p} < \infty \qquad (2.41)$$

In the lower limit the solution is nearly sinusoidal with m wavelengths fitted in a transit. The upper limit is the case where v consists of 2m secant hyperbolic pulses of alternating phase per transit. Requiring T_R/τ_p to remain finite restricts the solution to the range (2.40). Thus, a given system cannot make the transition between the two solutions (2.27a, b).

The time average power in the DM solution is given by

$$P = |v_o|^2 \left[\gamma^2 \frac{E(1/\gamma)}{K(1/\gamma)} + 1 - \gamma^2 \right] . \qquad (2.42)$$

In the limit $\gamma \to 1$ the S and AS expressions for P become identical. In the limit $\gamma \to \sqrt{2}$ the time average power in the AS solution approaches one-half its peak power as is characteristic of a sinusoidal waveform. Analogous to the S case we use (2.42) in (2.29b) and (2.30) to obtain constraints on the system parameters such that solu-

tions exist. The same relations (2.35), (2.36) and (2.37) as obtained for the S solution can be applied to the AS solution provided we make the substitution

$$\frac{E(\gamma)}{K(\gamma)} \rightarrow \left[\gamma^2 \frac{E(1/\gamma)}{K(1/\gamma)} + 1 - \gamma^2 \right] . \qquad (2.43)$$

The apparent singularity in (2.35) is treated by noting from (2.30) that the relation $1 + q - g = 0$ determines the time average power in the limit $\gamma \rightarrow \sqrt{2}$.

The steady state solutions for the same fixed set of system parameters q, P_A/P_L, and $\omega_L T_R$ as illustrated in the S case are shown for the AS case in Figure 10. The threshold value of g_0 is seen to be higher than in the S case. Furthermore, the field prior to the modelocking threshold is nearly sinusoidal, rather than constant, as in the S case. In otherwords, the AS solution is initiated by the beating of two adjacent cavity modes which are equidistant from line center and, hence, have equal gain. Since this is a special case, which can only be created by careful adjustment of the cavity length, we shall reserve further discussion of the AS solution until Section 2.8 and concentrate our efforts on the S solution.
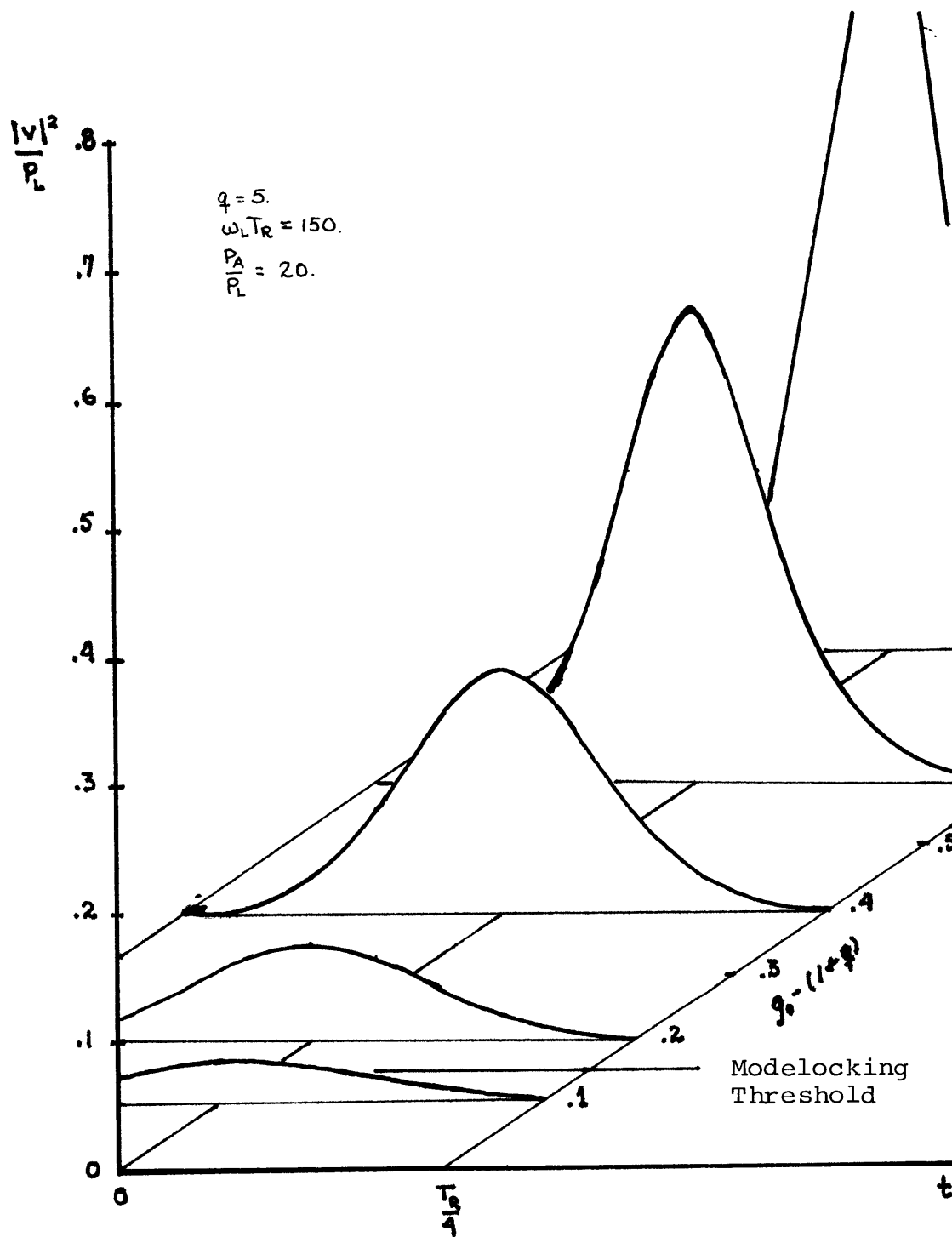
Figure 10: Antisymmetric Single Pulse Solutions for Increasing Small Signal Gain

Thus far we have treated only the steady state solutions to (2.23). In order to determine how the system reaches the steady state we must solve the full equation for $v(t, n)$. The solution is executed in two stages:

(1) The evolution of the system from the initial spontaneous emission noise to the first modelocking S solution corresponding to $\gamma = 0$ and

(2) The subsequent evolution of the system to the final steady state operating point.

2.3 The Modelocking Threshold

An understanding of the modelocking threshold is essential for the determination of the conditions for which the buildup of modelocking is statistical or deterministic. Previous authors have assumed that the initial lasing field is dominated by wideband spontaneous emission noise consisting of many bandwidth limited spikes per transit time T_R.[33,34] Although it is true that the signal in the laser, as in any oscillator, is initiated by noise, it is essential to note that only the spectral components of the noise in the region where gain exceeds loss are amplified, all others must decay. Modelocking initiates after the power in the cavity has built up to a point where the absorber saturation becomes significant. By that time the initial noise has been amplified over many transits through the gain medium, and the axial modes of the cavity are "well formed".

The issue of statistical versus deterministic buildup then boils down to the number of modes present in the cavity at the modelocking threshold. We show here that the proper design of a passively modelocked system for reliable operation should ensure that only a single mode (SM) field is present in the cavity at the modelocking threshold.

The general case of the buildup of modelocking is sketched in Figure 11. Lasing initiates when the small signal gain g_0
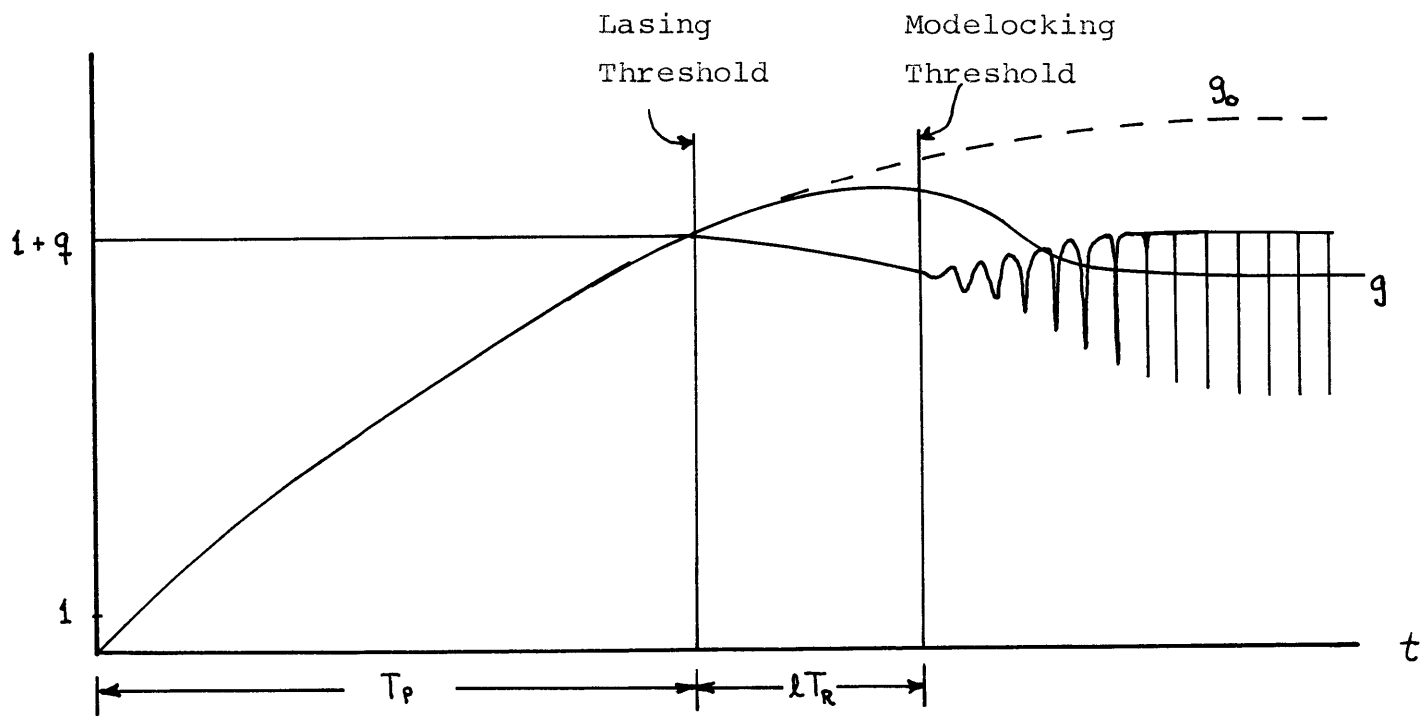
Figure 11: Transient Buildup of Modelocking System to the Steady State

first breaks above the small signal loss 1 + q. In other words, the time at which the gain of the mode at line center first exceeds the total loss--constant plus saturable--in the cavity is defined as the origin n = 0. In the region near the onset of lasing we assume that the saturation of the absorber is negligible. The initial buildup of the field is described by

$$\frac{1}{\Delta\omega_c T_R} \frac{\partial v(n,\ t)}{\partial n} = \left[g - (1 + q) + \frac{1 + q}{\omega_L^2} \frac{\partial^2}{\partial t^2} \right] v(n,\ t). \qquad (2.44)$$

We can express the field in the nth transit by a superposition of the cavity modes, namely

$$v(n,\ t) = \sum_m V_m \exp \left[j\ \frac{m2\pi t}{T_R} + \int^n \alpha_m(n)\ dn \right] \qquad (2.45)$$

where m is an integer which labels the modes, V_m is the amplitude and α_m is the gain coefficient characteristic of the mth mode.

Substitution of (2.44) in (2.45) gives an expression for the gain coefficient

$$\frac{1}{\Delta\omega_c T_R} \alpha_m(n) = g(n) - (1 + q) - \frac{1 + q}{\omega_L^2} \left(m\ \frac{2\pi}{T_R} \right)^2. \qquad (2.46)$$

Only modes close to line center (m = 0) experience growth. The spectral width of the lasing field is determined by the value of m for which $\alpha_m = 0$. The mode nearest line center (m = 0) experiences the most rapid growth due to the band narrowing effect of the gain dispersion. The number of modes present is further limited as power builds up in the cavity by the saturation of the gain medium. Thus, operation on the single mode (SM) nearest line center will dominate.

Let us first consider the case where the laser field is assumed to be SM just prior to the onset of modelocking. We wish to show that the buildup of modelocking for this case is determinsitic. Subsequently we shall examine the conditions for which the assumption of SM operation is valid in actual modelocked laser systems.

2.3.1 The Ideal Threshold

As the gain rises the SM field described by $v_o(n)$ grows to the point where the equations describing the subsequent growth of the field must include the absorber saturation. Hence, the equation governing growth becomes

$$\frac{dv_o}{dn} = \alpha_o(n) \; v_o(n) \qquad (2.47)$$

where α_o is given by

$$\frac{\alpha_o(n)}{\Delta\omega_c T_R} = g(n) - (1 + q) + \frac{q|v_o(n)|^2}{P_A} . \qquad (2.48)$$

Note that gain dispersion plays no role in determining α_o, the gain coefficient of the mode at line center. Since the field is "time independent" within T_R the saturated gain is

$$g(n) = \frac{g_o(n)}{1 + \dfrac{|v_o(n)|^2}{P_L}} . \qquad (2.49)$$

The modelocking threshold is determined by the value of $v_o(n)$ for which the first SM modelocking solution to (2.23)

is obtained. As shown by (2.33), the first solution is the
case where the SM waveform acquires a sinusoidal ripple,
with one half wavelength fitted in a round trip transit. Thus,
the modelocking threshold is defined by $n = \ell$ such that

$$\frac{T_R}{\tau_p(\ell)} = \omega_L T_R \sqrt{\frac{q}{2P_A(1 + q)}} \quad v_o(\ell) = \pi \qquad (2.50)$$

and we have

$$\frac{P_o(\ell)}{P_A} = \frac{2\pi^2}{q} \frac{1 + q}{\omega_L^2 T_R^2} . \qquad (2.51)$$

The SM field must build up to a value $|v_o(\ell)|^2 = P_o(\ell)$
before modelocking initiates. In contrast to the work of
previous authors who have noted the existence of a modelocking
threshold,[29,36] we have obtained a precise definition of the
threshold which has a direct physical interpretation. The
modelocking threshold occurs at the point where the power in
the SM field is sufficient to saturate the absorber, such
that the two modes adjacent to line center can reach thres-
hold, causing a buckling of the SM field.

To prove that the transition from the SM to the first
modelocking solution is deterministic, we now show that a

sinusoidal perturbation on the SM experiences more rapid growth than the SM. In other words, the system must mode-lock rather than continue to run in a single mode.

Returning to equation (2.22), we assume a perturbed solution of the form

$$v(n, t) = v_o(n) + \sum_{m \neq 0} \delta v_m \exp\left[jm\frac{2\pi t}{T_R} + \int^n \alpha_m(n) \, dn\right] \quad (2.52)$$

where $v_o(n)$ is the growing SM solution whose gain coefficient α_o is given by (2.48). The perturbation has been expanded in the cavity modes. Substituting (2.52) in (2.22), we find that to first order $\alpha_m(n)$ is given by

$$\frac{1}{\Delta\omega_c T_R} \alpha_m(n) = \left[g(n) - (1 + q) + \frac{3q}{P_A}|v_o(n)|^2 - \frac{1+q}{\omega_L^2}\left(m\frac{2}{T_R}\right)^2\right].$$

$$(2.53)$$

Since the perturbation is "orthogonal" to the single mode field over a cavity transit time, the saturated gain does not change to first order in the perturbation amplitude, and is still specified by (2.49). From (2.48) we see that the difference between the gain coefficient of the single mode

field and that of the perturbation is

$$\frac{1}{\Delta\omega_c T_R} (\alpha_m - \alpha_o) = \frac{2q}{P_A} |v_o|^2 - \frac{1 + q}{\omega_L^2} \left(m \frac{2\pi}{T_R} \right)^2 . \qquad (2.54)$$

Maximum growth is experienced by the perturbation for which m = 1. Setting $\alpha_1 = \alpha_o$ then establishes the value of P for which the perturbation growth first exceeds the SM growth. Clearly the threshold value of P predicted by (2.54) is the same as that given by (2.51). Thus, for P > P(ℓ) the sinusoidal perturbation grows faster than the SM. Consequently, once the threshold P = P(ℓ) is reached, the system must ease into the SM modelocking solution.

2.3.1 Actual Transient Behavior Near Threshold

We have shown that the buildup of modelocking is
deterministic if the lasing field is confined to a single
mode at the modelocking threshold defined by equation (2.51).
Here we investigate the conditions for which SM operation
of the modelocking threshold is assured.

The salient features of the buildup process are illus-
trated in Figure 11. Two mechanisms combine to limit the
bandwidth of the cavity field as the small signal gain rises
above the small signal loss line--first, the parabolic fre-
quency dependence of gain near line center and second, the
saturation of the gain as power builds up in the field. Of
course, in the absence of a saturable absorber, the gain ul-
timately settles to the loss line and the laser runs single
mode. It is clear, therefore, that the dynamic behavior of
the modelocked system will ensure SM operation at the mode-
locking threshold in two cases: 1. the gain rises suffici-
ently slowly, or 2. the gain saturates sufficiently easily
that only a single axial mode sees net gain at the point
where the threshold power is reached. In general, the system
can rely on a combination of the two cases enumerated above.
Thus, constraints are placed on the rate of increase of the
small signal gain and the relative magnitudes of the satura-

tion powers of the gain and loss media. Note that although the saturation power density is a fixed characteristic of each medium, the relative saturation powers can be varied by adjusting the relative beam diameters in the two media.

In order to describe the buildup regime accurately we allow the gain to rise at a rate specified by the pumping of the laser medium. We first consider the constraints on the buildup rate alone, i.e. where gain saturation does not play a significant role. The rise in the excess gain is assumed to be linear in the regime of interest, namely

$$g_0 - (1 + q) = \left(\frac{dg_0}{dn}\right)_0 n \qquad (2.55)$$

where the rate of increase at threshold $(dg_0/dn)_0$ is determined by the pumping mechanism. The buildup of power in the mth mode is governed by

$$\frac{dP_m}{dn} = 2 \alpha_m P_m. \qquad (2.56)$$

Making use of (2.55) we obtain

$$P_m(n) = P_m(0) \exp\left\{2\Delta\omega_c T_R \left[\left(\frac{dg_0}{dn}\right)_0 (n - n_m)^2 \right.\right.$$

$$\left.\left. - (1 + q) \left(\frac{2\pi m}{\omega_L T_R}\right)^2 (n - n_m)\right]\right\} \qquad n \geq n_m. \qquad (2.57)$$

$P_m(0)$ is the noise power in the mth mode at its threshold given by

$$P_m(0) = P_o(0) \left[1 - \left(\frac{2\pi m}{\omega_L T_R} \right)^2 \right] , \qquad (2.58)$$

and n_m is the pass at which each mode reaches the lasing threshold given by

$$n_m = \frac{(1 + q)}{(dg_o/dn)_o} \left(\frac{2\pi m}{\omega_L T_R} \right)^2 . \qquad (2.59)$$

The number of passes ℓ through the laser medium required for the power in the mode nearest line center to reach the modelocking threshold is determined by inverting (2.57) to obtain:

$$\ell^2 = \frac{\ln \left[\frac{P_o(\ell)}{P_o(0)} \right]}{2\Delta\omega_c T_R \left(\frac{dg_o}{dn} \right)_o} . \qquad (2.60)$$

Substituting for the threshold power $P_o(\ell)$ from (2.51) we can write

$$\ell^2 = \frac{1}{2\Delta\omega_c T_R (dg_o/dn)_o} \ln\left[\frac{2\pi^2(1 + q)}{(\omega_L T_R)^2} \frac{P_A}{q} \frac{P_A}{P_o(0)}\right].$$ (2.61)

The spectral width of the field at the modelocking threshold defined by ℓ can be determined by computing the decrease in power with increasing distance from line center, m. If we assume $n_m \ll \ell$, we can use (2.59) and (2.57) to obtain the expression

$$\frac{P_m(\ell)}{P_o(\ell)} \simeq \left[1 - \left(\frac{2\pi m}{\omega_L T_R}\right)^2\right] \exp\left[- 6\Delta\omega_c T_R (1 + q) \left(\frac{2\pi m}{\omega_L T_R}\right)^2 \ell\right]$$ (2.62)

whence we can define a modelocking threshold bandwidth

$$\omega_{th}^2 = \left(\frac{2\pi \ m_{th}}{T_R}\right)^2 = \frac{\omega_L^2}{6\Delta\omega_c T_R (1 + q) \ell}$$ (2.63)

at which the power has decreased by a factor greater than $1/e$. In the ideal case $m_{th} \to 1$, i.e., the laser bandwidth at the modelocking threshold contains only one cavity mode. The constraint on the initial rate of increase of the gain for which $m_{th} = 1$ is

$$\frac{1}{\Delta\omega_c T_R} \left(\frac{dg_o}{dn}\right)_o \leq 18 \left\{ (1 + q) \left(\frac{2\pi}{\omega_L T_R}\right)^2 \right.$$

$$\left. \ln \left[\frac{2\pi^2 (1 + q)}{(\omega_L T_R)^2 q} \frac{P_A}{P(0)}\right]\right\} \tag{2.64}$$

As we would expect, the restriction on the rate of increase of the gain is strongly dependent on the number of modes within the laser linewidth, $\omega_L T_R/\pi$. The larger the number of modes, the more slowly the gain must rise.

A plot of equation (2.64) is shown in Figure 12 for typical values of q and $P_A/P(0)$. The maximum rate of gain rise at threshold allowed for three different transient systems—TEA CO_2, Nd:YAG and Nd:Glass—is presented in Table II. By assuming a linear rise of the gain, we also obtain a conservative estimate of the minimum allowable pump time T_p^{min}, the time it takes the small signal gain to reach threshold (see Figure 11). The TEA CO_2 laser, having the narrowest linewidth of the three media, can tolerate the fastest gain risetime.

The pump times required of both the CO_2 and Nd:YAG lasers shown in Table II are within the normal operating bounds of these lasers. The time required for the small signal gain of the TEA CO_2 laser to reach maximum is typically 3 - 5 μs.[44] The actual pumping time of the Nd:YAG laser is
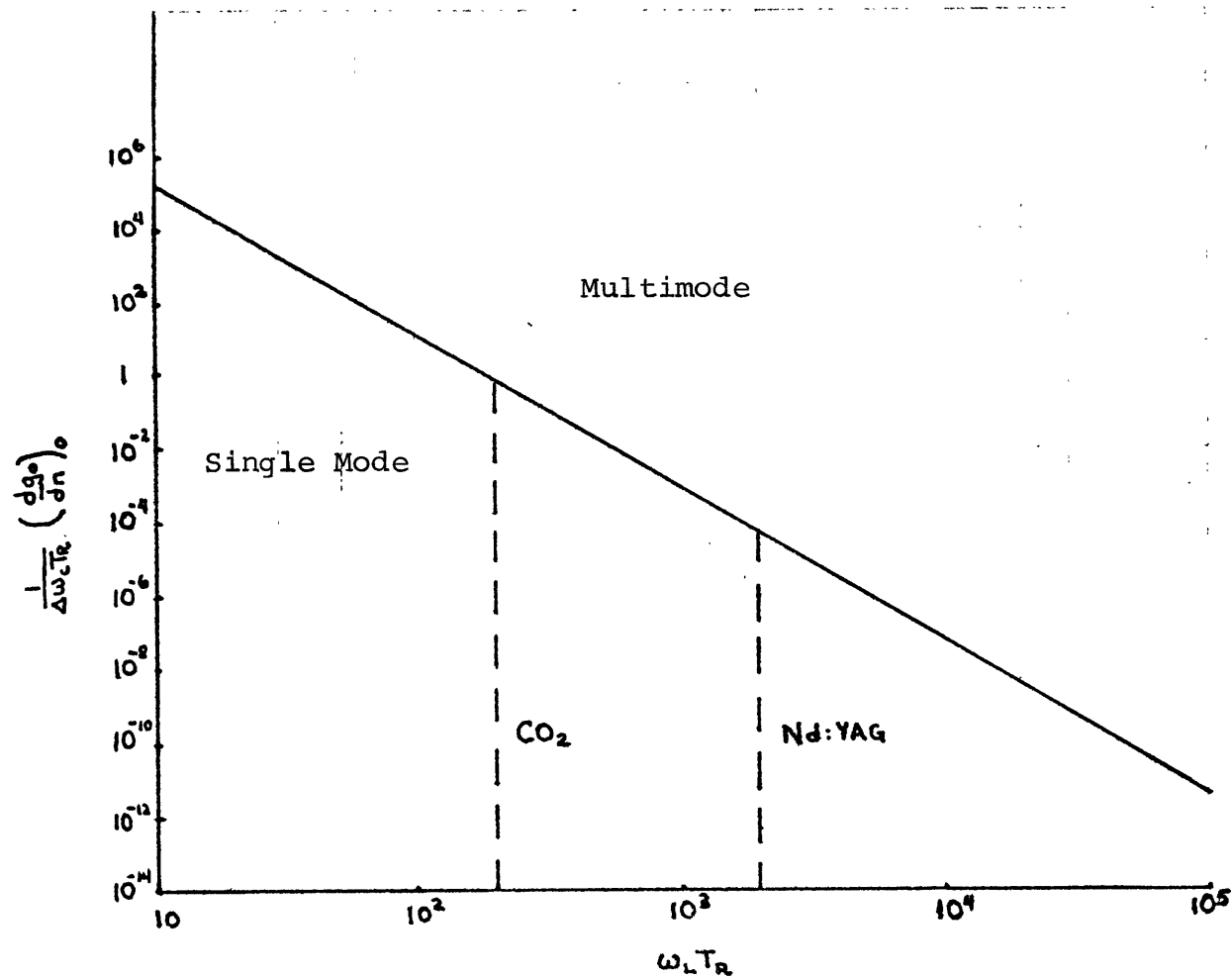
Figure 12: Rate of Increase of the Small Signal Gain to Ensure Single Mode Operation at the Modelocking Threshold

Table II

	CO_2	Nd:YAG	Nd:Glass
ω_L	10^{10} s^{-1}	$2 \cdot 10^{11}$ s^{-1}	$2 \cdot 10^{13}$ s^{-1}
T_R	20 ns	10 ns	10 ns
$\omega_L T_R$	200	$2 \quad 10^3$	$2 \quad 10^5$
$\Delta\omega_c T_R$	.1	.1	.1
$1 + q$	10	10	10
$\left(\dfrac{dg_o}{dn}\right)_o$	.1	10^{-5}	10^{-13}
T_p^{min}	2 μs	100 μs	10^4 s

on the order of hundreds of microseconds.[9]

The pump time required for modelocking the Nd:Glass laser, however, is clearly way out of line. The extremely small rate of gain rise at threshold could be achieved by having a fast initial rise which levels off near threshold-- in which case the allowed T_p could be much smaller than the 10^4 s indicated in Table II. Even so, the rate $(dg_o/dn)_o = 10^{-13}$ would be difficult to attain and more difficult to reproduce from shot to shot. Thus, the wide bandwidth of the Nd:Glass amplifier precludes consistent modelocking. The statistical model[34] of the buildup applies, as is betrayed by fluctuations in the laser output.[40] The only way to obtain reliable modelocking, which utilizes the largest possible fraction of the Nd:Glass linewidth, would be to devise a means to vary the bandwidth during the buildup, as shall be discussed in Chapter 3.

The finding that reproducible modelocking requires a slow rate of increase of the gain at the lasing threshold, is in agreement with the experimental observation that near threshold operation is required. The near threshold constraint can be relaxed if the gain medium saturates significantly before the modelocking threshold is reached. In this case we rely upon the settling of the saturated gain to the loss line to filter out all but the mode nearest line center before

modelocking initiates. The ideal case is one in which the rate of rise of the gain and saturation power of the gain are such that it has saturated to the loss line before the threshold power $P(\ell)$ is attained.

2.4   The Transient Evolution from Single Mode to Short Pulse

We have shown in the previous section that at a particular SM power level in the cavity the SM field must acquire a sinusoidal modulation. Once the SM field has "buckled", the absorber saturation ensures that the peak intensity of the field will experience the most rapid growth from one pass to the next. Thus, the waveform v(t, n) will continue to grow and narrow until the excess gain in the system is depleted, and the spectrum of the pulse runs up against the bandwidth of the laser medium.

The initial buckling of the SM field was shown to correspond to the "first" steady state modelocking solution in the limit $\gamma \rightarrow 0^+$. We now treat the transient evolution from the SM field to short pulse operation as a succession of quasi-steady state solutions to equation (2.22).

In order to determine precisely how the waveform evolves from the modelocking threshold to the steady state pulse, we constrain the buildup to be adiabatic. Because it is central to our treatment of the transient evolution and stability, the word "adiabatic" requires precise definition. Our usage is consistent with the discussion of adiabaticity presented by Kulsrud[45]

"Consider the classic one-dimensional problem
of an oscillator whose spring constant is slowly varied
by some external means, such as a varying temperature,
which only affects the motion through its spring con-
stant. The counterpart of this problem was first con-

sidered by Einstein at the Solvay Congress of 1911 on the old quantum theory. Lorentz asked how the amplitude of a simple pendulum would vary if its period were slowly changed by shortening its string. Would the number of quanta of its motion change? Einstein immediately gave the answer that the action, E/ω, where E is its energy and ω its frequency, would remain constant and thus the number of quanta would remain unchanged, if $(1/\omega)(d\omega/dt)$ were small enough."

The approach we take here is identical to Einstein's treatment of the pendulum. In our case the time average power is the slowly varying parameter which corresponds to the pendulum frequency. Thus, our statement of adiabaticity becomes $(1/P)(dP/dn) \ll 1$. We find a constant of motion of the system (2.73) which enables us to specify a unique solution to the modelocking equation for each value of time average power, in the same manner that the fixed action of the pendulum allows Einstein to specify the amplitude of the pendulum at each value of frequency.

Furthermore, we can determine how the time average power changes in our system by the use of energy conservation, just as one would use the amount of energy added to the pendulum to compute the change in ω. Conservation of energy in the case of modelocking requires setting the change in field energy in one transit equal to the energy supplied by the system in one transit, so that the total energy remains constant. The energy balance equation

$$\Delta W_{field} = - \Delta W_{system} \tag{2.65}$$

can be obtained directly from (2.22) by multiplying both

sides by $v^*(n, t)$ and integrating over one period or transit time. Thus, (2.65) becomes

$$\frac{d}{dn} \oint |v|^2 dt = 2\Delta\omega_c T_R \{[g - (1 + q)] \oint |v|^2 dt$$

$$+ \frac{q}{P_A} \oint |v|^4 dt - \frac{1 + q}{\omega_L^2} \oint \left|\frac{dv}{dt}\right|^2 dt \qquad (2.66)$$

where $\oint$ denotes integration over one period $-T_R/2 < t < T_R/2$.

We assume that the power in the field experiences a change over one transit time given by

$$P(n + 1) = [1 + 2\alpha(n)] P(n) \qquad (2.67)$$

where $\alpha(n)$ is the growth rate of the field to be determined from the energy balance equation. Thus, for two energy states which are differentially close, the left hand side of the energy balance equation becomes simply

$$\Delta W_{field} = \frac{d}{dn} \oint |v|^2 dt = 2T_R \alpha(n) P(n). \qquad (2.68)$$

In order to evaluate the change in the system energy we make use of the fact that the quasi-steady state solution for each value of n is given by (2.27a), namely

$$|v(n,\ t)|^2 = \frac{K[\gamma(n)]}{E[\gamma(n)]}\ P(n)\ dn^2\left[\frac{t}{\tau_p(n)}\ ,\ \gamma(n)\right] \qquad (2.69)$$

where

$$\frac{1}{\omega_L^2\tau_p^2(n)} = \frac{q}{2(1+q)}\ \frac{K[\gamma(n)]}{E[\gamma(n)]}\ \frac{P(n)}{P_A} \qquad (2.70)$$

$$2K[\gamma(n)] = \frac{T_R}{\tau_p(n)} \qquad (2.71)$$

and

$$g(n) = \frac{g_o(n)}{1 + \frac{P(n)}{P_L}}. \qquad (2.72)$$

Note that we limit our attention to solutions of multiplicity m = 1. The parameter $\gamma(n)$, which completely characterizes the solution, is determined by solving (2.75)-(2.79) simultaneously to obtain

$$\frac{P(n)}{P_A} \frac{1}{K[\gamma(n)]E[\gamma(n)]} = \frac{8(1 + q)}{q \; \omega_L T_R} . \qquad (2.73)$$

The left hand side of (2.73) is, in fact, a constant of motion. Substitution of (2.69) in the right hand side of (2.66) and equating to (2.68) gives the desired expression for $\alpha(n)$

$$\frac{1}{\Delta\omega_c T_R} \alpha(n) = [g(n) - (1 - q)]$$

$$+ [2 - \gamma^2(n)] \frac{qK[\gamma(n)]}{2E[\gamma(n)]} \frac{P(n)}{P_A} \qquad (2.74)$$

which is simply the effective time average net gain in the nth transit including the laser medium dispersion and absorber saturation.

The equations governing the transient buildup are now complete. The waveform $v(n, t)$ for each value of n is given by (2.69) where the constant $\gamma(n)$, the pulsewidth in each period $\tau_p(n)$, and the saturated gain $g(n)$ are determined by equations (2.70)-(2.72). The evolution of the nth waveform to the $(n + 1)^{th}$ waveform is dictated by equation (2.67), where conservation of energy constrains $\alpha(n)$ to be given by (2.74).

The initial condition of $P(n)$ was shown in the previous section to be

$$\frac{P(\ell)}{P_A} = \frac{2\pi^2}{q} \frac{1 + q}{\omega_L^2 T_R^2} .$$ (2.75)

The final steady state defined by

$$v(t, n + 1) = v(t, n)$$ (2.76)

requires that

$$\frac{\alpha}{\Delta\omega_c T_R} = g - (1 + q) + \frac{qP E[\gamma]}{2P_A K[\gamma]} [2 - \gamma^2] = 0 .$$ (2.77)

We recognize that (2.77) is the eigenvalue relation determined earlier to describe the general steady state solution. Equations (2.76) and (2.70)-(2.72) now uniquely specify the final steady state solution as was shown in section 2.2.

Typical plots of the buildup from the modelocking threshold are shown in Figures 13 and 14 for different values of the small signal gain g_o. In both cases the small signal gain is assumed to rise instantaneously to a constant value above the total loss line. In addition to the fixed parameters assumed earlier in Figures 4-9 we have set the constant cavity loss at 50% per pass $(\Delta\omega_c T_R = .5)$ for the sake of illustration.

The slow time evolution of the small signal and saturated
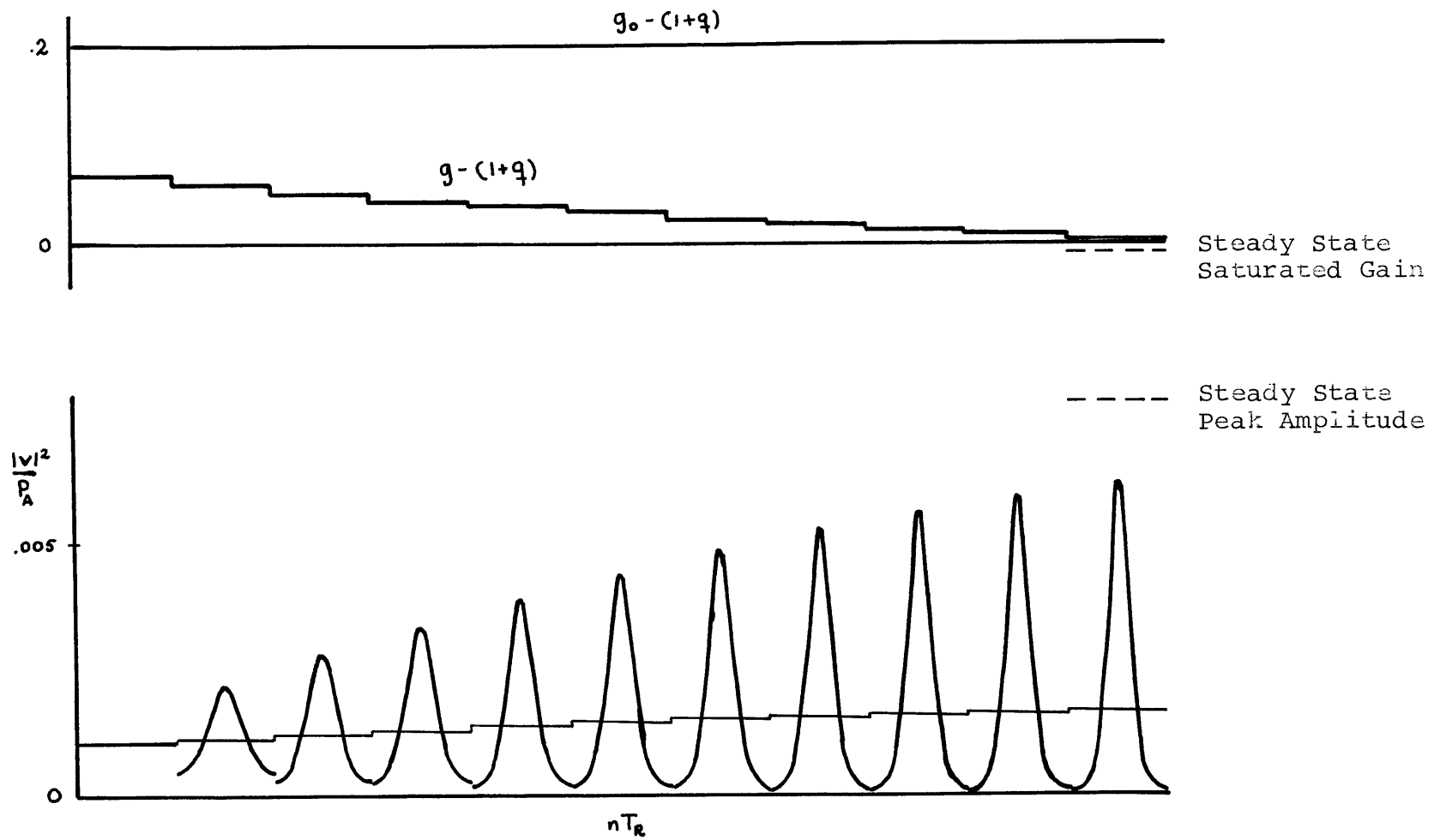
Figure 13: Transient Buildup for Small Signal Excess Gain of .2
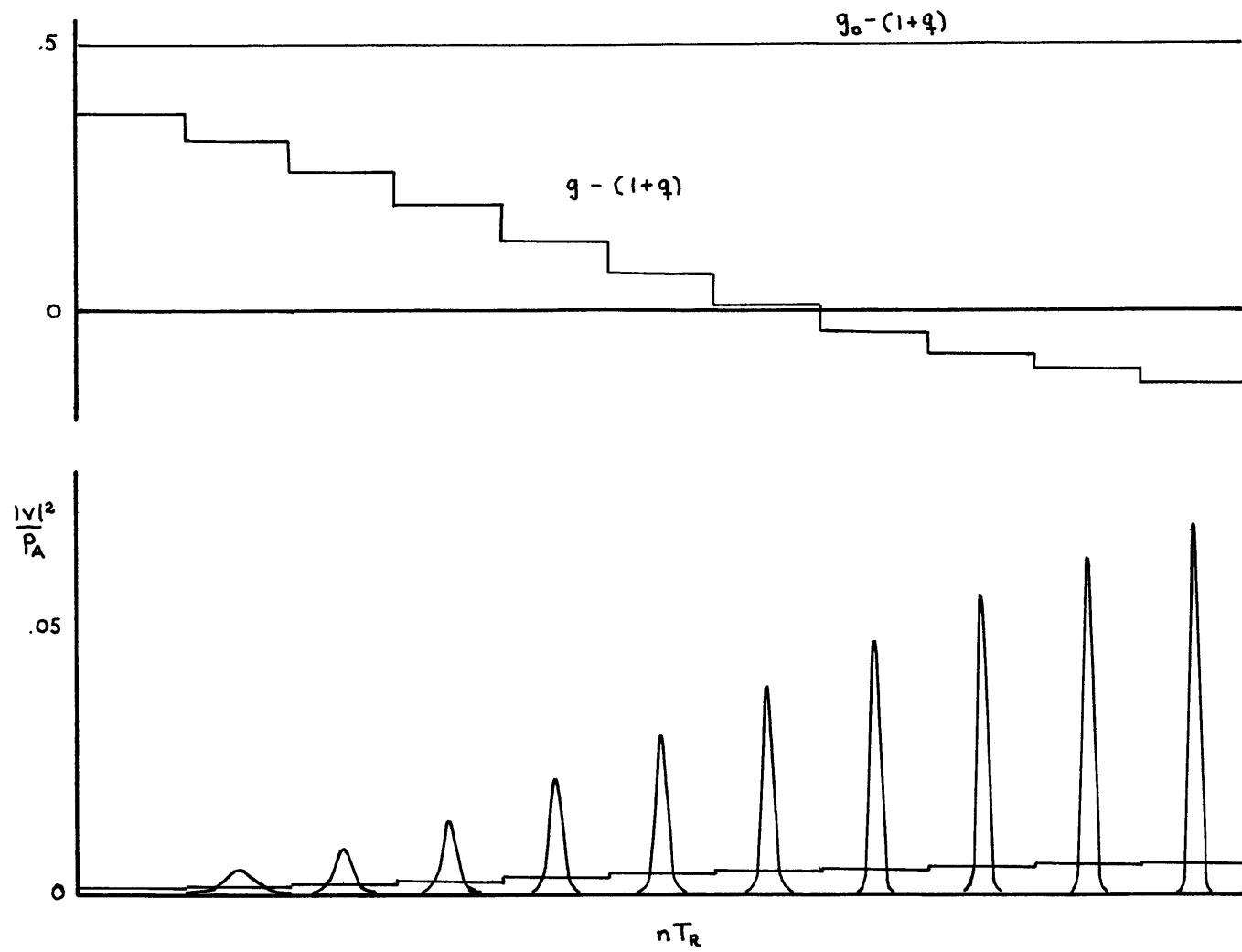
Figure 14: Transient Buildup for Small Signal Excess Gain of .5

gain is shown in the upper section of both Figures. The corresponding time average power and instantaneous power are shown in the bottom section. The steady state values of saturated gain, time average power, and peak power ultimately reached, are indicated by the dotted markings on the right hand side of the Figures. By comparing the waveforms in the two figures we see that the pulses obtained are sensitive to the excess gain.

Of course, in many modelocked systems (e.g. gain or Q switched lasers) an absolute steady state is never reached. This does not limit the effectiveness of the analysis, provided the net growth $\alpha(n)\, P(n)$ over the cavity transit time T_R remains small, such that the buildup and decay of the waveform v can be approximated by a succession of quasi-steady states. In fact, the analysis enables us to trace the complete evolution of transient modelocking from start to finish.

Before proceeding it is essential that we clarify the significance of the adiabatic gain coefficient (2.74). Equation (2.74) is an expression for the time average net gain in the nth transit and, as such, dictates the change in time average power from one pass to the next. The physical mechanism which causes change is the gain of the amplifying medium, which first rises due to pumping, and then saturates as the time average power builds up. The net laser gain over the

small signal loss is given by the first two terms of (2.74).
The net gain due to the combined absorber saturation and
laser dispersion is contained in the last term of the equation.
Note that the dispersion, represented by the γ^2 term, can
never counterbalance the absorber saturation, so that the net
effect of the two is always destabilizing. Consequently,
stabilization only occurs when the laser gain has saturated
to a point below the small signal loss line, such that the
terms of (2.74) sum to zero. It is also clear that the pulses
obtained never utilize the full laser bandwidth, but only that
fraction which is consistent with the power in the cavity.

A schematic picture of the transient evolution of mode-
locking is shown in Figure 15. We view the transient mode-
locked system as a series of black boxes representing the time
average net gain, $\alpha(n)$, over a transit. The field enters
the nth box in state n characterized by $P(n)$, and emerges
in state n + 1. The state of the system is determined by
the field before it enters the box. The only change experi-
enced by the field in traversing the box is that its energy
increases [we assume $\alpha(n) > 0$ for the sake of argument].
Between boxes, however, the field must satisfy the system
equation. It distributes its new found energy ΔW_{field} in
such a way that it acquires a new $(n + 1)^{th}$ amplitude, width
and shape, which is compatible with the new $(n + 1)^{th}$ system
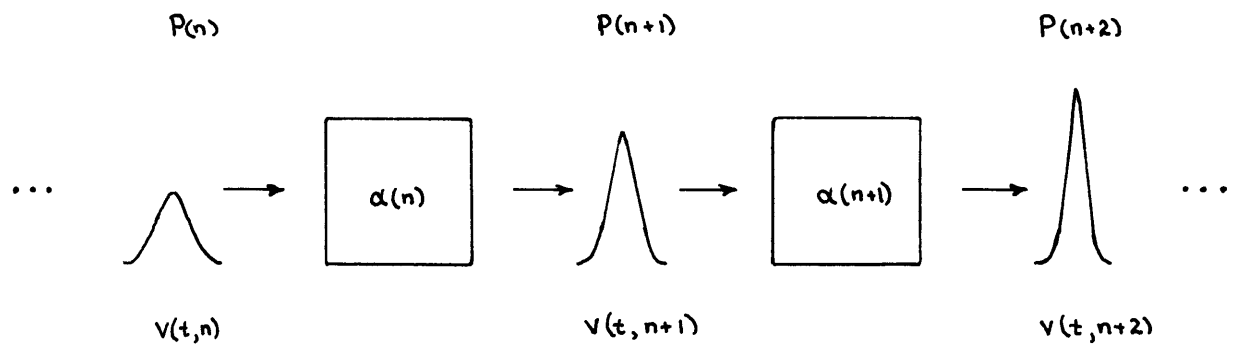
Figure 15:   Schematic Picture of Transient Evolution

state it has defined by extracting ΔW_{system}.

We have devised a specific means of connecting the quasi-steady state solutions to (2.22). Now we must examine the extent to which the adiabatic evolution of Figure 15 is an accurate description of transient modelocking. Two assumptions have been made:

1. Changes in both the field and the system over a single transit, which are due to or result in a change in the saturated gain, can be time averaged over the transit.

2. Of all possible waveform configurations, that which corresponds to the quasi-steady state solution at each value of n grows the fastest or decays the slowest.

We justify the first assumption as follows. From the start of our analysis the gain has been assumed constant over each transit and saturates only with the time average power in the field in each transit. Changes in the field are dictated by the existence of net gain. In determining net gain, since we are comparing the dispersion and saturable absorption, which operate on and vary with the instantaneous field, to the laser gain, which varies with the time average power in one transit, it is reasonable that we consider only the time average effects of the dispersion and absorption. Consequently,

net gain over one transit is only defined here as a time
average quantity. Of course, in considering changes in the
field which do not involve a change in the laser gain, i.e.,
a reshaping of the field which keeps the time average power
invariant, we must treat the operation of the dispersion on
and the response of the absorption to the instantaneous field.

Justification of the second assumption requires that we
test the stability of the quasi-steady state solutions against
all possible perturbations on each pass. The stability analy-
sis is carried out in the next section. We show that the ac-
ceptance of the first assumption stated above implies the
validity of the second.

2.5 Stability of the Steady State

We have yet to address ourselves to the crucial question of the stability of the steady state solutions which were derived in section 2.2 and which form the basis of the transient analysis in section 2.4. Indeed, two distinct steady state solutions for each set of system parameters were found to be possible in section 2.2. The stability of the solutions against small perturbations is investigated here.

A rigorous stability test requires proof that no perturbation of the steady state experiences unbounded growth. We assume

$$v(t) = v_s(t) + \delta v(t, n) \qquad (2.78)$$

where $v_s(t)$ is the steady state solution and $\delta v(t, n)$ is a perturbation. In order to facilitate the stability analysis we divide the perturbation into two components

$$\delta v = \delta v^N + \delta v^O \qquad (2.79)$$

defined such that

$$2 \int v_s \, \delta v^N \, dt = \delta P \qquad (2.80)$$

$$2 \int v_s \, \delta v^O \, dt = 0 \qquad (2.81)$$

where δP is the perturbation of the time average power.
The above representation divides the perturbation into a
perturbation δv^N which is not orthogonal to the steady
state and a perturbation δv^O which is orthogonal to the
steady state. Note that the orthogonality relations hold
only on the nth pass. In tracing the evolution of the per-
turbation, we must divide the perturbation into orthogonal
(OP) and nonorthogonal (NP) perturbations on each pass.

The NP causes a change in the time average power in
the system. Fundamental to our analysis is the concept of
adiabatic evolution. We assume that the power change due to
the NP causes a shift from the steady state solution to an
adjacent quasi-steady state solution. The OP perturbation
alone can only change the distribution of power in the steady
state waveform within one transit time without affecting the
time average power. Before treating the case of a general
perturbation, let us first examine separately the stability
of the purely NP and OP.

2.5.1 Non-Orthogonal Perturbations

In keeping with the schematic picture of the transient evolution presented in section 2.4, we can develop the physical picture of the effect of the NP shown in Figure 16. The system in the steady state is characterized by a zero gain coefficient. The overlapping perturbation appears on the kth pass. However, the perturbation is not "felt" until it makes a complete transit through the system. After the first pass the power in the field has changed by an amount

$$\delta P = 2 \oint v_s \, \delta v^N \, dt \tag{2.82}$$

due to the NP. The sign of δP may be positive or negative, i.e., the perturbation can either add to or subtract from the steady state power. Furthermore, in the adiabatic limit we are free to specify the shape of the perturbation, provided (1) it is completely overlapped by the steady state, (2) it introduces no drastic shape changes to the steady state, and (3) its symmetry matches that of the steady state. The precise shape chosen is discussed in the section on the OP to follow.

The important point to note from Figure 16 is that the presence of the NP disturbs the system over the first pass, such that the gain coefficient is no longer zero on the second pass, $\alpha(k + 1) = \alpha_p \neq 0$. From the adiabatic analysis
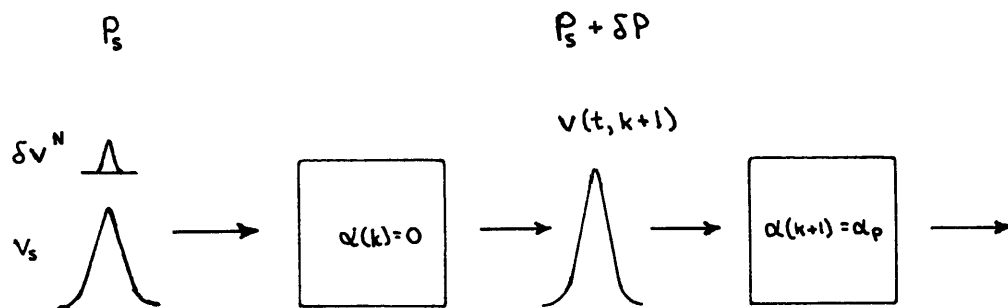
Figure 16: Schematic Picture of the NP Evolution

of section 2.4 we know that the evolution of the time average power is dictated by

$$P(n + 1) = [1 + 2\alpha(n)] \, P(n). \tag{2.83}$$

In the steady state the gain coefficient is zero so that $P(n + 1) = P(n) = P_s$. If, however, we perturb the steady state power

$$P_s \rightarrow P_s + \delta P(n)$$

the evolution of the perturbation is governed by

$$\delta P(n + 1) = [1 + 2\alpha_p] \, \delta P(n) \tag{2.84}$$

where

$$\alpha_p = \frac{d\alpha}{dP} \, P_s. \tag{2.85}$$

From (2.84) the stability criterion for the NP can be stated succinctly

$$\alpha_p \begin{cases} < 0 & \text{stable} \\ = 0 & \text{stability boundary} \\ > 0 & \text{unstable.} \end{cases} \tag{2.86}$$

In effect, we are testing the stability of the quasi-steady state solutions to (2.22) which are adjacent to the true steady state.

In order to determine the location of the stability boundary we now evaluate α_p. The gain coefficient of (2.74) is a function of both P and γ. Consequently, we can write (2.85) as

$$\alpha_p = \frac{d\alpha}{dP} P_s = \left[\frac{\partial \alpha}{\partial P} \bigg|_\gamma + \frac{\partial \alpha}{\partial \gamma} \bigg|_P \frac{d\gamma}{dP} \right] P_s.$$ (2.87)

The first term of (2.87) is due to the response of the system to the power change in the field, the second term is due to the shape change of the field. The derivative $d\gamma/dP$ can be evaluated by using the constant of motion (2.73) which results from the simultaneous satisfaction of the periodicity constraint (2.71) and the pulsewidth constraint (2.70), namely

$$\frac{P}{P_A} \frac{1}{K(\gamma) \, E(\gamma)} = \frac{m^2}{A}$$ (2.88)

where

$$A = \frac{q \, \omega_L^2 T_R^2}{8(1 + q)}$$ (2.89)

and we have included the multiplicity m.

From the steady state gain coefficient

$$\frac{\alpha}{\Delta\omega_c T_R} = g - (1 + q) + \frac{q}{2}\frac{P}{P_A}\frac{K}{E}(2 - \gamma^2)$$

(2.90)

and (2.88) we now determine

$$\frac{\alpha_p}{\Delta\omega_c T_R} = - \frac{g_o}{\left(1 + \frac{P_s}{P_L}\right)^2}\frac{P_s}{P_L} + \frac{K}{E}(2 - \gamma^2)\frac{q}{2}\frac{P_s}{P_A}$$

$$+ KE\frac{\frac{d}{d\gamma}\left[\frac{K}{E}(2 - \gamma^2)\right]}{\frac{d}{d\gamma}(KE)}\frac{q}{2}\frac{P_s}{P_A}.$$

(2.91)

The derivatives in the last term can be evaluated, but we leave them as is for the time being to facilitate the interpretation of the equation.

The first term of (2.91) is the stabilizing effect of gain saturation. The remaining terms result from the dispersion and the absorber saturation. Since KE and (K/E)(2 - γ^2) are monotonically increasing functions of γ, both of the last two terms are destabilizing. The condition for the

stability boundary, $\alpha_p = 0$, reduces to an equation in γ if we make use of (2.88) to substitute for P_s in terms of KE. Rather than attack the full equation from the start, however, it is helpful to solve it in two steps.

To begin with, we have noted that the last two terms of (2.91) are destabilizing. Consequently, if we neglect the last term in satisfying the condition $\alpha_p = 0$, we will obtain a necessary condition for the NP stability. In other words, we will determine at least part of the regime over which the solutions are unstable. In fact, the neglect of the last term gives us an extremely simple relationship for this first stability boundary which is directly related to the apices of the curves in section (2.35).

We know from (2.91) that

$$- \frac{g_o}{\left(1 + \dfrac{P_s}{P_L}\right)^2} + \frac{K}{E}(2 - \gamma^2)\frac{q}{2}\frac{P_L}{P_A} = 0, \tag{2.92}$$

whence the steady state power level P_1 at which the first stability boundary occurs is readily determined to be

$$\frac{P_1}{P_L} = \sqrt{\frac{2g_o}{q}\frac{P_A}{P_L}\frac{E}{K}\frac{1}{2 - \gamma^2}} - 1. \tag{2.93}$$

Solutions at power levels $P_s > P_l$ are unstable against the NP while those for which $P_s < P_l$ may or may not be stable depending upon the magnitude of the term in (2.91) which we have neglected.

It is of interest to determine where the first stability boundary occurs on our plots of P/P_L versus γ. From equation (2.35) we see that the power at the apices of the curves is given by

$$\frac{P_{sa}}{P_L} = \frac{1}{2} \left[\frac{2(1+q)}{q} \frac{P_A}{P_L} \frac{E}{K} \frac{1}{2 - \gamma^2} - 1 \right].$$
(2.94)

Substituting (2.94) in (2.93) we find that the power at the first stability boundary is related to that at the apex of a specific curve by

$$\frac{P_l}{P_L} = \sqrt{\frac{g_o}{1+q} \left(\frac{2P_{sa}}{P_L} + 1 \right)} - 1.$$
(2.95)

Note further that P_l can be related directly to the small signal gain and loss by making use of (2.38) to substitute for P_{sa}. At low power levels for which $g_o \simeq 1 + q$ and $2P_{sa}/P_L \ll 1$, the first stability boundary coincides with

the apex $P_1 \simeq P_{sa}$. The first stability boundary dictated by (2.95) is shown in Figures 4 and 5. The boundary is indistinguishable from the locus of apices. It is immediately apparent that the solution on the upper branch of the power curves are all unstable.

We are now prepared to consider the solution to the complete NP stability problem by finding the value of γ at which (2.91) changes sign. Evaluating the derivatives in (2.91) and using (2.88) to substitute for P_s, we obtain the condition for the stability boundary

$$- \frac{g_0}{\left[1 + \dfrac{8m^2(1 + q) P_A}{\omega_L^2 T_R^2 P_L} KE \right]^2}$$

$$+ \frac{qP_L}{P_A} \frac{K}{E} (2 - \gamma^2) \left[1 - \frac{2 \dfrac{E}{K} \dfrac{1}{2 - \gamma^2} - 1}{\dfrac{E}{K} \dfrac{1}{1 - \gamma^2} - 1} \right] = 0. \qquad (2.96)$$

Before proceeding with the solution to (2.96) one question comes to mind. Why have we used the power dictated by the periodicity constraint (2.88) to specify our steady state rather than the power determined by the eigenvalue relations

(2.35)? In reply we refer to Figure 17. The continuous lines are the loci of solutions dictated by the periodicity condition. The dotted lines are the loci of solutions dictated by the eigenvalue relation. Their intercepts define the steady state solution as discussed in section 2.2. In perturbing the steady state we have assumed from the start that the NP has the same symmetry properties as the steady state. In other words, the perturbation can not cause a timing shift of the steady state. Consequently, the perturbation does not change the periodicity of the solution. As indicated by the arrows in Figure 17, the perturbation can only shift the steady state along the locus of constant periodicity. In determining stability, therefore, we test the stability of the steady states defined by each point on the loci of constant periodicity.

An analytic solution for γ from (2.96) is not possible. However, the root γ_o of the equation is easily computed numerically. Steady state solutions found at values of γ less than the root γ_o are stable, while those at values of γ greater than γ_o are unstable. The stability boundaries are shown on the plots of inverse pulsewidth and time average power in Figures 18-20 for the system parameters of section 2.2. The boundaries are prescribed by evaluating the inverse pulsewidth and power at γ_o by equations (2.35) and (2.36).
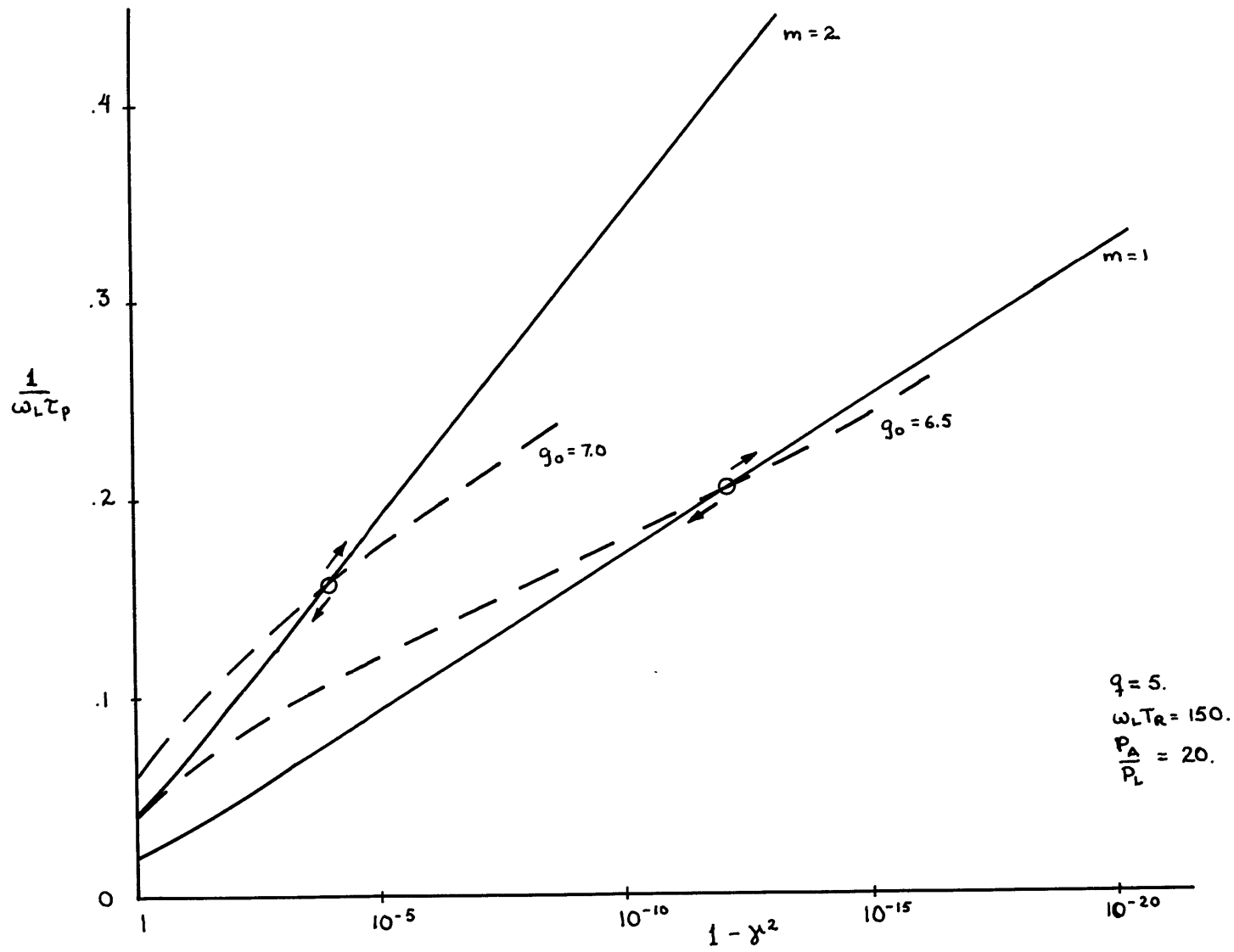
Figure 17:   Perturbation of the Steady State Operating Point
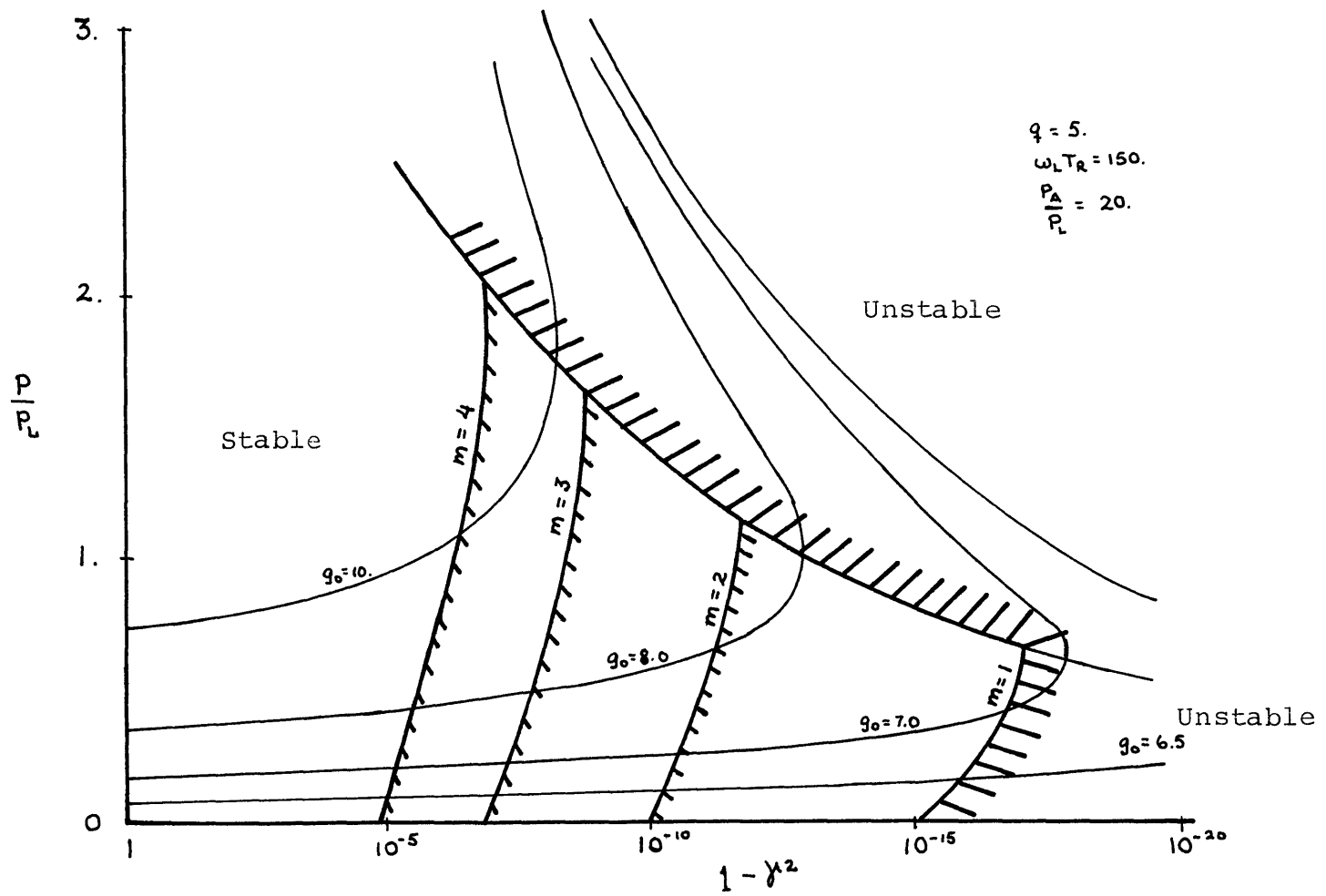
Figure 18: Stability Boundaries on Plot of Time Average Power
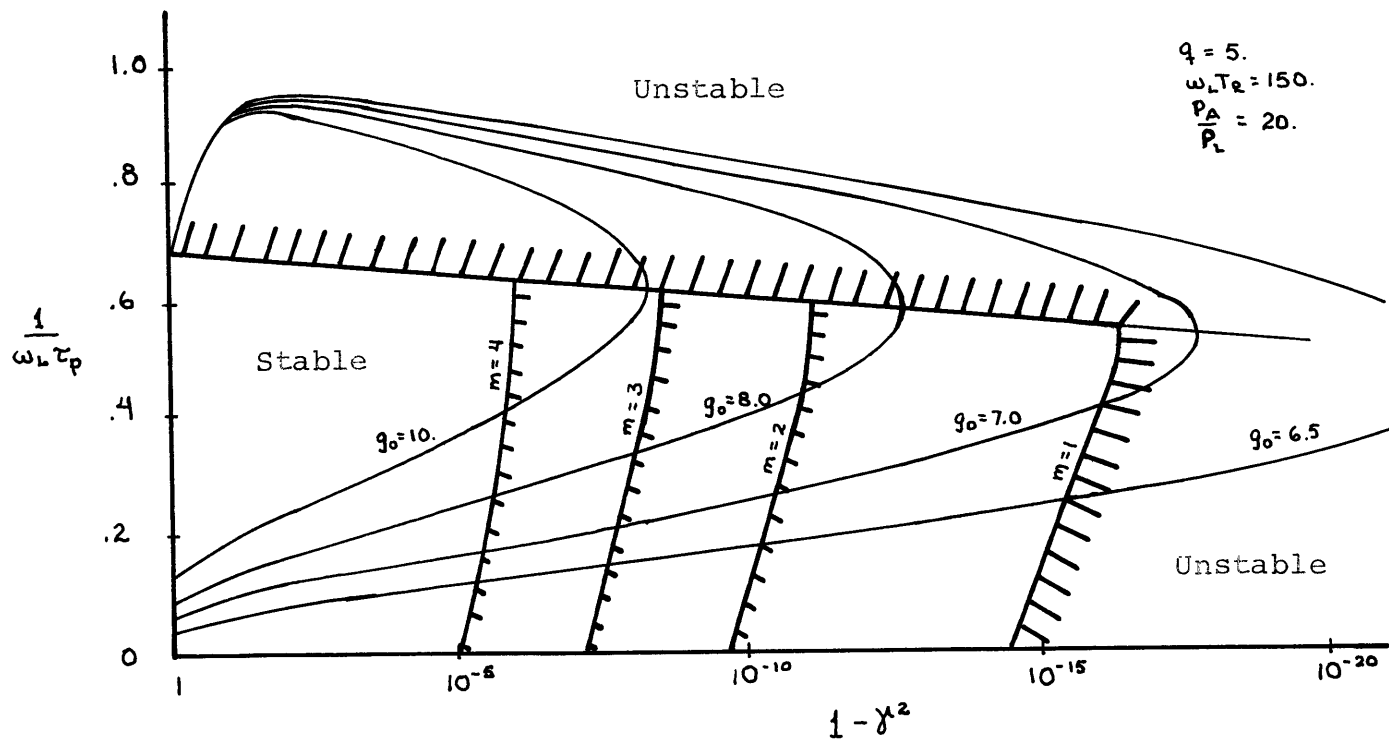
Figure 19:   Stability Boundaries on Plot of Inverse Pulsewidth
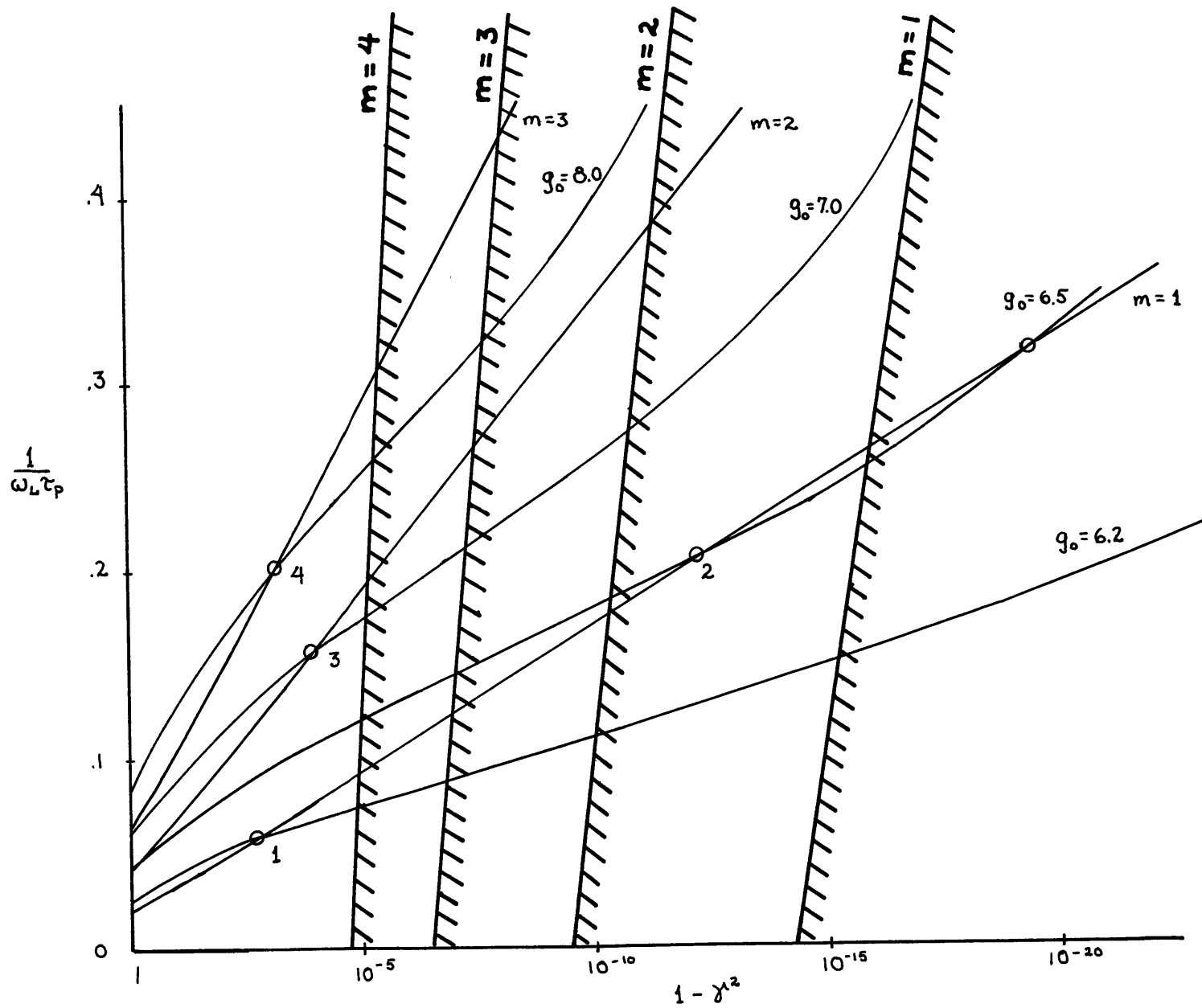
Figure 20: Detailed View of Stability Boundaries

Since each value of the multiplicity m has a different locus of constant periodicity each value of m defines its own stability boundary. For a given mulitplicity m, solutions found to the left of the boundary line labelled by m shown in Figures 18-20 are stable, while those found to the right are unstable. Note in Figure 20 that, in the case where two possible steady state operating points are found for m = 1, g_o = 6.5, the stability boundary passes between the two points! Thus, only the steady state corresponding to the smaller value of γ is stable. It appears, therefore, that for a given set of parameters a cw system must always settle on a unique steady state.

One qualifying remark must be made regarding our treatment of the stability of the multiple pulse solutions. We have treated the pulses within each transit as being independent of one another, whereas our requirement that the gain respond only to the time average power within a compete transit implies that they are coupled. If we adhere to our model of the gain response, then the multiple pulse solutions are clearly unstable to perturbations which add to one pulse and subtract from another within one transit, such that the gain remains invariant. If, on the other hand, we were to allow the gain to respond on a time scale comparable to or faster than T_R/m, such that stable m pulse solutions could be

found as prescribed above, then pulses of multiplicity m - 1

would become unstable since the relaxation of the gain medium

would allow net gain between pulses.

Thus, the precise description of a system in which both

stable single pulse and stable multiple-pulse solutions are

possible would require that we enlarge upon our simple two

level, single relaxation time model of the laser medium to

include at least two relaxation times. In fact, dye lasers,

on which both stable single and stable multiple pulse opera-

tion has been observed,[73] are characterized by many relaxa-

tion times which can be both faster and slower than the cavity

transit time.

Our treatment of stability against the NP perturbation

is now complete. To ensure stability we require $\alpha_p < 0$,

and we have mapped out regimes in parameter space where the

inequality holds. Taken by itself, however, the requirement

that the system be stable against the NP perturbation is a

necessary but not a sufficient condition for stability. We

have treated only a specific type of perturbation. In order

to generalize the analysis to include all possible perturba-

tions, we now turn our attention to the OP.

2.5.2 Orthogonal Perturbations

We assume at this point that the steady state operating point is in a regime where it is stable against the NP, i.e., $\alpha_p < 0$, and ask ourselves whether it is possible for the OP to cause instability. Since the OP is defined by

$$\delta P = 2 \oint v_s \, \delta v^O \, dt = 0$$

there is no change in the gain due to the perturbation. In the absence of gain saturation the modelocked system in the steady state does not "feel" the perturbation, its time average net gain remains zero. On the other hand, the OP feels the system. The shaping and growth or decay of the OP is dictated by the steady state it perturbs.

The evolution of the OP δv^O of the modelocking steady state is governed by the perturbed equation

$$\frac{1}{B} \frac{\partial \delta v^O}{\partial n} = \left[-(2 - \gamma^2) + \tau_p^2 \frac{\partial^2}{\partial t^2} + 6 \, dn^2 \left(\frac{t}{\tau_p} , \gamma \right) \right] \delta v^O \qquad (2.97)$$

where

$$B \equiv \frac{4m^2 (1 + q) \, \Delta\omega_c T_R \, K^2 (\gamma)}{\omega_L^2 T_R^2} \quad .$$

The right hand side of the equation has the form of a

Schrödinger equation whose wavefunctions $\{\phi_i(t), \phi(t, \lambda)\}$

comprise a complete orthonormal set, where $i = 1, 2, \ldots$

is a discrete index and λ is continuous.

The perturbation δv^O can be expanded in terms of the

wavefunctions

$$\delta v^O(n, t) = \sum_i a_i(n) \phi_i(t) + \int d\lambda \, a(n, \lambda) \phi(t, \lambda). \qquad (2.98)$$

Thus, the growth or decay of each component of the OP on

one pass is dictated by the sign of the eigenvalues $\{\lambda_i, \lambda\}$

associated with each wavefunction λ. In treating the evolu-

tion of the perturbation over several passes, however, we

must be careful. Since the wavefunctions ϕ_i are not neces-

sarily orthogonal to the steady state waveform v_s and the

coefficients a_i experience different growth or decay rates

depending upon the eigenvalues, the perturbation which is

orthogonal on the nth pass is no longer orthogonal on pass

n + 1. In other words, the perturbation which is initially

orthogonal provides coupling to the NP over successive

passes through the system. On each pass the total perturba-

tion can be split into an OP plus an NP

$$\delta v_O{}^O(n, t) \to \delta v^O(n + 1, t) + \delta v^C(n + 1, t) \qquad (2.99)$$

where the superscript c denotes the fact that the NP is
due to coupling.

By resorting to the schematic picture developed in sec-
tion 2.4 we can depict the evolution of the OP over several
passes as shown in Figure 21. Introduced at transit k, the
OP has no initial effect on the time average power. By
k + 1, however, some of its energy has been coupled into an
NP. The effect of the NP is only felt after another transit.
On each pass the OP is that which remains after the NP has
been subtracted out.

The change in the time average power due to the coupling
from the OP is

$$
\delta P_c = \oint \delta v^c \, v_s \, dt = \sum_i a_i(n + 1) \oint dt \, \phi_i(t) \, v_s(t, \, n)
$$

$$
+ \int d\lambda \, a(n + 1, \, \lambda) \oint dt \, \phi(t, \, \lambda) \, v_s(t, \, n) \qquad (2.100)
$$

where the new coefficients at (n + 1) are determined by

$$
a_i(n + 1) = a_i(n) \, e^{B\lambda_i} \qquad (2.101)
$$

$$
a(n + 1, \, \lambda) = a(n, \, \lambda) \, e^{B\lambda}
$$

Depending upon the relative signs and magnitudes of the various
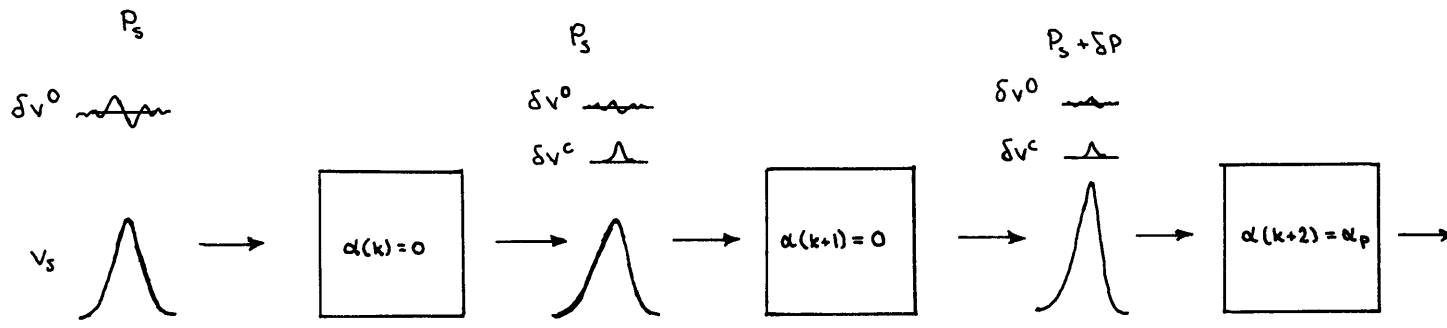
Figure 21: Schematic Picture of the OP Evolution

terms, the change in the time average power due to coupling can be positive, negative or zero. Whether or not the system is stable in the regime $\alpha_p < 0$ as defined in the previous section depends on the stability of the OP remaining after the coupling to the NP has been subtracted.

Thus far we have outlined a general approach to the stability of the OP. Let us now focus our attention on the specific problem at hand.

The bound state eigenfunctions and eigenvalues of the operator on the right hand side of (2.97) are

$$\phi_o = \sqrt{\frac{3\gamma^2}{2[(1 + \gamma^2)E - (1 - \gamma^2)K]}} \; cnx \; dnx, \quad \lambda_o = 3 \qquad (2.102)$$

$$\phi_1 = \sqrt{\frac{3\gamma^3}{2[(2\gamma^2 - 1)E + (1 - \gamma^2)K]}} \; snx \; dnx, \quad \lambda_1 = 3(1 - \gamma^2) \quad (2.103)$$

$$\phi_2 = \sqrt{\frac{3\gamma^4}{2[(2 - \gamma^2)E - 2(1 - \gamma^2)K]}} \; snx \; cnx, \quad \lambda_2 = 0 \qquad (2.104)$$

where $x = t/\tau_p$. The eigenvalues of the continuum states are all negative, i.e. $\lambda < 0$. The overlap of the bound state wavefunctions of the perturbed equation with the steady state

can be computed to be

$$\oint \phi_0 \, v_s \, dx = v_0 \, \frac{N_0(\gamma)}{K(\gamma)} \left[\frac{1}{\gamma} \sin^{-1} \gamma + 1 - \gamma^2 \right] \tag{2.105}$$

$$\oint \phi_1 \, v_s \, dx = \oint \phi_2 \, v_s \, dx = 0 \tag{2.106}$$

where $N_0(\gamma)$ is the normalization of ϕ_0 given in (2.102).
Thus, only one of the discrete wavefunctions overlaps with
the steady state.

Two points regarding the stability of the OP are im-
mediately apparent. First, as found by Haus,[24] the solution
is astable ($\lambda_2 = 0$) with respect to the timing perturbation
ϕ_2, so-called because it is the derivative of the steady state.
Second, the solution is unstable with respect to perturbations
of the form ϕ_1. As given by (2.103) the growth of the per-
turbation ϕ_1 over each pass is

$$a_1(n + 1) = a_1(n) \, e^{\lambda_1 B} \tag{2.107}$$

where

$$\lambda_1 B = \frac{12 m^2 (1 + q) \, \Delta\omega_c T_R}{\omega_L^2 \, T_R^2} \, K^2(\gamma)(1 - \gamma^2) \tag{2.108}$$

Since $1 - \gamma^2$ approaches zero faster than $K^2(\gamma)$ approaches infinity it is clear that $\lambda_1 B$ is zero in the limit $\gamma \to 1$ where ϕ_1 becomes indistinguishable from ϕ_2. To give a feeling for how rapidly $\lambda_1 B$ approaches zero we know that at $(1 - \gamma^2) = 10^{-2}$ the product $(1 - \gamma^2) K^2(\gamma) = 3.7 \times 10^{-2}$. For a sizeable linewidth transit time product, $\omega_L T_R$, therefore, the instability of the ϕ_1 component is very weak even for poorly defined pulses.

The behavior of the $\phi_o(t)$ and continuum components $\phi(t, \lambda)$ of the OP is not as readily determined. Indeed, the ϕ_o component appears to be unstable for all values of γ. Our only hope for proving stability is that the coupling to the NP is sufficient to offset the growth of the ϕ_o component on each pass. We recall at this point that we have not yet completely specified the form of the NP. Since the stability of the NP is solely dependent upon stability against changes in the time average power, we are free to choose the shape of the NP due to coupling, δv^c, provided the relationship

$$\delta P_c = \oint \delta v^c \, v_s \, dt \qquad (2.109)$$

is satisfied. The obvious choice to make to simplify the analysis is

$$\delta v^C = b_o(n) \; \phi_o(t) \tag{2.110}$$

where

$$b_o(n) = \frac{\delta P_c(n)}{\oint \phi_o \, v_s \, dt} \; ,$$

so that coupling occurs only from the lowest wavefunction, ϕ_o, of the perturbed well. Note that in setting the NP to be of the form of $\phi_o(t) = N_o \; cnx \; dnx$ we satisfy the three constraints required of the NP in the analysis of the previous section: That it (1) be completely overlapped by the steady state, (2) introduce no drastic shape changes to the steady state and (3) have the same symmetry as the steady state.

After one transit the OP can then be written as

$$\delta v^O(t, \, n + 1) = a_o(n) \left[e^{B\lambda_o} - \frac{b_o(n)}{a_o(n)} \right] \phi_o(t)$$

$$+ \; a_1(n) \; e^{B\lambda_1} \; \phi_1(t) \; + \; a_2(n) \; \phi_2(t)$$

$$+ \int d\lambda \; e^{B\lambda} \; a(n, \, \lambda) \; \phi(t, \, \lambda) . \tag{2.112}$$

The stability of the ϕ_1 and ϕ_2 components has already been discussed. Since the continuum states are all decaying ($\lambda < 0$), the stability of the remaining terms reduces to the criterion that the ϕ_0 component be stable:

$$0 < e^{B\lambda_0} - \frac{b_0}{a_0} < 1. \tag{2.113}$$

The proof that (2.113) holds is straightforward. From our requirement that the total OP be orthogonal to the steady state we find that the coefficients of the lowest bound state and the continuum states are related by the conditions

Pass n: $a_0(n) \oint dt\ \phi_0(t)\ v_s(t,\ n) + \int d\lambda\ a(n,\ \lambda)$

$$\int dt\ \phi(t,\ \lambda)\ v_s(t,\ n) = 0 \tag{2.114}$$

Pass n + 1: $a_0(n) \left[e^{B\lambda_0} - \frac{b_0(n)}{a_0(n)} \right] \oint dt\ \phi_0(t)\ v_s(t,\ n)$

$$+ \int d\lambda\ e^{B\lambda}\ a(n,\ \lambda) \oint dt\ \phi(t,\ \lambda)\ v_s(t,\ n) = 0$$

In other words, the lowest bound state $\phi_0(t)$ and the con-

tinuum states $\phi(t, \lambda)$ must counterbalance each other to ensure zero overlap with the steady state v_s at each pass through the system. The contribution of the continuum states to the overlap ultimately must decay from one pass to the next due to the fact that their eigenvalues are negative. Consequently, the ϕ_o contribution to the overlap ultimately must decay in order to maintain the orthogonality of the perturbation (2.112). We use the word "ultimately" because the evolution of the continuum states, being governed by a continuous sum or integral of decaying expontentials, can experience initial growth, but must decay in the long run. On the pass at which the sum of the continuum states begins to decay the OP stability condition (2.113) is satisfied.

2.5.3   The General Perturbation

In review of the stability analyses of the   NP   and

OP , we see that we have expanded the general perturbation

in the wavefunctions of the perturbed equation excluding

gain saturation (2.97)

$$\delta v(t, \; n) = a_o{}^N(n) \; \phi_o(t) \; + \; a_o{}^O(n) \; \phi_o(t) \; + \; a_1(n) \; \phi_1(t)$$

$$+ \; a_2(n) \; \phi_2(t) \; + \; \int d\lambda \; a(n, \; \lambda) \; \phi(t, \; \lambda)$$

$$\underbrace{\phantom{a_o{}^N(n) \; \phi_o(t)}}_{\delta v^N(t, \; n)} \qquad \underbrace{}_{\delta v^O(t, \; n).} \qquad (2.115)$$

By doing so we assume a specific form of the   NP.   The evolu-

tion of the   NP   obeys the perturbed equation which includes

gain saturation and to which ϕ_o is clearly not a wavefunc-

tion.   Strictly speaking, therefore, the gain saturation term

must introduce coupling from the   NP   to the   OP.   However,

our assumption that changes which involve gain variation can

be treated by averaging over a transit time enables us to

argue that the purely   NP   merely causes a shift from the

steady state to an adjacent quasi-steady state, whose stability

is in question.   Since we consider only the response of the

system to the change in time average power, δP,   caused by

the NP, the precise shape of the NP is not important and the coupling from the NP to the OP can be neglected.

Thus, the only coupling treated is from the OP to the NP as discussed in section 2.5.2. We conclude that all components of the OP except ϕ_1 and ϕ_2 are always stabilized by coupling to the NP. The ϕ_1 and ϕ_2 components are degenerate and astable in the limit of well separated pulses. The condition for NP stability, $\alpha_p < 0$, is not only necessary but is sufficient to prove stability against all perturbations.

2.5.4 Comparison of Our Results to Those of Haus

The results of our analysis of the steady state mode-locking solutions and their stability differ from those of Haus.[24] The difference stems from our explicit inclusion of the periodicity constraint of the system and our use of the adiabatic gain coefficient in determining stability.

Although the steady state solution curves we obtain appear similar to Haus's curves, we should note that the abscissa in our case is $1 - \gamma^2$, while that used by Haus is the parameter $qK/(1 + q)$ (not to be confused with the complete elliptic integral of the first kind), where he defines

$$K \equiv \frac{1}{4} \frac{P_L}{P_A} \omega_L T_R.$$

Buried in K is the fact that Haus has assumed a secant hyperbolic pulse shape and accounts for the periodicity in determining the power in the pulse. By explicitly including the effect of the periodicity in determining the pulse shape as well as the pulse power, we have obtained a more accurate description of the steady state. Furthermore, our approach enables the separate consideration of the parameters P_A/P_L and $\omega_L T_R$ in determining the steady state operating point.

As noted in the previous section, the assumption of

adiabatic evolution, which underlies our stability analysis, obviates the infinite coupled mode analysis posed by Haus by allowing us to ignore coupling from the NP to the OP. The stability analysis then reduces to determining whether the adiabatic gain coefficient becomes positive or negative, or remains zero when perturbed from its steady state value of zero. We automatically account for the shape change of the perturbed solution by using the constant of motion (2.88).

2.5.5 Stability of the Quasi-Steady State

The stability problem takes on a slightly different complexion when we discuss the quasi-steady states of a transient system. The quasi-steady state is inherently unstable against the NP, so it is necessary for us to be more precise in defining what we mean by a "stability" analysis. What we wish to determine is the validity of the analysis. In other words, does the evolution of the field proceed as a succession of quasi-steady state pulses, or can instabilities which cause a break-up of the pulse solutions grow faster than the solution itself?

Since we accept the instability against the NP, the stabilizing influence of gain saturation is not essential to our argument. The quasi-steady state is evolving according to the dictates of the time average net gain α. We have already treated the question of stability by expanding the perturbation in the eigenfunctions of (2.97). The fastest growing component, and, in fact, the only growing component in the limit $\gamma \to 1$, is $\phi_o(t)$. But $\phi_o(t)$ corresponds to a sharpening or broadening of the solution which occurs in making the transition from one quasi-staady state to the next. No break-up of the pulse solution is possible. Thus, the adiabatic assumption is justified.

The fact that gain saturation need not play an important

role in transient systems is the fundamental reason why transient passively modelocked systems are easier to find than cw passively modelocked systems. In the cw system a comparitively "soft" gain medium is necessary to ensure the stability of the steady state over many transits. In fact, the condition $P_A/P_L >> 1$ must be satisfied to find steady state solutions. Since the gain only lasts for a finite time in the transient system, long term stability is not an issue. The saturation power of the laser medium need not be small. Stability becomes a question of relative growth--what waveform grows the fastest and how much does it grow while the gain lasts? We have shown that the fastest growing waveform during the buildup is that of the quasi-steady state of a perturbation which sharpens it. Growth can occur until the assumption that we operate in a regime where the absorber is weakly saturated breaks down. The topic of strong absorber saturation is taken up in section 2.7.

2.6 Generalization of the Modelocking Media

The constraints applied to the amplifying and absorbing media in section 2.1 are restrictive. In particular, we limited our analysis to a two level gain medium whose relaxation time was slow compared to the cavity transit time and a two level absorbing medium whose relaxation time was fast compared to the field variation within one transit. In general, the amplifying and absorber media are multiple level systems which may have many characteristic relaxation times and saturation powers. Here we show how the analysis can be extended to describe these more complex systems.

The most obvious extension of the theory is to cases where the various relaxation times of the two media can be lumped into two categories--those which are slow compared to T_R and those which are fast compared to the time variation of $v(t)$. In this case each medium can be characterized by a fast and a slow saturation power. The response of the gain medium becomes

$$g\left(t, \frac{d}{dt}, n\right) v(t, n) = g(n) \left[1 - \frac{|v(t, n)|^2}{P_{LF}} + \frac{1}{\omega_L^2} \frac{\partial^2}{\partial t^2}\right] v(t, n)$$

$$(2.116)$$

where

$$g(n) = \frac{g_O(n)}{1 + \dfrac{P(n)}{P_{LS}}}$$

while that of the absorber becomes

$$q(t, n)\, v(t, n) = q(n) \left[1 - \frac{|v(t, n)|^2}{P_{AF}} \right] v(t, n) \qquad (2.117)$$

where

$$q(n) = \frac{g_O}{1 + \dfrac{P(n)}{P_{AS}}}$$

and the subscripts F and S refer to fast and slow.

The case where the laser medium has a fast relaxation time has been discussed by Haus.[24] The decrease in the gain in response to the instantaneous field works against pulse formation we must require that

$$\frac{q(n)}{P_{AF}} > \frac{g(n)}{P_{LF}} \qquad (2.118)$$

for modelocking to be possible. In other words, the fast response of the absorber must overpower the fast response of the laser medium.

The slow response of the absorber has interesting consequences in transient systems. If the absorber loading decreases with increasing time average power in the laser the pulses do not necessarily narrow as shown in Figures 14 and 15 and may, in fact, broaden. Thus, the bleaching of the absorber on a slow time scale provides a simple explanation for the observation in Nd:glass systems that the shortest pulses are at the beginning of the modelocked train.[46]

In order to ensure pulse shortening during the buildup the criterion

$$P_{AS} > P_{LS} \tag{2.119}$$

must be met, so that the absorber loading does not decrease appreciably in comparison to the saturated gain.

The treatment of media which have relaxation times which are less than the cavity transit time, but comparable to or greater than the time variation of $v(t)$ has been carried out elsewhere and will not be considered here. The case in which both the gain medium and absorber fall in this category has been treated in detail by Haus.[25] The case where only the absorber relaxation time is varied is analyzed by Hagelstein and Ausschnitt.[42] Thus, the theory has been shown to be applicable to the whole range of absorbing and

amplifying media which can be described phenomenologically
by relaxation times and saturation powers.

2.7 Strong Saturation of the Absorber

The modelocking equation derived by Haus and used in the previous sections to describe the transient evolution of passive modelocking is limited to the case of weak absorber saturation where the expansion (2.21) is valid. We now address ourselves to the general case where the absorber can be strongly saturated and the full expression for the absorber response must be used in (2.17). The regime in which short pulse solutions to the new equation exist is limited. It is clear that in the case where the power is sufficient to bleach the absorber fully pulse solutions to the modelocking equation are not possible, and the laser will run single mode.

The steady state modelocking equation for the case of strong absorber saturation becomes

$$\left[1 + \frac{q}{1 + \dfrac{|v(t)|^2}{P_A}} - g - \frac{1 + q}{\omega_L^2} \frac{\partial^2}{\partial t^2} \right] v(t) = 0 \qquad (2.120)$$

which is the equation of motion of a particle in the potential well

$$U(v) = - q\, P_A \ln \left[1 + \frac{|v|^2}{P_A} \right] + (g - 1)|v|^2 - C.$$

Expanding the logarithmic term we obtain

$$U(v) = - q|v|^2 + \frac{q|v|^4}{2P_A} - q\frac{|v|^6}{3P_A^2} + \ldots + (g - 1)|v|^2 - C.$$

<div align="right">(2.121)</div>

We recognize that to second order in the expansion we obtain the potential for the case of weak saturation (2.26). Since the logarithm is monotonically decreasing we see that the "well" is formed by the fact that the positive excess gain term $(g - 1)|v|^2$ offsets the initial decrease of the negative first order loss term $q\,v^2$. Ultimately, however, as $|v|^2/P_A$ increases, the third order term of the logarithm, $q|v|^6/3P_A^2$, dominates and the potential decreases. The point at which the third order term becomes dominant determines the existence of solitary pulse solutions. Since modelocking solutions are confined to the region of the "well" we need only carry out the expansion of the absorber loss to third order as shown in (2.121). Higher order absorber loss terms contribute to the potential only in the region of large $|v|^2/P_A$ outside the well and hence, are not of interest.

Thus, we are able to confine our attention to the equation

$$\left[1 + q - g - \frac{q|v|^2}{P_A} + \frac{q|v|^4}{P_A^{\,2}} - \frac{1 + q}{\omega_L^{\,2} \tau_p^{\,2}} \frac{\partial^2}{\partial t^2}\right] v = 0 \qquad (2.122)$$

in our discussion of strong absorber saturation. As in the case of weak absorber saturation the solitary pulse solution to (2.122) corresponds to the case of $C = 0$ in (2.121). The solitary pulse solution is given by

$$v(t) = \frac{v_o}{\sqrt{(1 - \beta^2) \cosh^2\left(\frac{t}{\tau_p}\right) + \beta^2}} . \qquad (2.123)$$

By direct substitution of (2.123) in (2.122) the pulse parameters v_o, τ_p and β are determined by the eigenvalue relations

$$1 + q - g = \frac{1 + q}{\omega_L^{\,2} \tau_p^{\,2}} \qquad (2.124)$$

$$\frac{q|v_o|^2}{P_A} = \frac{2(1 + q)}{\omega_L^{\,2} \tau_p^{\,2}} (\beta^2 + 1) \qquad (2.125)$$

$$\frac{q|v_o|^4}{P_A^{\,2}} = \frac{3(1 + q)\beta^2}{\omega_L^{\,2} \tau_p^{\,2}} . \qquad (2.126)$$

Solving for the peak amplitude and the parameter β we obtain

$$|v_o|^2 = \frac{3}{4} P_A \left[1 - \sqrt{1 - \frac{16}{3} \frac{(1 + q - g)}{q}} \right] \qquad (2.127)$$

$$\beta = \sqrt{\frac{3}{16} \frac{q}{(1 + q - g)}} \left[1 - \sqrt{1 - \frac{16}{3} \frac{(1 + q - g)}{q}} \right] . $$

$$(2.128)$$

To discuss the solution we identify three conditions of interest defined by

$$\left.
\begin{array}{ll}
1. & 1 \ll \\[2ex]
2. & 1 < \\[2ex]
3. & 1 =
\end{array}
\right\} \quad \frac{3q}{16(1 + q - g)} . \qquad (2.129)$$

For condition 1. the time average power is such that $\beta \simeq 0$ and the solution is seen to reduce to the secant hyperbolic pulse found in the case of weak absorber saturation. In the power regime where condition 2. holds assumes a finite value and (2.122) shows that the pulse

broadens at the peak while its tails remain unaffected. As condition 3. in approached $\beta \to 1$ and the solitary pulse solution ceases to exist. However, condition 3. does not preclude the existence of periodic solutions or, for that matter, the single mode solution. The condition for which even periodic pulse solutions are not possible is obtained from the general solution to the strong saturation case discussed below.

In general, the constant C is nonzero and the solution to (2.122) is periodic with two possible time dependences (see Appendix A):

$$S: \quad v(t) = v_o \sqrt{\frac{1 - \gamma^2 \, sn^2 \, (t/\tau_p, \, \gamma)}{1 - \beta^2 \, sn^2 \, (t/\tau_p, \, \gamma)}} \qquad 0 < \beta < \gamma < 1$$

$$(2.130a)$$

$$AS: \quad v(t) = v_o \; \frac{cn \, (t/\tau_p, \, 1/\gamma)}{\sqrt{1 - (\beta/\gamma)^2 \, sn^2 \, (\, t/\tau_p, \, 1/\gamma)}} \qquad 1 < \gamma$$

$$0 < \beta < \gamma.$$

$$(2.130b)$$

As in the weak saturation case we shall concentrate our attention on the regime $0 < \gamma < 1$. The constants γ and β

are related to C by the roots of the potential function $U(v)$. Since the potential is cubic in v^2 there are three roots $v_-^2 \leq v_o^2 \leq v_+^2$ which we define as shown in Figure 22. In the region of interest the roots are pure real. The solution oscillates in the well between v_-^2 and v_o^2. In terms of the roots, γ and β are given by

$$\gamma^2 = \left| \frac{v_o^2 - v_-^2}{v_+^2 - v_-^2} \right| \frac{v_+^2}{v_o^2} \tag{2.131}$$

$$\beta^2 = \frac{v_o^2}{v_+^2} \gamma^2. \tag{2.132}$$

Substitution of (2.130a) in (2.122) gives the eigenvalue relations

$$1 + q - g = \frac{(1 + q)}{\omega_L^2 \tau_p^2} G_{\gamma\beta} \tag{2.133}$$

$$\frac{q|v_o|^2}{2P_A} = \frac{(1 + q)}{\omega_L^2 \tau_p^2} G_{\beta\gamma} \tag{2.134}$$

$$\frac{q|v_o|^4}{P_A^2} = \frac{3(1 + q)}{\omega_L^2 \tau_p^2} \frac{\beta^2(1 - \beta^2)}{(\gamma^2 - \beta^2)} \tag{2.135}$$
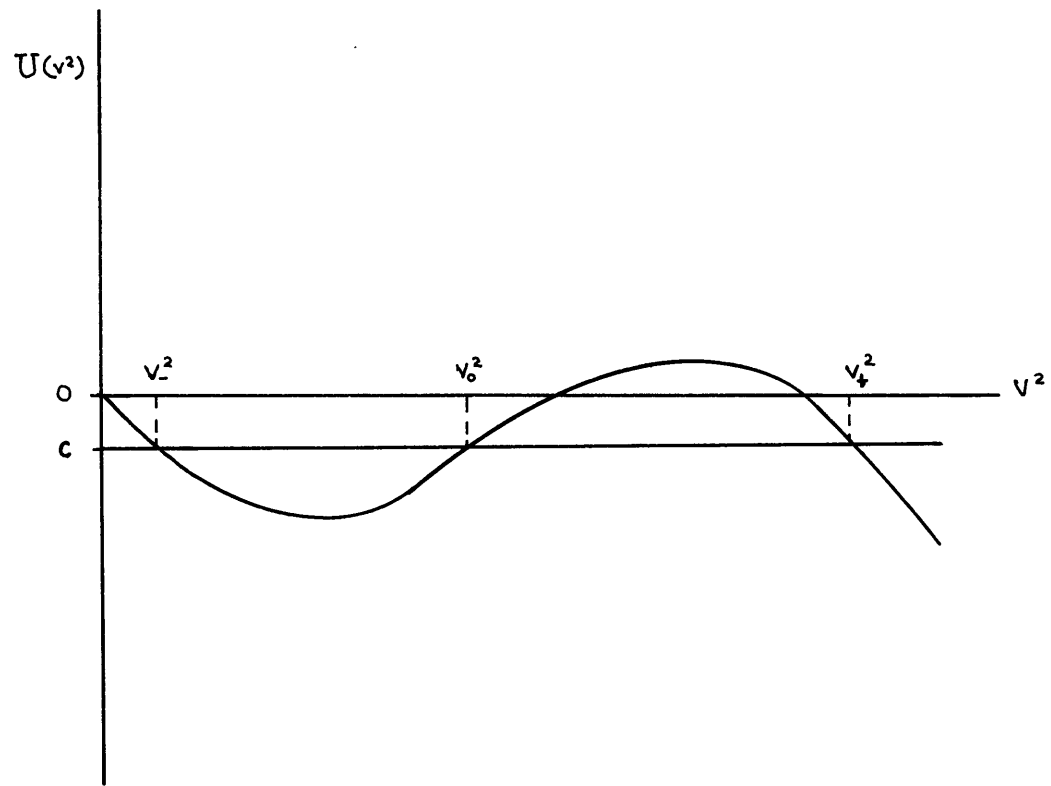
Figure 22: Potential Well of Strong Saturation Equation

where $G_{\gamma\beta}$ and $G_{\beta\gamma}$ are defined in Appendix A. In the limit $\beta \to 0$ the equations reduce to those of the weak saturation case. In the limit $\gamma \to 1$ the equations reduce to those of the strong saturation solitary pulse solution.

The requirement that the periodicity of the solution equal the transit time T_R sets the same constraint as in the weak saturation limit, namely

$$2m \, K(\gamma) = \frac{T_R}{\tau_p} . \tag{2.136}$$

Furthermore, the time average power in a single transit is determined by substituting (2.130a) in (2.5). The power is expressible in terms of Jacobi's Zeta-function.[43]

$$P = |v_o|^2 \left\{ 1 - \frac{1}{\beta} \sqrt{\frac{\gamma^2 - \beta^2}{1 - \beta^2}} \, Z(\phi, \gamma) \right\} \tag{2.137}$$

where $\phi = \sin^{-1}(\beta/\gamma)$.

Although the algebra is more complex, the steady state operating point of the system for a given set of system parameters can be found in the same manner as for the weak saturation case. We have one additional unknown, β, to determine and one additional eigenvalue equation (2.135). The actual computation of the operating point will not be carried out

here since the results differ from the weak saturation case only in that the pulses obtained flatten at the top when their peak power becomes a significant fraction of the absorber saturation power $(|v_o|^2 \lesssim P_A)$.

One further consequence of the strong saturation analysis is that the power range for which modelocking solutions can be obtained is restricted. The criterion for perturbation growth on the SM field (2.62) becomes

$$\frac{(\alpha_m - \alpha_o)}{\Delta\omega_c T_R} = \frac{2q}{P_A} v_o^2 - \frac{4q}{P_A^2} v_o^4 - \frac{1 + q}{\omega_L^2} \left(m \frac{2\pi}{T_R} \right)^2 > 0. \qquad (2.138)$$

The value of the threshold power $P_m(\ell)$ is then given by

$$\frac{P_m(\ell)}{P_A} = \frac{1}{2} \left[1 \pm \sqrt{1 - \frac{2(1 + q)(2\pi m)^2}{q \, \omega_L^2 T_R^2}} \right]. \qquad (2.139)$$

The smaller value of P_1 is the threshold at which the SM field goes unstable. The higher value of P_1 is the point at which the SM field becomes stable again due to the ultimate dominance of the $|v|^6/P_A^2$ term in the potential. We conclude, therefore, that for the purposes of modelocking the

absorber is fully bleached when $P = P_1^+ \simeq P_A$ and the system reverts to stable SM operation. The condition (2.47) determined earlier for the existence of modelocking solutions is usually more restrictive except in cases of small absorber loading. For typical modelocking parameters, namely $q \gg 1$ and $P_A \gg P_L$, (2.47) requires $P \leq P_A/2$.

Note further that each set of values of P_m determines the range for the existence of the solution of multiplicity m per transit time. Thus, the maximum number of pulses per period allowed for a given modelocked system is determined by

$$m = \sqrt{\frac{q}{1+q}} \; \frac{\omega_L T_R}{2\pi} \qquad \text{(smaller integer)} \qquad (2.140)$$

for which $P \simeq P_A/2$. A power regime $P_A/2 \lesssim P \lesssim P_A$ exists for which both single mode operation and modelocked operation are unstable. We expect the laser output in this regime to be characterized by irregular spiking.

The main conclusion to be drawn from the strong saturation analysis is that it plays little or no role in steady state modelocked systems. The constraints placed on the operating conditions by the inclusion of the strong saturation effect are usually less restrictive than the stability and existence criteria already established for modelocking solutions. In other words, stable steady state modelocking solutions are

mostly found in regimes where the weak saturation approximation
(2.21) is valid.

As noted in section 2.5.4, however, the existence and
stability criteria for steady state solutions do not apply
to the quasi-steady state. The quasi-steady state solutions
of a transient system are, by definition, unstable. Thus, the
effects of strong saturation, which are not readily observable
in cw systems, should be seen in transient systems.

2.8   The Antisymmetric Pulse

In section 2.2 we obtained two steady state solutions to the modelocking equation. However, in our subsequent treatment of the transient evolution we ignored the anti-symmetric (AS) pulse solution (2.27b). We return here to consider its significance in greater detail.

The existence of the AS solution is a consequence of the discrete mode spectrum of the cavity field or, in other words, the periodicity of the laser cavity. In the limit of a continuous spectrum both periodic solutions (2.27a) and (2.27b) approach the solitary secant hyperbolic pulse. The fixed periodicity of the cavity, however, lifts the degeneracy of the two solutions. Since the AS pulse train consists of pulses of alternating phase, an even number of pulses must be fitted into the transit time, whereas all multiples of the S pulse solution are allowed.

The contrast between the S and AS solutions becomes particularly evident in the analysis of the transient buildup. As noted in section 2.2 it is clear that the AS solution cannot buildup from a single mode field in the cavity. Thus, its threshold condition must differ from that of the S so-lution. This is reasonable since the discrete nature of the field spectrum is most strongly felt near threshold.

The discrete mode spectrum allows, in fact, two possible initial conditions for the buildup. In the case where one cavity mode is closer to line center than all the others the cavity field must evolve to SM operation prior to modelocking. However, in the special case where two cavity modes are equidistant from the laser line center the field must evolve to double mode (DM) operation. The field prior to modelocking becomes

$$v(t, n) = v_O(n) \cos \left[\frac{2\pi}{T_R} t \right] \tag{2.141}$$

the sinusoidal beating of the two cavity modes nearest line center.

The AS modelocking threshold is determined by the value of $v_O(n)$ for which the cavity field makes the transition from the sinusoidal beat to the first AS modelocking solution of (2.23), at which point the waveform in the cavity becomes

$$v(t, n) = v_O(\ell) \text{ cn } (t/ \tau_p, 1/\sqrt{2}) . \tag{2.142}$$

As in the S case we can solve for $v_O(\ell)$ by making use of the eigenvalue relations and periodicity condition (2.29b) - (2.40b), i.e.

$$\frac{T_R}{\tau_p(\ell)} = \omega_L T_R \sqrt{\frac{q}{P_A(1 + q)}} \; v_o(\ell) = 4K(1/\sqrt{2}).$$ (2.143)

The time average power in the DM field must be

$$\frac{P_{DM}(\ell)}{P_A} = \frac{8K^2 \; (1/\sqrt{2})(1 + q)}{\omega_L T_R \; q}$$ (2.144)

before modelocking initiates.

The subsequent evolution of the AS solution from the modelocking threshold to well separated pulses can be treated in a manner directly analogous to the S solution. The adiabatic gain coefficient becomes

$$\frac{\alpha_{AS}}{\Delta\omega_c T_R} = g - (1 + q) + \frac{q}{2}(2 - \gamma^2) \left[\frac{K(1/\gamma)}{\gamma^2 \; E(1/\gamma) + K(1/\gamma)(1 - \gamma^2)} \right] \frac{P}{P_A}$$

(2.145)

and the associated quasi-steady state solutions are determined by (2.27b), (2.29b)-(2.40b).

Because the system's choice of the S or AS solution

is dependent upon the initial conditions and the solutions only become degenerate in the limit $T_R/\tau_p \to \infty$, the solutions are mutually exclusive in a given physical system. In other words, a modelocking system designed such that the initial cavity field is SM will always generate pulses of the form (2.27a), while the system designed such that the initial field is DM will generate pulses of the form (2.27b). Note further that the design of the former is much less critically dependent on the mode positioning under the gain profile than the latter. Indeed, stable AS pulse modelocking should be difficult to achieve. By the same token stable S pulse modelocking requires adjustment of the cavity length such that one mode is near line center.

III. Experiment

As verification of the theory presented in Chapter II we report here the first matching of the pulses generated by a transient modelocked laser to those predicted by the closed form transient theory. The system employing a TEA CO_2 laser modelocked by an SF_6 saturable absorber was chosen for the experiment because it generates nanosecond pulses which are readily observable on a fast oscilloscope. For the sake of comparison, forced modelocking experiments were also performed using a Ge acousto-optic intracavity modulator.

The setup for the modelocking experiments is described in section 3.1. Characterization of the system parameters is carried out in section 3.2. Section 3.3 presents the results of the matching of the experimental passively mode-locked pulses. In section 3.4 the forced modelocking experiments and their comparison to passive modelocking are discussed.

3.1 Experimental Setup

The modelocked system is depicted in Figure 23. The major components--cavity, amplifier, absorber/modulator and detector--are described below.

The cavity consists of a 4.5 m radius 80% reflecting Ge mirror and a 80ℓ/mm flat grating blazed for 10.6 μ to limit the laser operation to a single CO_2 transition. The total cavity length is 3.52 m. The cavity is "folded" by means of two totally reflecting Ge mirrors located near its center. Apertures placed at both ends of the cavity are adjusted to ensure operation on the fundamental transverse mode.

The CO_2 amplifier is a pin-resistor discharge tube. The overall length consists of two tubes sealed together by copper sheeting external to the tube. Sharpened needles inserted every 0.5 cm in line along the length of each tube make up the cathode. The anode is composed of the metal leads of 1 kΩ carbon film resistors inserted at positions diametrically opposed to the needles. Separation between the cathode and anode is 2.5 cm.

The amplifying medium is a 2:1:6 mix of CO_2:N_2:He gas. The gases are mixed in a tank before flowing them through the discharge tube. The flow rate of each gas is measured using a Matheson flow meter. The pressure is measured at the exhaust port with a Matheson absolute pressure gauge. In the
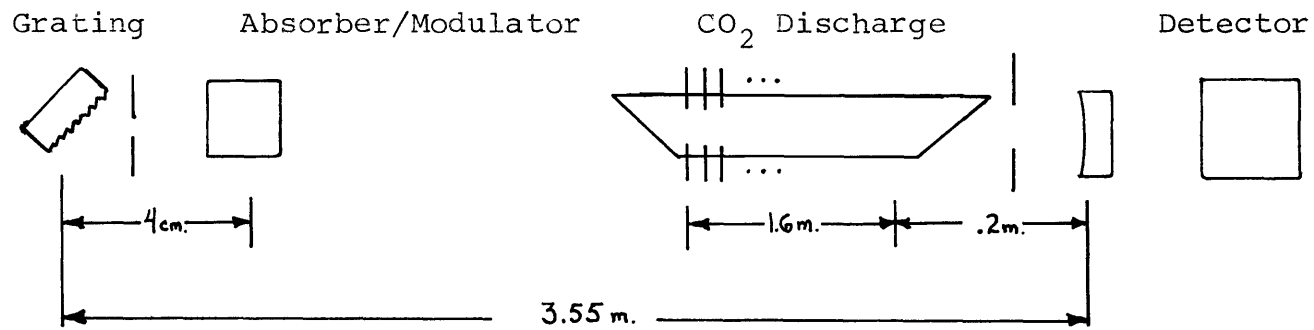
Figure 23: Modelocked TEA CO_2 Laser Oscillator

experiments conducted the pressure was varied between 200
and 600 torr.

The SF_6 cell consists of two circular NaCl windows
50 mm in diameter encased in a cylindrical aluminum holder.
A 1 mm metal spacer around the circumference of the cell
separates the windows. Ports through the Aluminum case and
spacer provide access to the gas line and pump. The windows
are sealed to the case by epoxy.

The modulator used for the forced modelocking experiments
is an antireflection coated single-crystal Ge acousto-optic
modulator. A $LiNbO_3$ piezoelectric transducer bonded to the
[111] surface provides coupling between the applied RF and
the acoustic wave. The $LiNbO_3$ has a broad resonance near
20 MHz, and the Ge crystal has narrow ($\sim$10 KHz) acoustic
resonances 210 KHz apart in the vicinity of 20 MHz.

The modulator was driven as illustrated in Figure 24.
In order to minimize heating of the modulator a pulsed RF
source is created by mixing the continuous output of a GR
Bridge Oscillator with the pulse from a GR 1340 Pulse Gener-
ator. The RF pulse is then amplified by an HP 230B Power
Amplifier to a peak power of approximately 4 W before being
applied to the modulator transducer. Operation on an acoustic
resonance of the crystal is ensured by monitoring the reflected
power from the crystal. A minimum in reflected power seen on
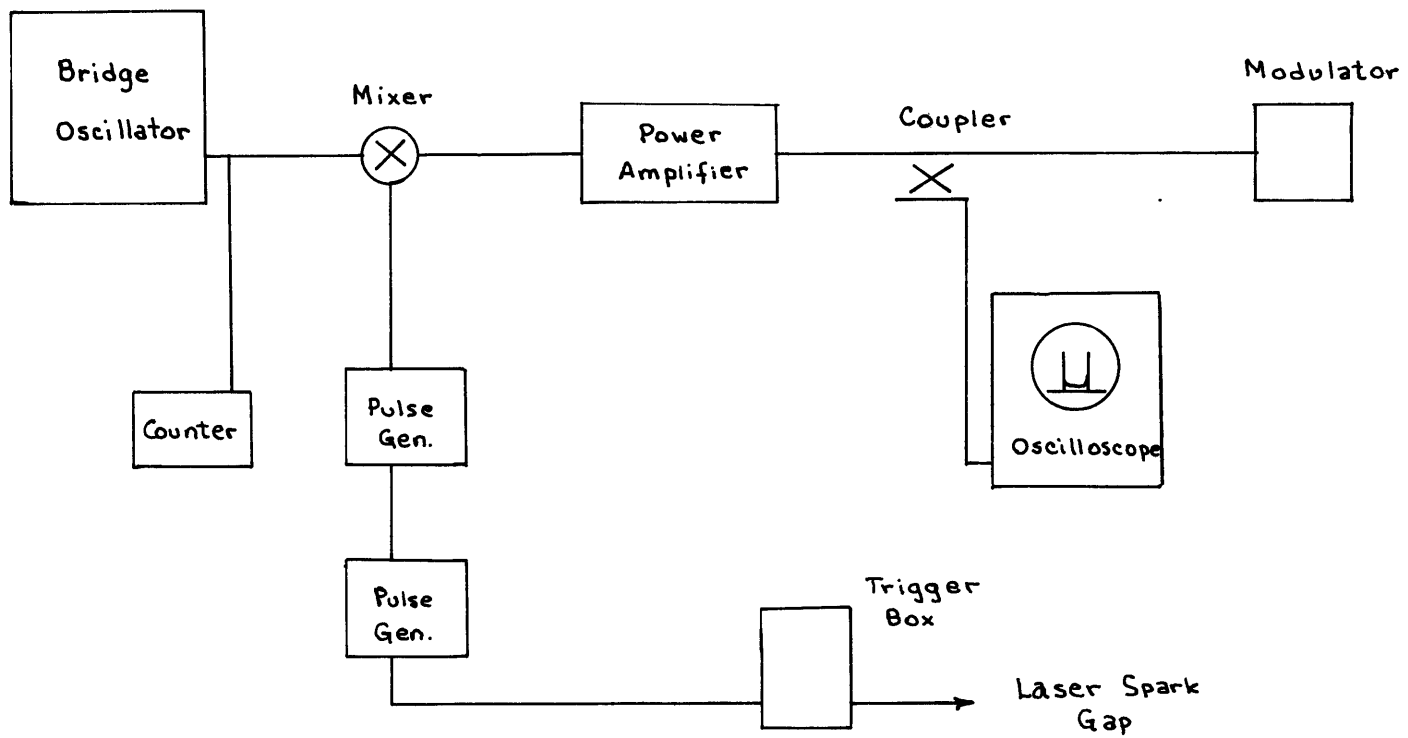
Figure 24: Modulator Drive Schematic

the oscilloscope indicates the line center of the resonance. For modelocking experiments, the RF is applied to the modulator at least one millisecond prior to the firing of the laser discharge, in order to guarantee modulation during the laser pulse.

Both nitrogen cooled Au:Ge and helium cooled Cu:Ge detectors were used to measure the output of the laser. The Au:Ge detector combined with a 7904 Tektronix oscilloscope has a rise time < 2 ns. The Cu:Ge detector 7904 oscilloscope combination has a risetime < 1 ns. Convex mirrors focused the laser radiation onto the detector crystals. The detector sensitivity was calibrated with the chopped output of a cw CO_2 laser against a Scientech 3602 energy meter. Calibrated $Ca F_2$ attenuators were positioned between the laser and the detector to ensure operation in a linear regime of the detector.

The faster Cu:Ge detector was used to measure the individual modelocked pulses. In measuring the overall TEA pulse, however, the slower Au:Ge detector was used.

3.2 Determination of the System Parameters

The complex energy level structure of both CO_2 and SF_6 makes the modelocked system difficult to characterize. In particular, the assumption of two level media which runs throughout most of the theoretical analysis of Chapter II is an oversimplification. Saturation phenomena in CO_2 and SF_6 are characterized by a host of saturation powers and relaxation times. A precise matching of the transient theory to experiment would require an elaboration of the theory along the lines indicated in section 2.6, an accurate determination of the relevant parameters of CO_2 and SF_6, and a monitoring of the amplifier gain and absorber loss during the TEA pulse. In such an approach, however, the law of diminishing returns rapidly takes hold. The inherent simplicity of the theory becomes obscured. The excess gain in the cavity is difficult to measure with sufficient accuracy to obtain a meaningful match to the experimental results.

The approach taken here in characterizing the modelocked is to demonstrate the approximate validity of the simple two-level media model adopted in the theory over the range of parameters studied. Rather than characterize each medium separately, the system is viewed as a whole, and the medium parameters are determined to be consistent with the two-level model, published data, and the output observed from the laser.

3.2.1 Modelocked Laser Output

Examples of the TEA laser output for free-running, passively modelocked and forced modelocked operation are shown in Figure 25. In the absence of any intracavity mode-locking element the laser exhibits the multimode output of Figure 25a. The random beat signal, which is periodic in the cavity transit time, is a consequence of the fact that the transient gain shoots well above the cavity loss line. Lasing takes place on many cavity modes, despite the fact that the gain medium is homogeneously broadened.

Figure 25b shows the laser output in the case of forced modelocking when the modulator is tuned to the cavity mode spacing. The peak power of the modelocked pulses increases over that of the free running oscillator while the time average output power decreases slightly due to the insertion loss of the modulator.

Passive modelocking by means of the 1 mm SF_6 absorbing cell reduces the output power of the laser due to the requirement of near threshold operation. The photograph in Figure 25c shows three successive shots of the laser. Superpositions of many shots of the passively modelocked laser are shown in Figure 26a, b to demonstrate reproducibility. A more detailed view of two pulses of a single shot is shown in Figure 26c. The fact that modelocking occurs on every firing of the laser
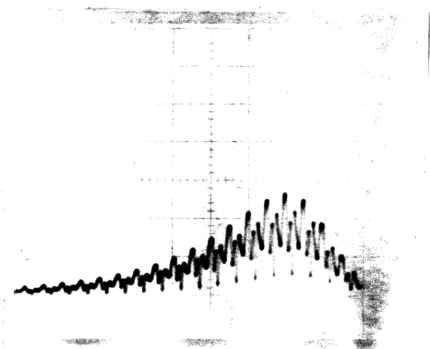
(a)   Spontaneous Locking

6 KW/D.

50 ns/D.
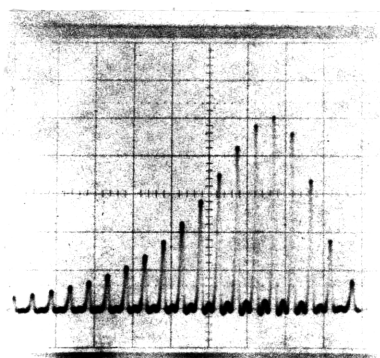
(b)   Forced Modelocking

6 KW/D.

50 ns/D.

f_m = 20.576 MHz
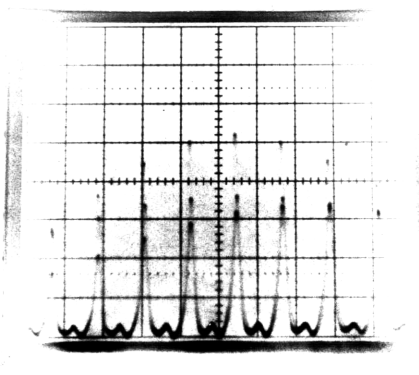
(c)   Passive Modelocking

.12 KW/D.

20 ns/D.

p_L = 255 torr

p_A = 80 torr

← t

Figure 25: Modelocked Laser Output
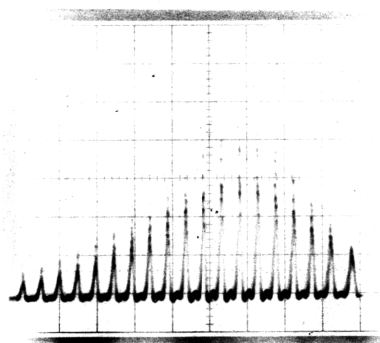
(a)   30 shots

        .24 KW/D.

        50 ns/D.

        p_L = 395 torr

        p_A = 80 torr
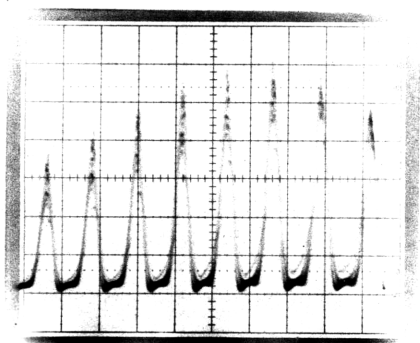
(b)   25 shots

        .12 KW/D.

        20 ns/D.

        p_L = 277 torr

        p_A = 80 torr
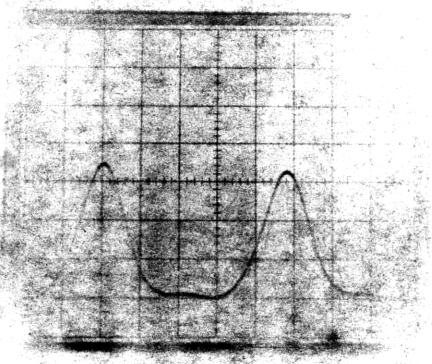
(c)   1 shot

        .24 KW/D.

        5 ns/D.

        p_L = 277 torr

        p_A = 80 torr

Figure 26:   Shot-To-Shot Reproducibility of Passive Mode-Locking

discharge supports the basic premise of the theory that the buildup is deterministic, rather than the statistical selection of a noise spike. As we shall see, the considerable shot-to-shot amplitude variation can be attributed to gain variation rather than any inherent statistics of the buildup.

3.2.2 Small Signal Gain

Measurements of the transient small signal gain of the pin-type TEA laser amplifier have been reported by previous authors.[44,47] In the 200-600 Torr pressure regime they indicate a gain duration on the order of 10 μs. Since the passively modelocked TEA pulse is less than 250 ns in duration, the small signal gain can be considered constant during the pulse. The fact that passive modelocking requires near threshold operation then dictates that it is the maximum value of small signal gain which is of interest to us.

The maximum small signal gain was measured over a range of operating conditions--laser pressure and capacitor voltage --by adding loss to the cavity until the laser quenched. The loss was introduced by filling the absorber cell with SF_6. The small signal absorption of SF_6 was then determined by measuring the transmission of the cell external to the cavity (see Chapter IV). The detailed passive modelocking experiments were carried out on the P(24) transition of CO_2 where the SF_6 small signal absorption was measured to be .19 $\pm$ .02 cm^{-1} torr^{-1} in good agreement with published values.[48,49] The curves of the peak gain versus capacitor voltage with the total laser pressure as a parameter are shown in Figure 26 for the P(24) transition. The dotted line indicates an absorber loading corresponding to 80 torr of SF_6 where most of the modelocking experiments were conducted.
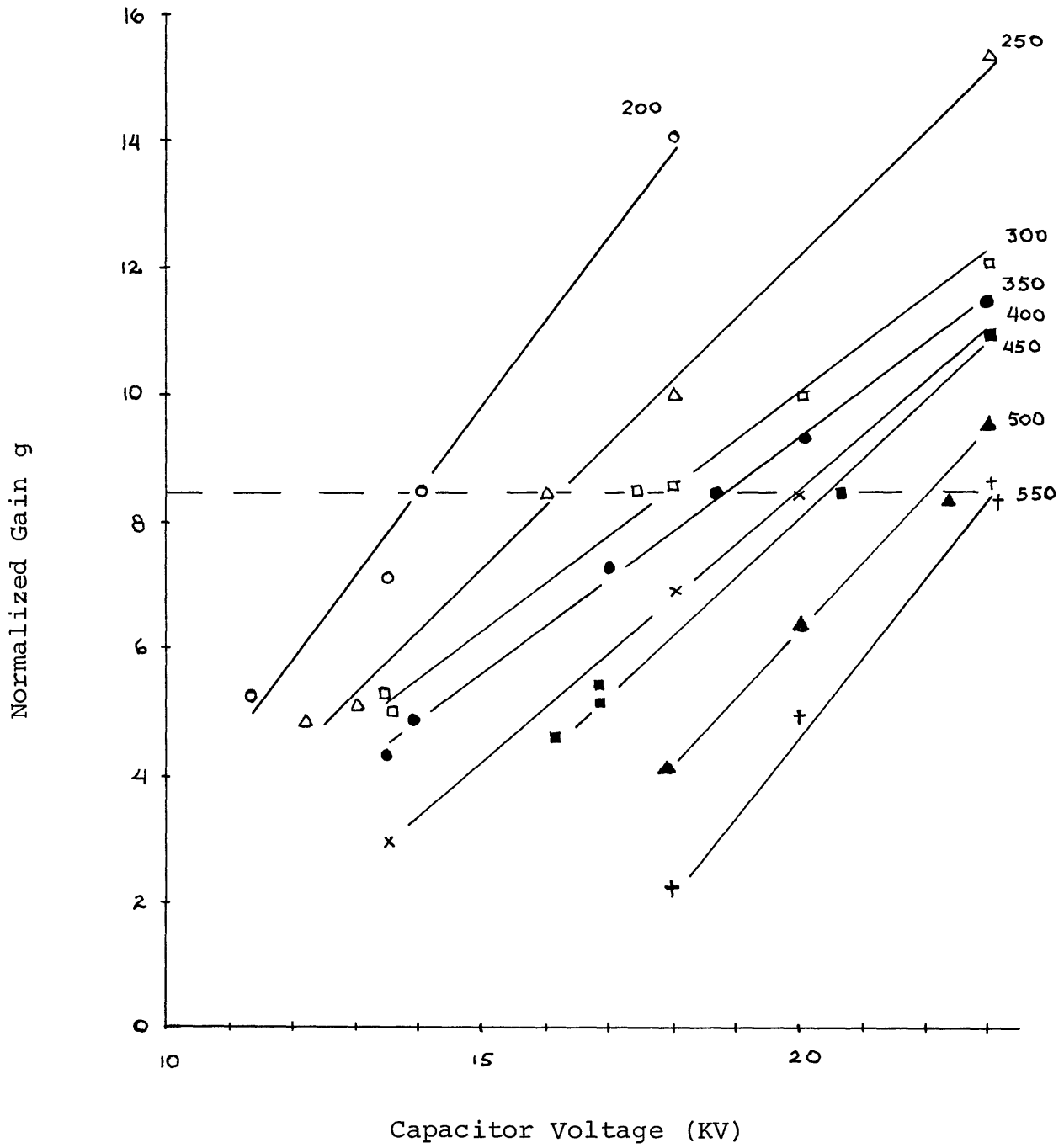
Figure 27: Normalized Round Trip Small Signal Gain
Versus Capacitor Voltage

3.2.3 Saturation Powers

Both the CO_2 amplifier and the SF_6 absorber can be characterized by relaxation times which are "fast" and "slow" compared to the passively modelocked pulses generated by the system. At the SF_6 pressure used in our experiments the only fast relaxation time characterizes the rotational relaxation. The slow relaxation times are associated with the equilibration among the vibrational levels. The still slower rate at which vibrational energy is converted into kinetic energy of the gas can be neglected altogether, since it is slow compared to the duration of the TEA pulse. In the case of the CO_2 amplifier, both the rotational relaxation and the intramode vibrational equilibration can be faster than the modelocked pulse. (Details of the CO_2 relaxation processes are discussed in Appendix B.) The slow relaxation is the rate of intermolecular vibrational equilibration between the symmetric stretch and bending modes, which governs the relaxation of the lower level of the lasing transition.

An experimental and theoretical study of SF_6 saturation is carried out in Chapter IV. Here our objectives are less ambitious. We justify the application of the simple two level models of the amplifier and absorber used in the theory of passive modelocking to the $CO_2 - SF_6$ system. In doing so, we obtain an estimate of the ratio of saturation powers P_{AF}/P_{LS}.

To estimate the saturation powers of the media we make
use of the well-known expression for the saturation intensity
of a two-level medium

$$I_s = \frac{\hbar \omega_o}{\sigma \tau} \qquad (3.1)$$

where σ is the optical cross-section of the levels in question
and τ is their relaxation time. Let us first compute the
fast saturation powers of CO_2 and SF_6 in order to check
the criterion (2.118) that the absorber response overpower the
laser response. As mentioned above, the fastest response of
both media is due to rotational bleaching.

In CO_2 the cross-section of the rotational levels di-
rectly interacting with the field at line center is

$$\sigma_L = \frac{\lambda^2}{4\pi} \frac{T_2}{\tau_s} \qquad (3.2)$$

where $T_2 \simeq .65 \cdot 10^{-7}$ s $\cdot$ torr is the dephasing time,[50]
and $\tau_s \simeq 5$ s is the spontaneous relaxation time.[51] Using
$\lambda \sim 10^{-3}$ cm we obtain $\sigma_L \cong 1.2 \cdot 10^{-15}$ cm^2 $\cdot$ torr. The
saturation intensity for rotational bleaching can now be eval-
uated from (3.1)

$$I_{LF} = \frac{\hbar\omega_o}{\sigma_L^{24} T_2} = 2.4 \cdot 10^2 \text{ W} \cdot \text{cm}^{-2} \cdot \text{torr}^{-2} \qquad (3.3)$$

where we have assumed that rotational equilibration occurs in one collision, i.e., the rotational relaxation time equals T_2.

As shall be shown in Chapter IV, the cross-section of the rotational levels of SF_6 directly interacting with the radiation of the $P(J)$ transition of the $10.6~\mu$ branch of CO_2 is given by

$$\sigma_A^{~J} = \frac{\alpha_o^{~J}}{\beta N} \qquad (3.4)$$

where $\alpha_o^{~J}$ is the small signal absorption coefficient of SF_6 on the $P(J)$ transition, β is the fraction of absorbing molecules which interact directly with the radiation, and N is the number of molecules per unit volume. The small signal absorption on the $P(24)$ transition $\alpha_o^{24} \sim .2 \text{ cm}^{-1} \cdot \text{torr}^{-1}$,[48] and the fraction of absorbing molecules $\beta \sim .003$,[52] so that substitution in (3.4) gives $\sigma^{24} \simeq 10^{-15}$ cm^2. Rotational equilibration in SF_6 has been measured to occur at a rate $4.5 \cdot 10^7 \text{ s}^{-1} \cdot \text{torr}^{-1}$.[52] Thus, the saturation intensity is given by

$$I_{AF} = \frac{\hbar\omega_o}{\sigma_A^{24} \cdot T_A} \simeq 8 \cdot 10^2 \ W \cdot cm^{-2} \cdot torr^{-1} \qquad (3.5)$$

The ratio of the fast saturation powers for the two media is given by

$$\frac{P_{AF}}{P_{LF}} = \frac{I_{AF}}{I_{LF}} \frac{P_A}{P_L^2} \frac{A_A}{A_L} \qquad (3.6)$$

where $P_{A, L}$ is the pressure and $A_{A, L}$ is the cross-sectional area of the beam. For the cavity geometry of our experiment the ratio $A_A/A_L \sim .25$. Over the 200 - 600 torr total pressure range of the laser medium, and at the 80 torr pressure of SF_6, the ratio of the fast saturation powers is computed to be in the range

$$1.9 \cdot 10^{-4} < \frac{P_{AF}}{P_{LF}} < 1.7 \cdot 10^{-3}. \qquad (3.7)$$

Clearly, the rotational saturation of the laser medium is negligible compared to that of the absorber.

On a time scale which is long compared to the rotational rate, we can treat the kinetics of the rotational-vibrational population as a two-level system by introducing an effective

stimulated cross-section[53]

$$\sigma_L^{~J} = \sigma_L~W(J) \cong \sigma_L~\frac{4hc~BJ}{k_b T_g}~e^{-\hbar cBJ^2/k_b T_g} \tag{3.8}$$

where $B = .37~\text{cm}^{-1}$ is the rotational constant,[53] k_b is Boltzmann's constant and T_g is the gas temperature. The weighting factor on the right hand side takes into account the equilibrium population distribution among the rotational levels of the upper and lower vibrational states. On the P(24) transition the weighting factor is $W(J) = .063$, assuming $T_g = 300°K$. Thus, the effective cross-section of the P(24) transition becomes $\sigma_L^{~24} \simeq 7.5 \cdot 10^{-17}~\text{cm}^2$ torr. Because the effective cross-sction is so much smaller than σ_L, the fast saturation of the intramode vibrational levels can also be neglected in comparison to the rotational bleaching of SF_6.

In determining the saturation power for the response of CO_2 which is slow compared to both the modelocked pulsewidth and the rotational relaxation rate, we again make use of the effective cross-section defined above. Proceeding with our characterization of the lasing transition as a two-level medium, we recognize that the "bottleneck" rate for the TEA laser operation is the intramolecular V-V relaxation from

the lower level of the transition. The rate is fast, measured as $z_{12} = 3 \cdot 10^5 \; s^{-1} \; torr^{-1}$ for pure CO_2,[54] because of the near resonance of the (100) level of the symmetric stretch mode with the (020) level of the bending mode (see Appendix B).

From (3.1) we can now estimate the "slow" saturation intensity as

$$I_{LS} = \frac{\hbar \omega_o \; z_{12}}{\sigma_L \; 24} \simeq 16 \; W \cdot cm^{-2} \cdot torr^{-2} \tag{3.9}$$

where we have assumed that the V-V rate z_{12} depends only on the partial pressure of CO_2 in the $CO_2:N_2:He$ mix of $2:1:6$.[54] Replacing I_{LF} in (3.6) by I_{LS} we can compute the ratio of the fast saturation power of the absorber to the slow saturation power of the laser medium to be in the range

$$2.7 \cdot 10^{-3} < \frac{P_{AF}}{P_{LS}} < 2.5 \cdot 10^{-2} \tag{3.10}$$

over the 200 to 600 torr total pressure range of the laser.

In our case, therefore, even the slow response of the laser medium can be neglected in comparison to the fast

response of the absorber. Indeed, since we require that the time average power in the field be less than the absorber fast saturation power for the modelocking equation to apply, the relations (3.7) and (3.10) indicate that modelocking can only occur in the small signal regime of the laser medium. The buildup and decay of the field is determined simply by the time variation of the small signal gain.

The slow response of SF_6 is more difficult to determine due to the strong hot band contribution to absorption on the P(24) transition. An experimental and theoretical study of the SF_6 saturation is conducted in Chapter IV, where it is shown that the slow saturation of SF_6 can also be neglected for the experiments discussed here.

3.3 Matching of the Experimental Pulse Shapes

The theory developed in Chapter II predicts that each pulse in the modelocked train is a quasi-steady state pulse of the form

$$I(t, n) = I_0(n) \ dn^2 \left[\frac{t}{\tau_p(n)} , \gamma(n) \right] \qquad 0 < \gamma < 1 \qquad (3.11)$$

where dn is a Jacobian elliptic function of argument t/τ_p and modulus γ. The time t is "local" to one roundtrip transit T_R through the modelocked system, while n is an integer which counts the number of transits. The peak intensity $I_0(n)$, width $\tau_p(n)$ and modulus $\gamma(n)$ are specified by the system characteristics on the nth pass and by requiring the solution (3.11) to be periodic in the cavity roundtrip transit time.

The output of the laser consists of a "long" pulse approximately 250 ns in duration which modulates the short, 2 ns - 10 ns, modelocked pulses. In matching our experimental results we must match both the overall TEA pulse and the individual modelocked pulses under the TEA pulse envelope.

To begin with, we assume the small signal gain to have a parabolic time dependence in the near threshold regime of interest here. Lasing on the mode nearest line center ini-

tiates when the gain equals the loss. We assume the initial power in the field to be that of one photon, namely

$$\frac{\hbar\omega_o}{T_R} = 7.7 \cdot 10^{-13} \text{ W.}$$

As shown in Figure 28, successful modelocking requires that the gain be adjusted such that the modelocking threshold defined by (2.51) is reached well after the gain has peaked. If the threshold is reached too soon, the field intensity can grow to a point where it fully bleaches the absorber, and modelocking ceases to be possible. This is confirmed experimentally by the fact that, as the small signal gain is increased, a dramatic increase in TEA pulse power is observed in passing from the regime of consistent modelocking to the regime of erratic self-locking.

Plots of small signal gain, $g_o(n)$, the time average gain coefficient $\alpha(n)$, and the overall TEA pulse envelope for a simulated case of transient modelocking are shown in Figure 28. The simulation corresponds to an experiment in which the laser is operated at a total pressure of 451 torr. From the linewidth dependence on pressure of 4.5 MHz $\cdot$ torr^{-1}, and the 24 ns transit time, we determine $\omega_L T_R = 153$. The constant cavity loss, due to the 20% transmitting mirror, diffraction grating and salt windows, is estimated as

$\Delta\omega_c T_R$ = .4. The addition of 80 torr of SF_6 to the 1 mm cell introduces a normalized loading q = 7.5 to the cavity on the P(24) transition, where the small signal absorption is .19 $cm^{-1} \cdot torr^{-1}$.

The dependence of the small signal gain on the number of passes through the system is taken to be

$$g_o(n) = g_m \left[1 - \left(\frac{n - n_o}{n_p} \right)^2 \right] \qquad (3.12)$$

where g_m is the maximum gain, n_p is the pump time in number of passes required for the gain to reach g_m, and n_o is one-half the time that net gain exists in the system given by

$$n_o = n_p \sqrt{g_m - (1 + q)} \ . \qquad (3.13)$$

From the small signal gain measurements that Lyon[44] conducted on the pin-type TEA CO_2 laser at 350 torr, we estimate the gain rise time to its peak value to be 6 μs. Dividing by the 24 ns roundtrip cavity transit time we find n_p = 250.

A modelocked laser pulse from the actual system charac-

$q = 7.5$

$g_m = 9.04401$

$\omega_L T_R = 153.$

$\Delta \omega_c T_R = .4$

$n_p = 250$
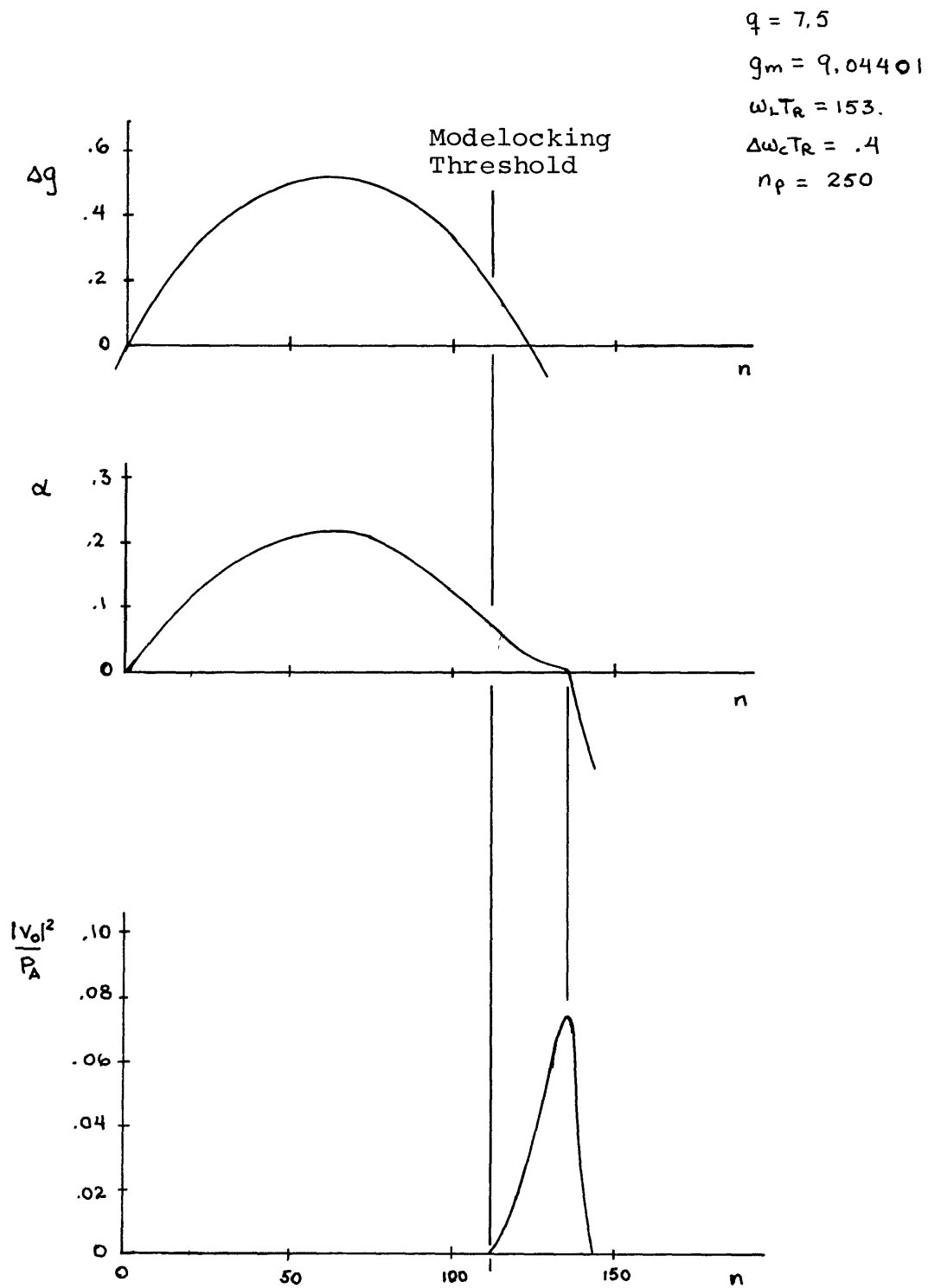
Figure 28: Simulation of Transient Modelocking for a
Parabolic Small Signal Gain

terized by the parameters given above is shown in Figure 29.
The asymmetry of the pulse predicted in Figure 28 is readily
apparent, namely a slowly rising front edge and rapidly fal-
ling trailing edge. (Note that time is reversed in Figure 29
because it is a contact print of the actual photograph.)
Furthermore, the widths of the experimental and theoretical
pulses are in good agreement.

Matching of individual modelocked pulses in the pulse
train was also carried out. By using the delayed sweep
capability of the 7B92 time base plug-in of the 7904
oscilloscope, pulses near the peak of the laser pulse could
be accurately measured. Two pulses just beyond the peak are
shown in Figure 30 for three successive shots of the laser.
The solid lines are tracings of a 3:1 enlargement of the
oscilloscope trace. The pulses on the right hand side of
Figure 30 and in subsequent Figures 31 - 34 have been
matched to the function given in (3.11) at different values
of the modulus γ, keeping the periodicity fixed at the
24 ns cavity transit time. The matching parameter γ is
related to the system parameters. For all cases considered
here, the absorber loading is fixed at q = 7.5 corresponding
to 80 torr of SF_6 at P(24). In accordance with the
findings of section 3.2.3, the ratio of the absorber fast
saturation power to the laser slow saturation power is

Experiment

.24 KW/D.

p_L = 451 torr

p_A = 80 torr

Δg_m = .5

Theory

$\omega_L T_R$ = 153

q = 7.5

Δg_m = .54401

n_p = 250

$\Delta \omega_c T_R$ = .4

t (.1 μs/D)
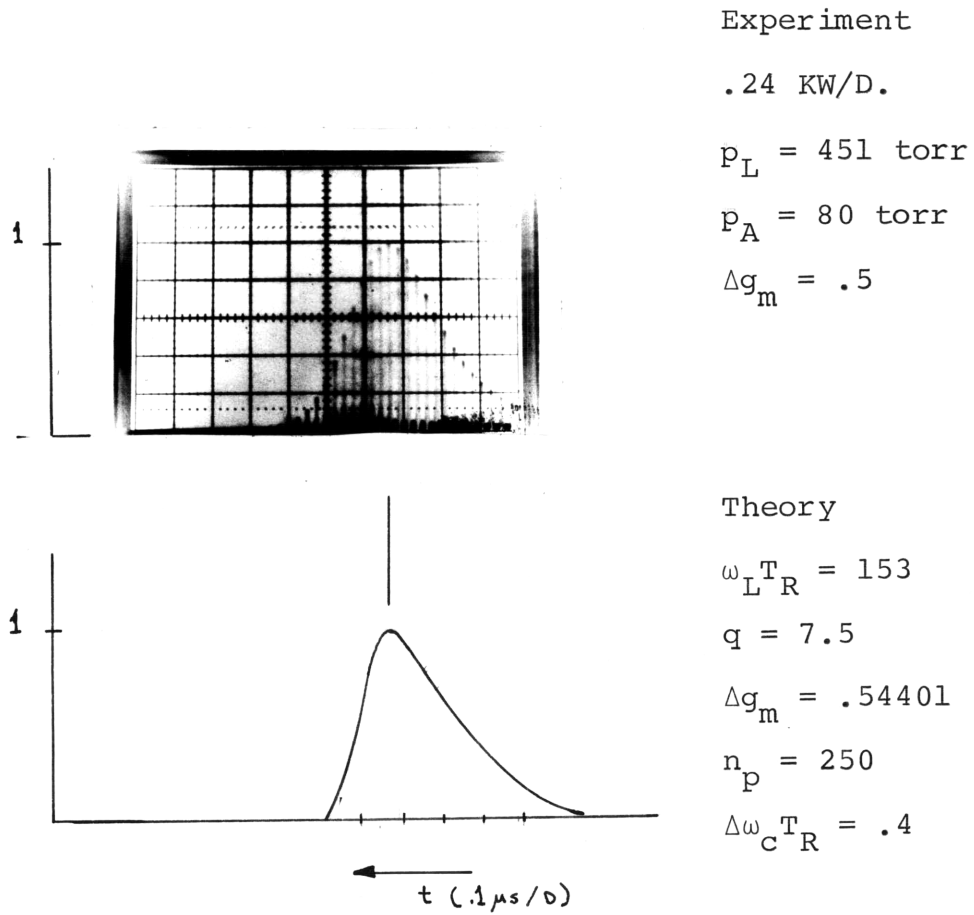
Figure 29: Comparison of Theoretical and Experimental
TEA Pulse Showing Asymmetry Match

$q = 7.5$

$\Delta\omega_c T_R = .4$

$n_p = 250$

$1 - \gamma^2 = 3.5 \cdot 10^{-6}$

$\Delta g_m = .54402$

$1 - \gamma^2 = 2.7 \cdot 10^{-5}$

$\Delta g_m = .54401$

$1 - \gamma^2 = 7.1 \cdot 10^{-4}$
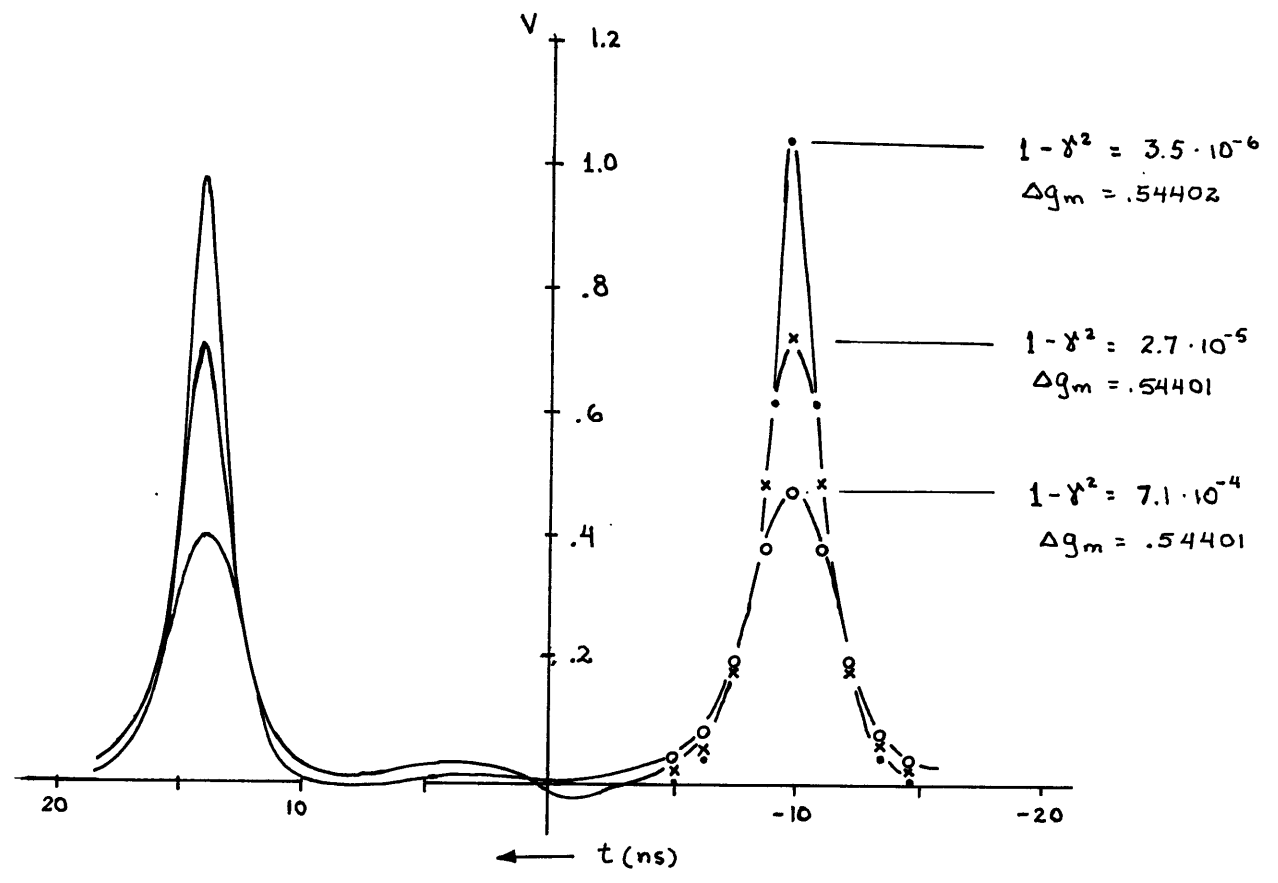
$\Delta g_m = .54401$

Figure 30:   Pulse Shape Match for $\omega_L T_R = 153$

$q = 7.5$

$\Delta g_m = .54401$

$\Delta \omega_c T_R = .4$

$n_p = 250$

V

.8

.4

$1-\gamma^2 = 7.7 \cdot 10^{-5}$

20　　　10　　　　　　-10　　　-20

t (ns)
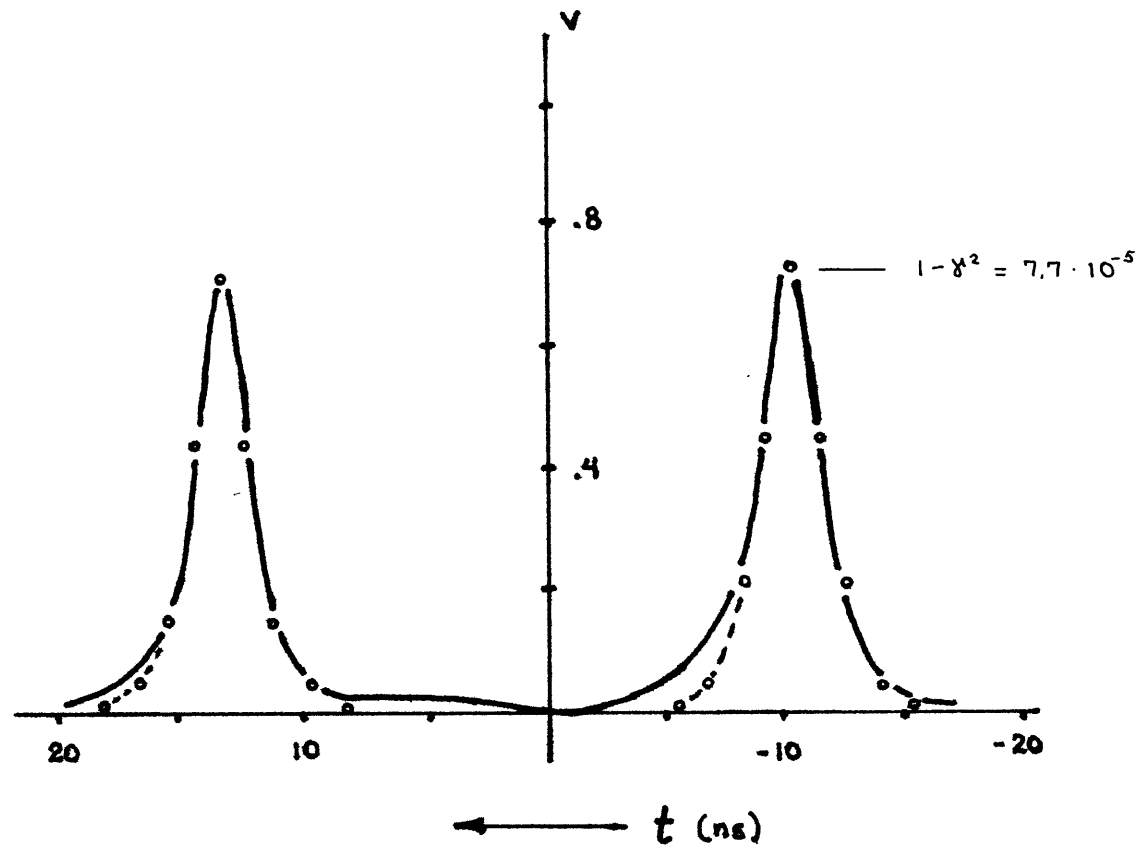
Figure 31:　Match of Successive Pulses for　$\omega_L T_R = 153$

$q = 7.5$

$\Delta g_m = .54531$

$\Delta \omega_c T_R = .4$

$n_p = 250$

$1 - \gamma^2 = 2.9 \cdot 10^{-6}$

$1 - \gamma^2 = 4.6 \cdot 10^{-6}$

t (ns.)
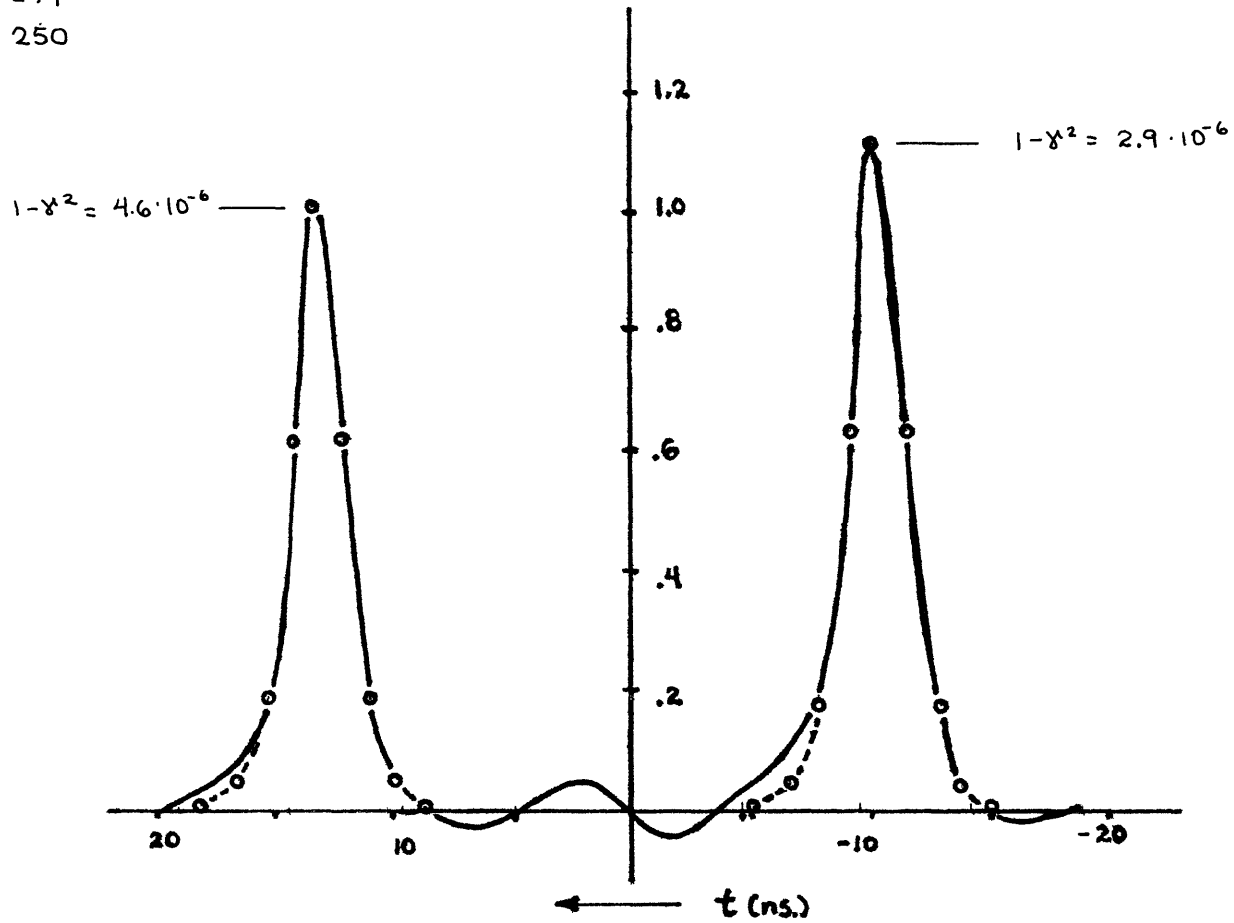
Figure 32: Match of Successive Pulses for $\omega_L T_R = 140$

$q = 7.5$

$\Delta g_m = .5497$

$\Delta \omega_c T_R = .4$

$n_P = 250$

$1 - \gamma^2 = 5.0 \cdot 10^{-3}$

$6.9 \cdot 10^{-3}$

$.5$

$.4$

$.3$

$.2$

$.1$

20

10

-10

-20

$t \ (ns.)$
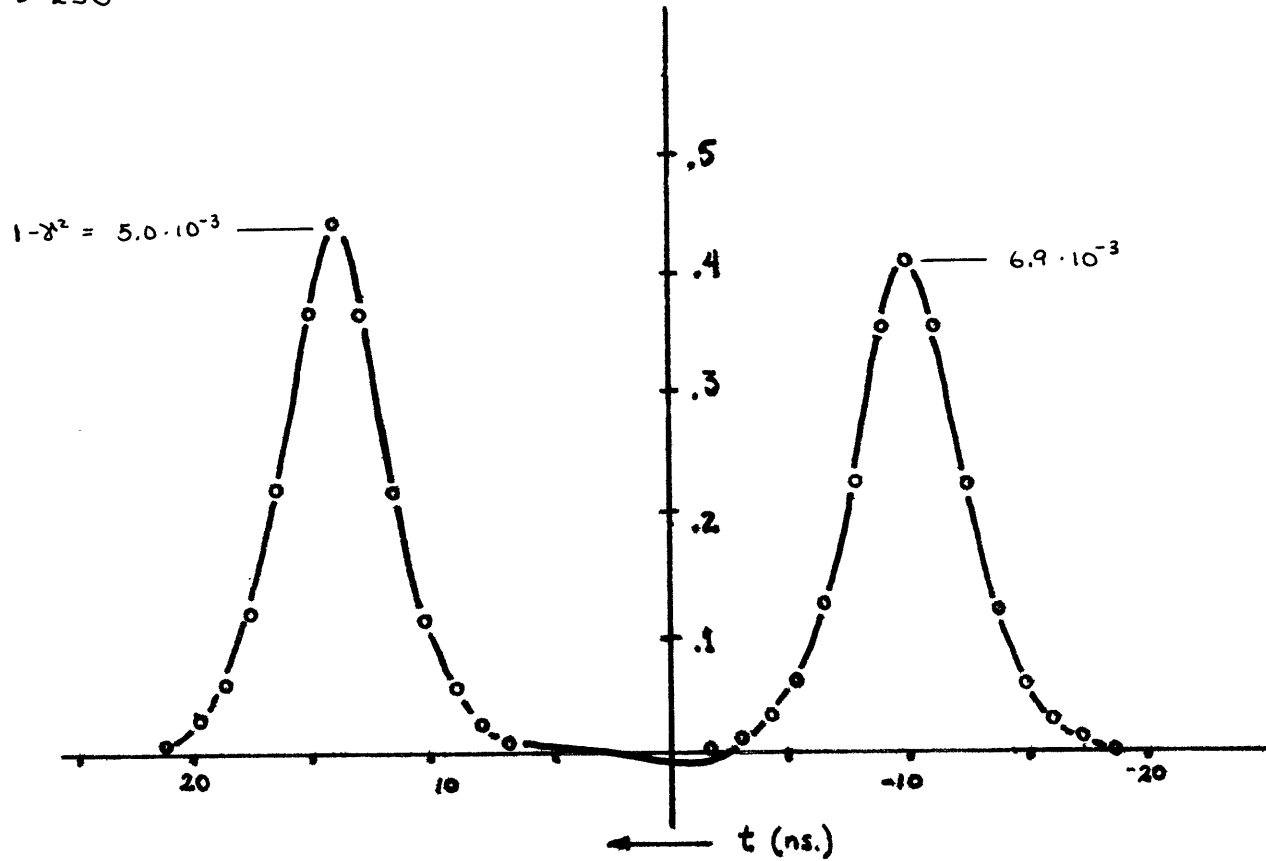
Figure 33:   Match of Successive Pulses for $\omega_L T_R = 102$

$q = 7.5$

$\Delta g_m = .544$

$\Delta \omega_c T_R = .4$

$n_p = 250$

$1 - \gamma^2 = .17$
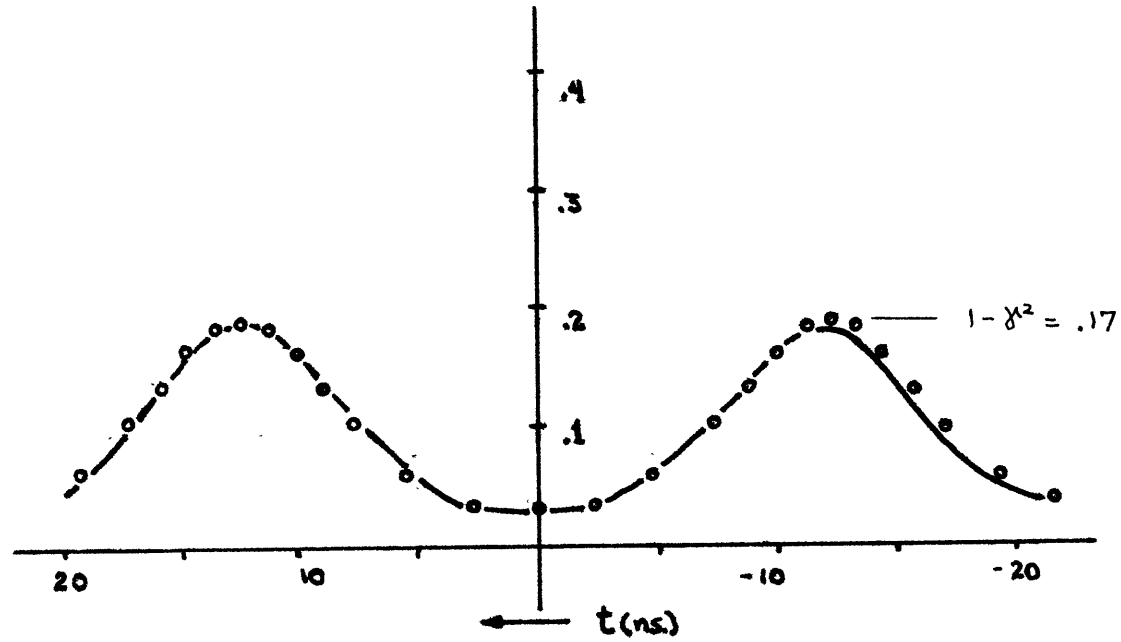
Figure 34: Match of Successive Pulses for $\omega_L T_R = 85$

neglected, $P_{AF}/P_{LS} = 0$, and all other saturation powers
are assumed to play no role. Furthermore, the gain rise
time to its peak value is assumed to be 6 µs. For a given
value of laser pressure, i.e. $\omega_L T_R$, the only system para-
meter varied in matching the pulses is the peak value of the
small signal gain, g_m.

In each case g_m is varied until a good pulsewidth
match to the experimental pulse is found for a pulse near
the peak of the theoretical pulse train. The value of g_m
used to match each set of pulses, and the value of $1 - \gamma^2$
associated with each pulse are indicated on the figures. The
match of theoretical and experimental pulse shapes is excel-
lent. Discrepancies in the tails of the pulses and the slight
ringing between pulses can be attributed to the detector
response.

A plot of the pulsewidth versus inverse laser linewidth
is shown in Figure 35 for the matched pulses. Although the
pulses tend to shorten with increasing laser linewidth, there
is no discernible functional dependence. This is not sur-
prising in light of the fact that equation (2.70) predicts a
dependence

$$\tau_p = \frac{1}{\omega_L v_o} \sqrt{\frac{(1 + q) P_A}{2q}} \, . \tag{3.14}$$
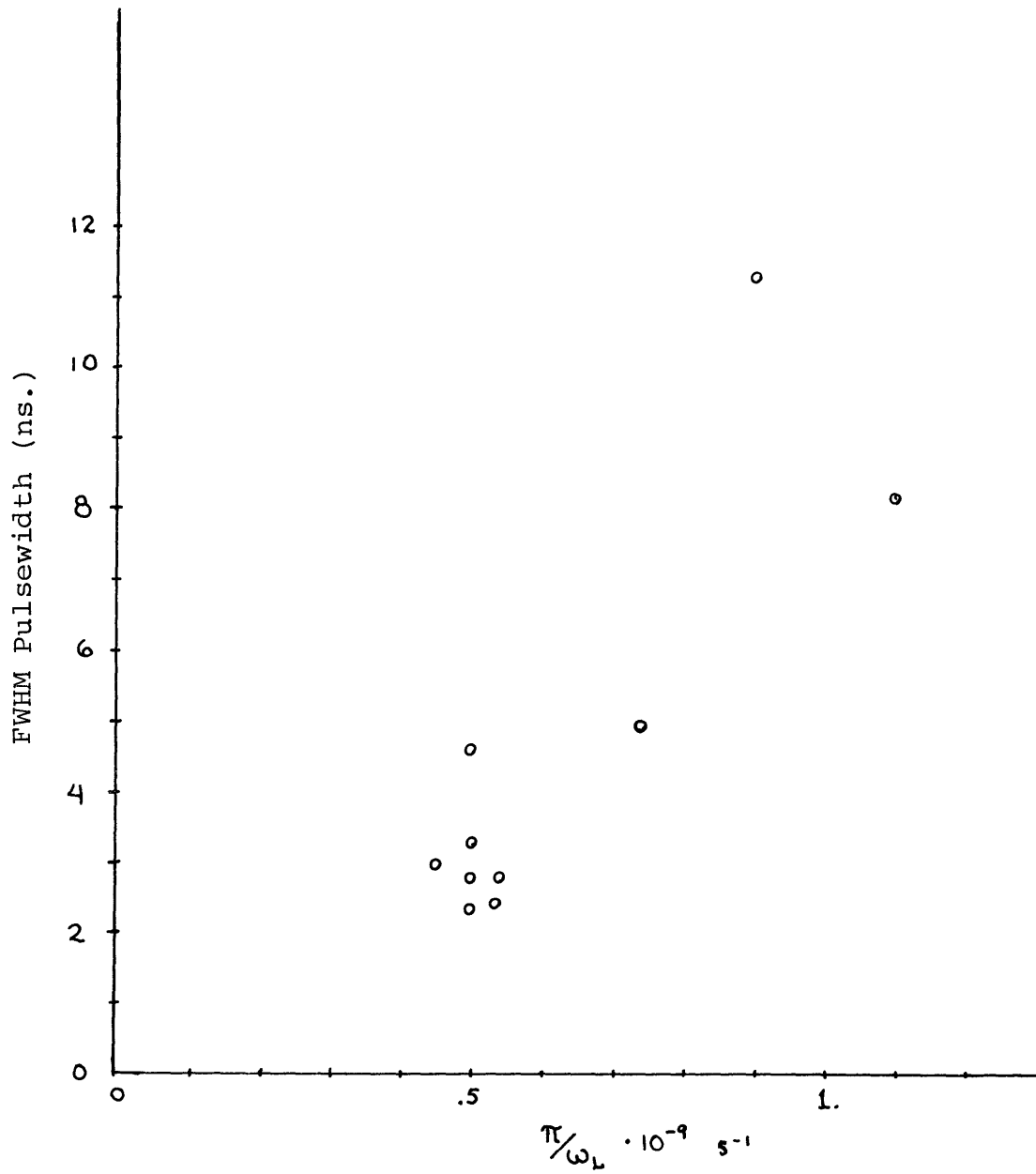
Figure 35: Experimental Modelocked Pulsewidth
Variation with Laser Linewidth

The peak amplitude of the pulse, v_o, is a sensitive function of the small signal excess gain. Furthermore, bounds are set on the values of excess gain $\Delta g_m = g_m - (1 + q)$ at a given ω_L for which modelocking is possible. If Δg_m is too small, the threshold power for modelocking is never reached, and the system runs single mode. If Δg_m is too large, the power in the cavity builds up to a point where the absorber is fully bleached, and the system exhibits only erratic self-locking behavior.

Having matched the experimental pulse shapes to those predicted by theory, we now examine the variation of the relative amplitudes of the predicted pulses to the relative amplitudes experimentally observed. The results are plotted in Figure 36, where we normalize all amplitudes to that of the highest pulse. The predicted "tracking" of the pulse amplitude is seen to be in good agreement with the amplitude variation observed.

The absolute amplitude of the highest measured pulse was determined to be 1.5 KW. Accounting for the 20% mirror transmission, this indicates an intracavity amplitude of 7.5 KW. The peak power predicted for the matching pulse is one-tenth of the absorber saturation power. From the number for I_{AF} given in (3.5) and the calculated beam cross-section of $\sim .2$ cm^2 in the absorber, we determine an amplitude of 1.3 KW. The approximate factor of 6 difference
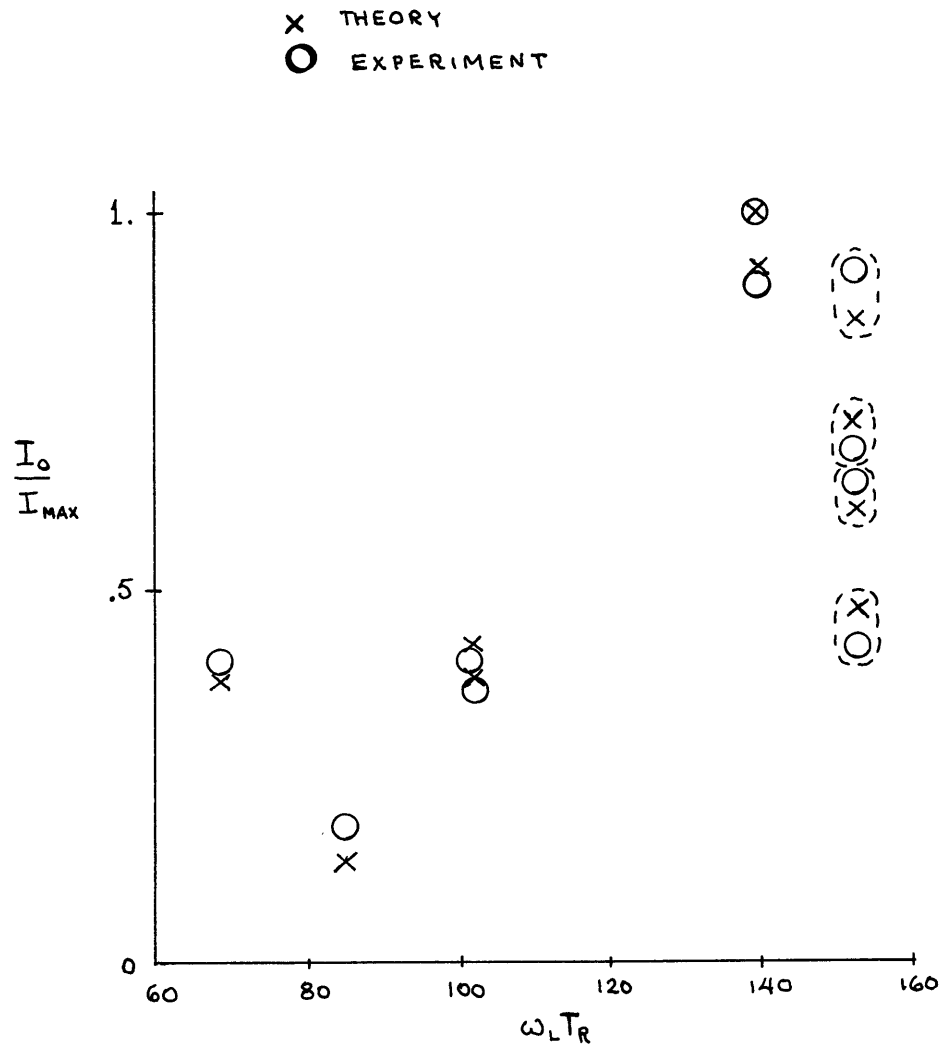
Figure 36: Comparison of Theoretical to Experimental
Amplitudes for Matched Pulses

between the absolute values of peak pulse amplitude is not surprising in light of the assumptions built into the theory, and the assumptions we have made about the behavior of CO_2 and SF_6.

Estimates of the maximum small signal gain, g_m, during operation of the system, were obtained by monitoring the voltage applied to the discharge capacitors and making use of the curves in Figure 27. A comparison with the values used in matching the modelocked pulses is shown in Table III Agreement is within experimental error. The error in the estimates of g_m is, admittedly, too large to enable any conclusive statements. A careful measurement of the excess gain of the system during the laser pulse would be necessary to obtain a more definitive confirmation of the theory.

In review, we summarize the comparison of theory to experiment as follows:

1. Qualitative agreement in the prediction of overall laser pulse shape and variation with system parameters.

2. Excellent modelocked pulse shape agreement.

3. Accurate prediction of modelocked pulse amplitude variation with system parameters.

4. Order of magnitude agreement in the prediction of the absolute amplitude of the modelocked pulse.

Table III

Maximum Excess Gain for Modelocking

$\omega_L T_R$	Δg_m Experimental	Δg_m Theoretical
153	.5	.54
140	.7	.54
102	.2	.55
85	.3	.55
68	.4	.55

5. Agreement with measured maximum small signal gain

    within experimental error.

Taken together, the five points of comparison provide a

strong case for the validity of the theory.

One conclusion that stems from our analysis and which

our experiments support, is that the shortest pulse occurs

at the peak of the modelocked train. This appears to disa-

gree with the observation of Feldman and Figueira,[39] on a

CO_2 laser modelocked with a p-type Ge absorber, that the

pulse shortened continuously along the train. A possible

explanation for the disagreement lies in the difference in

intracavity intensity between our system $\sim$ 10 kW/cm^2 and

theirs $\sim$ 10 MW/cm^2. In our system we were able to neglect

the gain saturation because of the low power level in the

cavity. In their system gain saturation and saturation

broadening are major effects. The depletion of the gain and

associated broadening of the laser linewidth leaves only the

Ge absorber to shape the decaying pulse. Consequently, the

analysis of Feldman and Figueira, in which they consider only

narrowing of the modelocked pulse due to the fast absorber

saturation on successive passes, is applicable to their system.

In our system, however, the gain dispersion remains a major

factor in determining the pulse shape throughout the buildup

and decay of the modelocked pulse, and the succession of quasi-

steady states analysis is valid.

3.4 Forced Modelocking Experiments

As a comparison to the performance of the passively modelocked system we also conducted forced modelocking experiments in the same laser cavity by replacing the absorber cell with a Ge acousto-optic modulator.

Examples of the individual modelocked pulses obtained from the forced modelocked system are shown in Figure 37. Each photograph shows the overlap of three shots of the laser. The output of the forced modelocked system is noticeably more stable from shot-to-shot than that of the passively modelocked system. Furthermore, the requirement of near threshold operation, so critical to the reproducibility of passive modelocking, is of little consequence in the forced modelocked system.

Both the improved stability and the ability to modelock well above threshold can be explained by the fact that, from the onset of lasing, one intracavity modulation tuned to the cavity roundtrip transit time $(\omega_M = 2\pi/T_R)$ discriminates against growth of the field propagating around the cavity which is not in synchronism with transmission maximum of the modulator. In other words, there is no modelocking threshold distinct from the lasing threshold. The fact that loss modulation dictates a maximum gain at a single time within the round trip transit leads to rapid pulse formation. Hence,
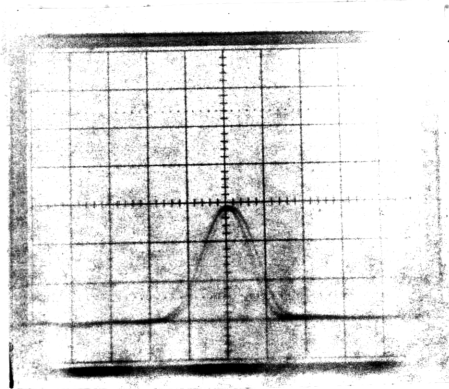
3 shots

2 ns/D.

p_L= 504 torr
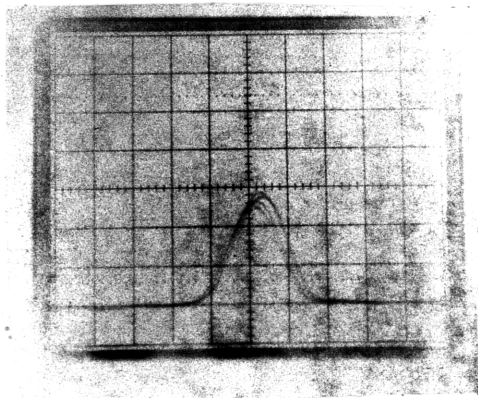
3 shots

2 ns/D.

p_L= 450 torr

Figure 37:   Forced Modelocked Pulses

for sufficient depth of modulation, modelocking occurs even though the excess gain in the cavity is large.

The equation governing the evolution of tuned forced modelocking is similar to that of passive modelocking:

$$\frac{\partial v(t,\ n)}{\partial n} = \Delta\omega_c T_R \left[g \left(1 + \frac{1}{\omega_L^2} \frac{\partial^2}{\partial t^2} \right) - (1 + M \sin^2 \omega_M t) \right] v(t,\ n)$$

(3.15)

where $M/2$ is the normalized modulation depth, and the modulation frequency ω_M is assumed equal to the cavity mode spacing. Again we have a gain minus loss equation governing the evolution of the waveform $v(t,\ n)$. The shaping of the field on each pass is now dictated by the competition between the gain dispersion and the forced modulation rather than the passive modulation due to the absorber bleaching.

The solution to (3.15) can be attacked in the same manner as was carried out for passive modelocking in Chapter II. The periodic steady state solutions to (3.15) are Mathieu functions.[55] In the regime of well separated modelocked pulses, however, the modulation function can be expanded to first order, $\sin^2 \omega_M t = \omega_M^2 t^2$ and the solutions become gaussians:[56,57]

$$v = \frac{v_o}{\sqrt[4]{\pi}\ \tau_p{}^2}\ \exp\left(-\frac{t^2}{2\tau_p{}^2}\right) \tag{3.16}$$

where the pulsewidth is determined from the eigenvalue relations to be

$$\tau_p = \sqrt[4]{g/M}\ \frac{1}{\sqrt{\omega_L \omega_M}}\ . \tag{3.17}$$

Excluding the weak dependence on saturated gain, the width of the forced modelocked pulse is seen to depend only on the fixed system parameters. As one might expect, this contrasts sharply with the pulsewidth equation for passive modelocking (3.14) in which the pulsewidth is found to vary inversely with the peak amplitude of the pulse.

The validity of the pulsewidth relation (3.17) was verified by taking measurements of pulsewidth versus pressure on our system. The crystal was driven at its 20.7859 MHz resonance where the reflected power was kept less than 5%. The absolute single pass modulation depth at the resonace, $\Delta\omega_c T_R M/2 = .08 \pm .01$, was determined prior to mounting the modulator in the modelocked system by measuring the transmission of the driven modulator to the cw 10.6 μ output of a

low pressure CO_2 laser. The modulation depth relative to the estimated cavity loss $\Delta\omega_c T_R \cong .4$, then becomes $M \simeq .4$. The normalized maximum gain g_m was kept at a value of 7.5 by varying the capacitor voltage with pressure as prescribed by the curves in Figure 27.

From the numbers given above we compute the linewidth dependence of τ_p as

$$\tau_p \cong .73 \cdot 10^{-7} \; \frac{1}{\sqrt{\nu_L}} \; s \tag{3.18}$$

where $\nu_L = \omega_L/\pi$ is the full linewidth in MHz. The linewidth was determined from the total laser pressure by the relation $\nu_L = 4.5$ MHz/torr. A comparison of the pulsewidths measured and the theoretically predicted relation (3.18) is shown in Figure 38. Agreement between theory and experiment is excellent. The validity of the forced modelocking theory applied to the transient system lends further credence to the passive modelocking theory, since the theories make similar fundamental assumptions about the system behavior.
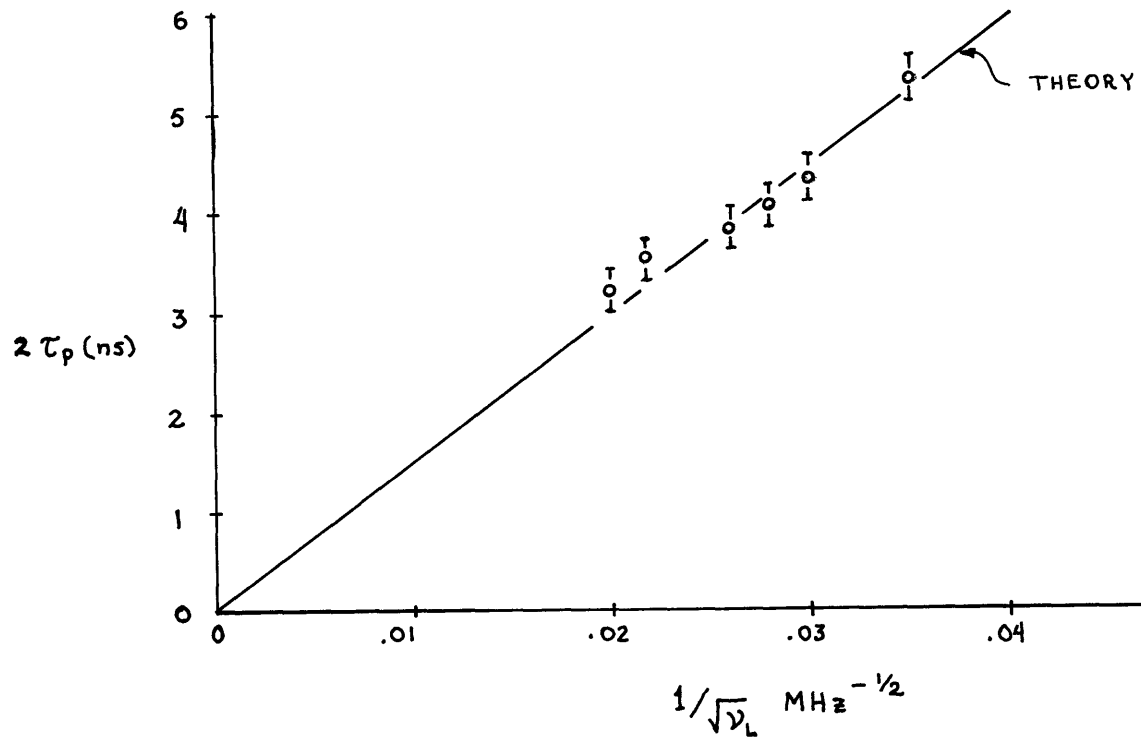
Figure 38: Forced Modelocked Pulsewidth Dependence on
Laser Linewidth

IV. Short Pulse Saturation of High Pressure SF_6

Interest in the short pulse saturation properties of SF_6 stems from its usefulness as a Q switching[58,59] and modelocking[5,8] element for the P branch of the 10.6 μ band of the CO_2 laser. More recently, work on laser isotope separation using SF_6 has intensified that interest.

Our primary motivation in carrying out the present study of SF_6 short pulse saturation is to determine the characteristics of the medium appropriate to modelocking the high pressure CO_2 laser. The modelocking mechanism is the bleaching of the SF_6 absorption on the time scale of the modelocked pulses. Thus, the absorption must, in part, be due to a set of levels having a relaxation time on the order of or less than the typical width of the modelocked pulse. In other words, the attenuation experienced by an intense pulse of duration τ_p in propagating through a cell of SF_6 should be less than that experienced by a long pulse signal of the same energy. By long pulse we mean a pulse of duration T_p greater than that of the modelocked pulse, but less than the V - T relaxation time of SF_6, i.e.,

$$\tau_p \ll T_p \ll T_{V-T}.$$

We have completed a set of experiments which verify this fact. By alternately irradiating a cell of SF_6 with the single mode output and the modelocked output of a high pressure TEA CO_2 laser we have measured the difference in transmission of the cell for equal values of the total energy in the TEA pulse.

The complexity of the energy level structure of SF_6, shown in Figure 39, makes it difficult to analyze. Models developed by Burak et al[60] and Brunet[62] show excellent agreement with experiments on the cw saturation of SF_6. Closer scrutiny of these experiments reveals that the only sensitive parameter is the "bottleneck" V - T relaxation, which may not even be identical to the one measured by ultrasonic dispersion experiments.[63]

The response of SF_6 to short pulses, however, is not well understood. The experiments can be interpreted in different ways. Steinfeld et al[49] set up a model which explains their double resonance results. The risetime of the 16 μ radiation measured by Knudtson and Flynn[64] can be explained by a similar model. The basic postulate of the model is that all modes of SF_6 come to equilibrium quickly. Their experiments can be explained even if this is only partly true. In addition, the model completely neglects the fast V-V process within the pumped (ν_3) mode. The more recent model adopted
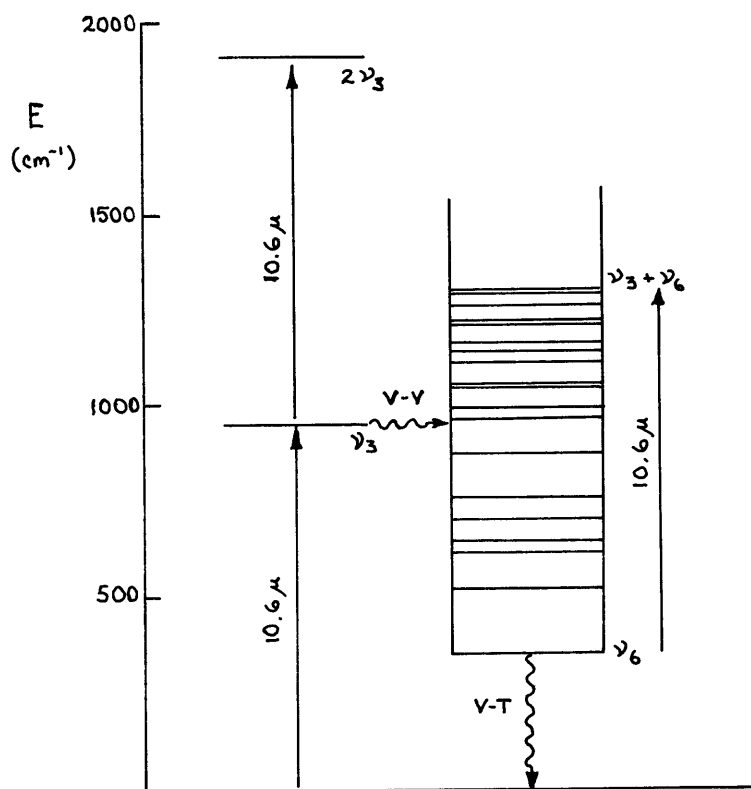
Figure 39:   Energy Level Diagram for SF_6

by Oppenheim and Kaufman[59] includes the V-V process, but is unrealistic in that it assumes an instantaneous relaxation rate for the excited state transition. Pulse transmission measurements have also been performed by Armstrong and Gaddy,[65] but their model ignores V-V equilibration and neglects the $\nu_3 \rightarrow 2\nu_3$ excited state absorption. The model's prediction of a $\nu_6 \rightarrow \nu_3 \rightarrow \nu_6$ relaxation time which is much faster than gas kinetic and a V-T time which is at least two times faster than previously determined values[62,63] is a measure of its weakness.

We have developed a simple closed form theory to explain the saturation curves for both the single mode and modelocked TEA pulse. The lower absorption seen by the modelocked TEA pulse is shown to be due to the increase in rotational bleaching. Our approach is similar to that of Oppenheim and Kaufman in that initially we consider only the absorption of the ν_3 mode and neglect the coupling to other vibrational modes of the molecule. Our model can be extended, however, to include the effect of additional modes, provided we make simplifying assumptions about the molecule. Furthermore, in contrast to previous work, we include the three fold degeneracy of the ν_3 mode and the saturation of the excited state absorption $\nu_3 \rightarrow 2\nu_3$ as influenced by the fast V-V relaxation process.

In section 4.1 we describe our experimental results.

The theory is presented in three sections, 4.2-4.4, corresponding to the major effects considered: (1) Saturation due to the pumping of the vibrational manifold, (2) bleaching of the rotational levels interacting directly with the incident radiation, and (3) pressure and power broadening of the absorbing transitions. A comparison of theory to experiment is presented in section 4.5.

4.1 Measurements

The transmission of SF_6 at the P(16) and P(22) lines of the 10.6 μ band of the TEA CO_2 laser was measured over a range of SF_6 pressures and TEA pulse intensities. The experimental setup is shown in Figure 40. Two distinct cases were compared:

1. Transmission of a single mode TEA pulse shown in Figure 41 through a 1 mm long cell containing SF_6.

2. Transmission of a modelocked TEA pulse shown in Figure 41 through the same cell. The modelocked TEA pulse consisted of a train of 2 ns pulses spaced 24 ns apart, thus giving a 12:1 peak power enhancement over the single mode TEA pulse of equal total energy.

In both cases the TEA pulse was generated by a three electrode CO_2 laser operated at a total pressure of 460 Torr, with a CO_2:N_2:He gas mix of 2:1:4. An intracavity aperture limited the operation of the laser to the fundamental transverse mode. Allowed to run freely, the TEA laser output showed erratic self locking. Consistent single mode operation was achieved with a 2.5 cm long intracavity cell of low pressure SF_6 (< 2 torr). On the other hand, consistent modelocking was produced by an intracavity acousto-optic modulator tuned to the cavity mode spacing at approximately
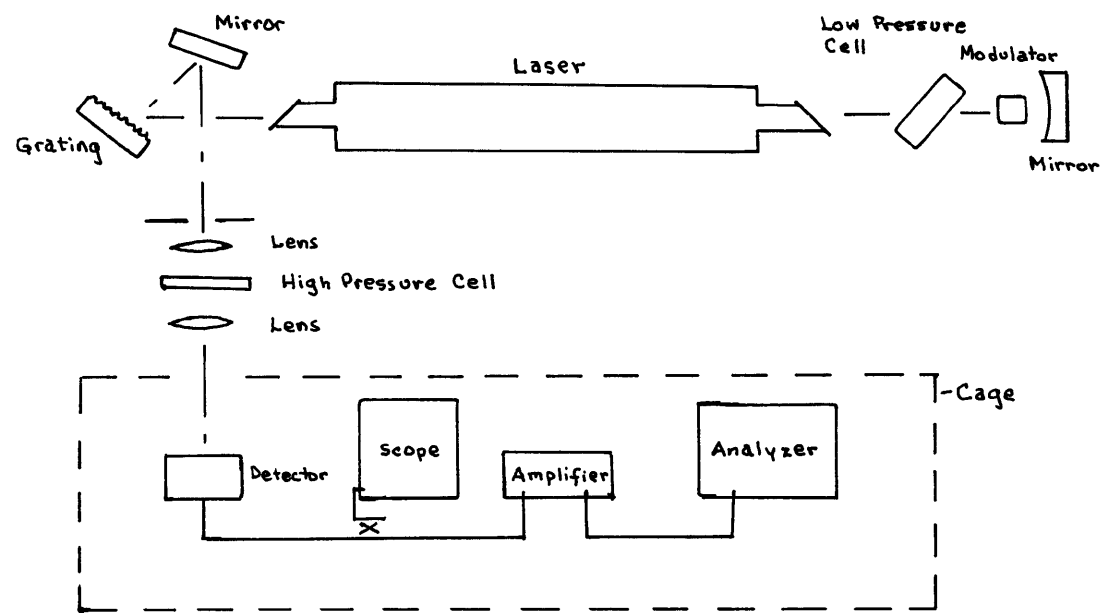
Figure 40: Experimental Set-Up for Measurement of SF$_6$ Saturation

Single Mode

20 ns/D

Modelocked

20 ns/D

2 Modelocked Pulses

5 ns/D
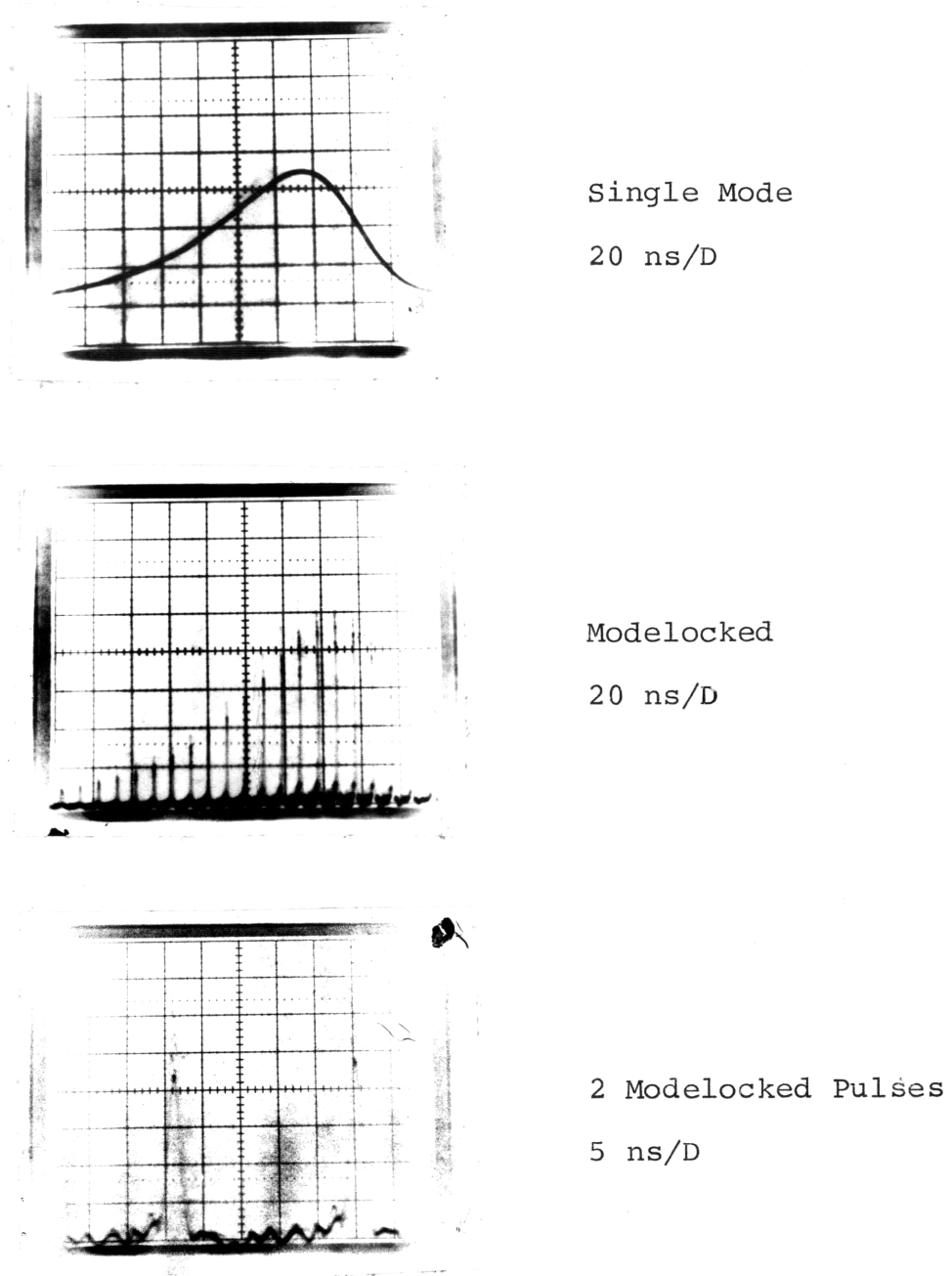
Figure 41: Pulses Incident on SF_6 Cell

42 MHz.

The output of the TEA laser was passed through a 3 mm aperture to ensure a nearly uniform intensity distribution across the beam and focussed by a salt lens to a .2 mm diameter spot inside the SF_6 cell. A second lens recollimated the beam before it was detected by a Au:Ge detector. Different values of input intensity were achieved by placing calibrated CaF_2 attentuators in the path of the beam. From the detector the signal was amplified by an amplifier which was slow ($\sim$ 5 μs) compared to the TEA pulse ($\sim$ 250 ns) so that its response depended only on the total energy in the TEA pulse. The amplifier output was then fed into a RIDL 400 channel pulse height analyzer which displayed the distribution of transmitted TEA pulse energy for successive shots of the laser. The use of the analyzer enabled us to distinquish between shot to shot fluctuations in the laser output energy ($\sim$ 10%) and differences in absorber transmission.

Results of the transmission measurements at various SF_6 pressures for the P(16) and P(22) lines of 10.6 μ CO_2 output are shown in Figures 42 and 43 respectively. The mode-locked pulse transmission is always higher than that of the single mode pulse. Furthermore, we observe that the saturation curves appear to be roughly asymptotic to the small signal absorption values measured by Wood et al.[48] indicating that the absorption cross-section does not change appreciably with pressure.
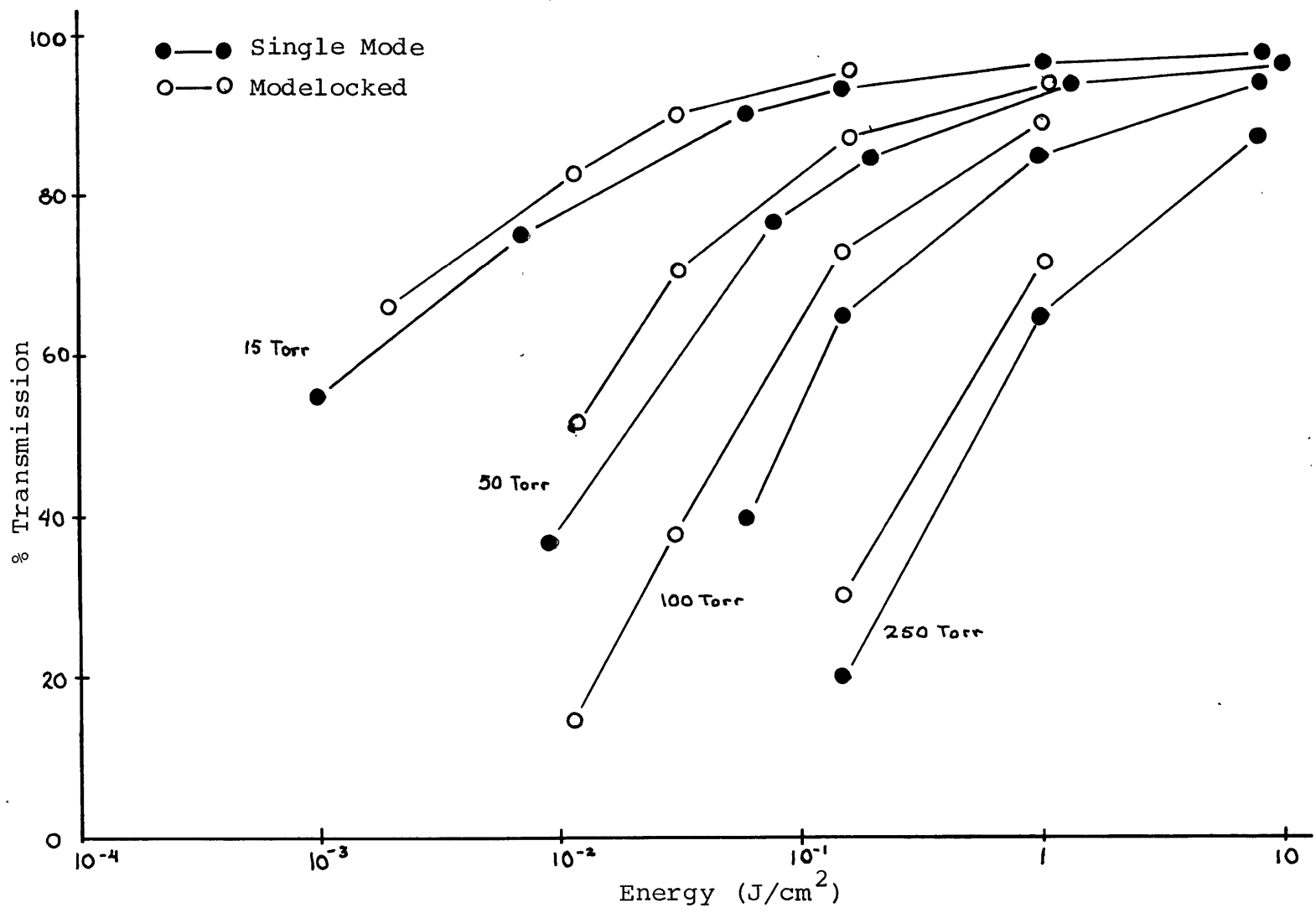
Figure 42: Transmission Measurements on P(16)
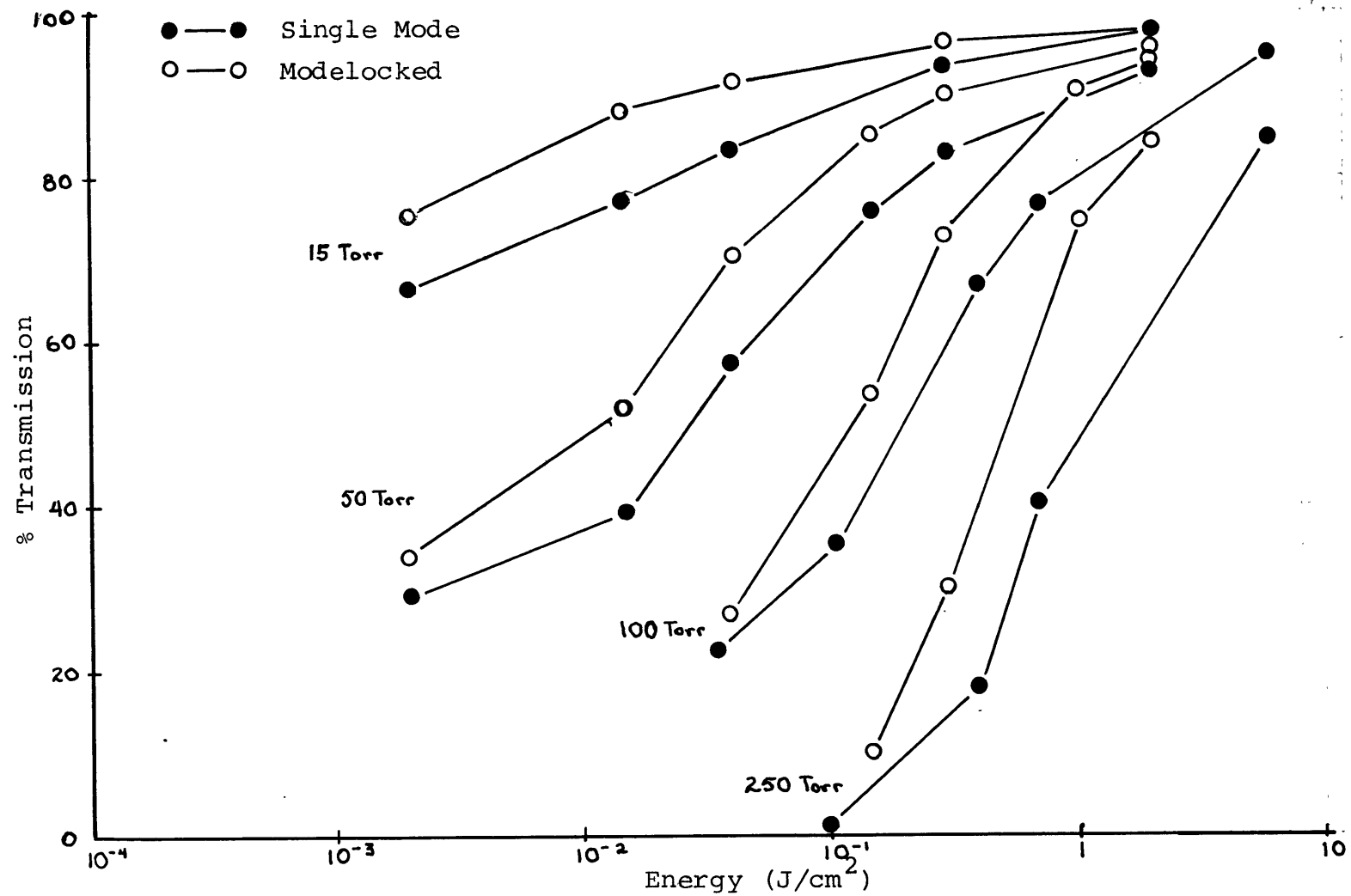
Figure 43: Transmission Measurements on P(22)

4.2 Pumping of the Vibrational Manifold

In order to describe the saturation behavior of SF_6 for the different lines of the 10.6 μ band we must consider the response of both the ground state and the excited state absorption. We adopt a model shown in Figure 44, which is similar to those described by Burak et al,[60] Brunet[62] and Oppenheim.[59] In our model we take into account the fast V-V processes that will thermalize any given vibrational mode at a vibrational temperature T_V. A theoretical justification for the use of "box" models will be given in a forthcoming publication.[66] The following notation is used:

N_1, N_2, N_2', N_3 Population densities in the three vibrational levels which are directly interacting with the incident field.

N_{11}, N_{22}, N_{33} Population densities which do not interact directly with the field.

σ_ν Absorption corss-sections of the rotational levels which interact directly with the incident field.

R   Rotational relaxation rate.
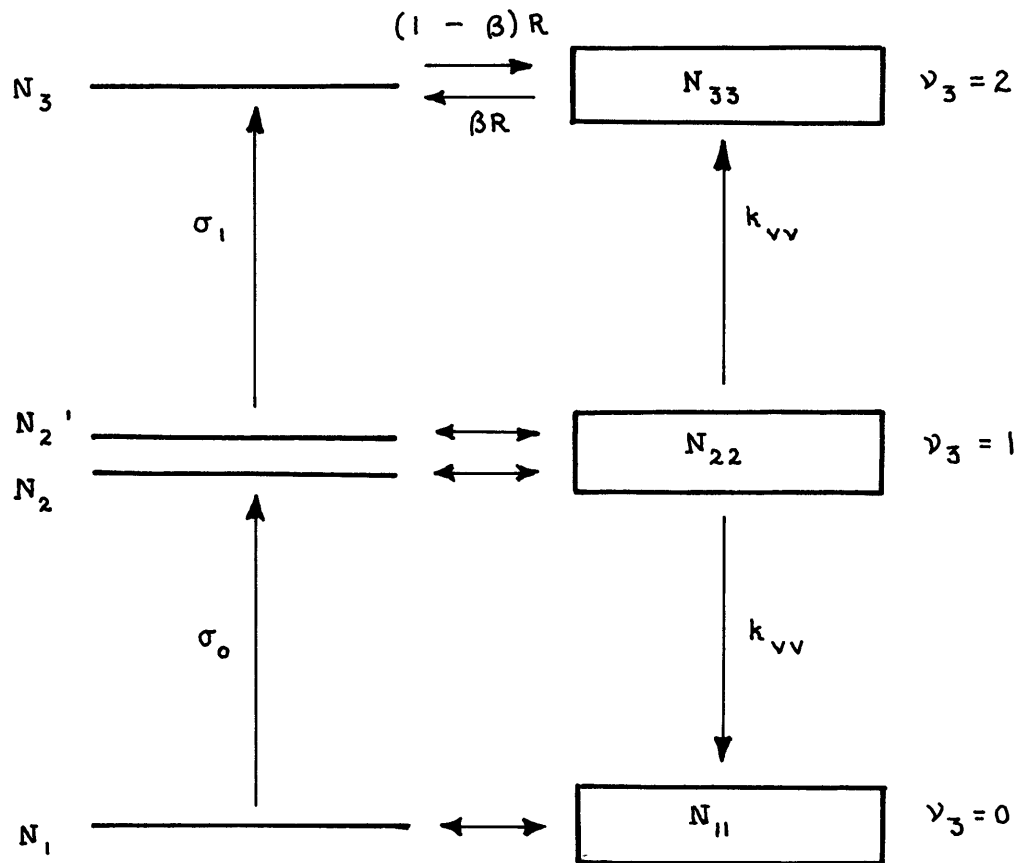
Figure 44: Model of SF_6 Energy Levels

β_ν Fraction of total number of molecules in the νth vibrational level which interact directly with the field.

k_{vv} Rate constant for equilibration among the vibrational levels.

We have omitted any reference to the V-T relaxation time because it is slow compared to our pulse duration. Measured values of the V-T rate place it at 95 μs/torr[61] which is much greater than our 250 ns pulsewidth even at 250 torr, the maximum pressure used in our experiments.

The absorption coefficient for the medium modelled in Figure 44 is given by

$$\alpha = \sigma_o \left[N_1 - \frac{g_1}{g_2} N_2 \right] + \sigma_1 \left[N_2' - \frac{g_2}{g_3} N_3 \right] \qquad (4.1)$$

where g_ν is the dengeneracy of the νth vibrational level. From the symmetry properties of the SF_6 molecule we know the ν_3 mode is three fold degenerate so that the level degeneracies are given by

$$g_1 = 1, \quad g_2 = 3, \quad g_3 = 6.$$

We neglect the absorption contribution of vibrational states higher than the first excited state because of the increasing anharmonicity of the vibrational mode. Furthermore, we should note the following: $N_\nu = \beta_\nu N_{\nu\nu}$. Pressure and power broadening influence both β_ν and σ_ν in such a way that, in a continuous spectrum like SF_6, the product $\sigma_\nu \beta_\nu$ is constant. This results in an absorption coefficient that is independent of pressure or power for a given vibrational population $N_\nu + N_{\nu\nu}$. Increasing the pressure or the laser power results in an increase in β_ν and a decrease in σ_ν--the only direct influence being on the "effective" rotational relaxation rate $\beta_\nu R$.

To determine the absorption seen by the TEA pulse we shall assume that both the rotational and vibrational levels remain in thermal equilibrium. The assumption is justified by the fact that both the rotational relaxation rate and the vibrational equilibration rate, measured as 10^7 sec^{-1} - torr^{-1} and $10^5 - 10^6$ sec^{-1} - torr^{-1} [63] respectively, are short compared to the pulsewidth in the range of pressures we have investigated. The assumption that thermal equilibrium is maintained among both the rotational and vibrational levels in the presence of the incident field can be expressed mathematically as follows:

R-T Equilibrium: $$\frac{N_\nu}{N_{\nu\nu}} = \frac{\beta_\nu}{1 - \beta_\nu}$$ (4.2)

V-V Equilibrium:
$$\frac{N_{22}}{N_{11}} = \frac{g_2}{g_1} \exp\left(-\frac{\hbar\omega_{12}}{kT_V}\right) \ ,$$

$$\frac{N_{33}}{N_{22}} = \frac{g_3}{g_2} \exp\left(-\frac{\hbar\omega_{23}}{kT_V}\right) \tag{4.3}$$

where ω_{ij} is the transition frequency and T_V is the vibrational temperature. Since the V-T time is slow, all of the incident energy absorbed by the medium is distributed throughout the vibrational manifold. Thus, saturation occurs as the ν_3 mode of the medium is pumped to a higher vibrational temperature T_V. For sufficiently high absorbed energy, $kT_V \gg \hbar\omega_{12}$, $\hbar\omega_{23}$, the population difference between the absorbing levels goes to zero and the medium is totally bleached.

Assuming that coupling to the other vibrational modes can be neglected, the total absorbed energy is equal to the energy in the ν_3 manifold

$$E_{abs} = \sum_\nu N_\nu{}^t \tag{4.4}$$

where $N_\nu{}^t$ is the total density of molecules having energy ε_ν above the ground state. According to the Maxwell-Boltzmann distribution law the numbers $N_\nu{}^t$ are given by

$$N_\nu{}^t = \frac{Ng_\nu \exp\left(-\dfrac{\varepsilon_\nu}{kT_\nu}\right)}{Q} \qquad (4.5)$$

where N is the total population density and Q is the partition function of the ν_3 vibrational mode. Using (4.5) the expression for the absorbed energy becomes

$$E_{abs} = \frac{N}{Q} \sum_\nu g_\nu \, \varepsilon_\nu \, \exp\left(-\frac{\varepsilon_\nu}{kT_\nu}\right) \qquad (4.6)$$

which can be rewritten as[66]

$$E_{abs} = Nk \, T_V{}^2 \frac{1}{Q} \frac{dQ}{dT_V} \, . \qquad (4.7)$$

The partition function for the triply degenerate ν_3 mode is given, in the harmonic oscillator approximation, by

$$Q = [1 - \exp(-\hbar\omega_o/kT_V)]^{-3} \qquad (4.8)$$

where $\hbar\omega_o$ is the energy separation between levels, assumed to be constant.

Substituting (4.8) in (4.7) and defining $\gamma \equiv \hbar\omega_o/kT_V$ we obtain the expression for the absorbed energy

$$E_{abs} = \frac{3N \, \hbar\omega_o}{e^\gamma - 1} \qquad (4.9)$$

which is Planck's law for a triply degenerate vibrational mode. Alternatively we can express the vibrational temperature in terms of the number of photons absorbed per molecule $n_p \equiv E_{abs}/N\hbar\omega_o$:

$$T_V = \frac{\hbar\omega_o}{k \, \ln \left(\dfrac{3 + n_p}{n_p} \right)} . \qquad (4.10)$$

Returning to equation (4.5) we see that the number of molecules in a given level of the ν_3 manifold is given in terms of the number of absorbed photons by

$$N_\nu{}^t = (1 + \beta_\nu) N_{\nu\nu} = N g_\nu \left(\frac{3}{3 + n_p} \right)^3 \left(\frac{n_p}{3 + n_p} \right)^\nu . \qquad (4.11)$$

We now assume

$$\beta_1 = \beta_2 = \beta_2{}' = \beta_3 \equiv \beta \ll 1 \qquad (4.12)$$

namely, that only a small fraction of the molecules in each

level interacts with the radiation (this number has been estimated to be $\sim .003$[52] for $P(20)$). Equation (4.11) combined with (4.1) gives the dependence of the absorption coefficient on the number of absorbed photons:

$$\alpha \simeq \beta N\sigma_o \left(\frac{3}{3 + n_p}\right)^4 \left(1 + \kappa \frac{3n_p}{3 + n_p}\right) \tag{4.13}$$

where $\kappa = \sigma_1/\sigma_o$. The small signal absorption coefficient is, therefore,

$$\alpha_{n_p \to 0} = \alpha_o = \beta N\sigma_o. \tag{4.14}$$

The absorption coefficient is related to the field intensity I by

$$\alpha = -\frac{1}{I}\frac{dI}{dx}. \tag{4.15}$$

For an optically thin sample of length ℓ (4.15) can be written in terms of the incident intensity and the time rate of change of the number of absorbed photons per molecule

$$I_{in} - I_{out} = I_{in}\,\ell\alpha = \hbar\omega_o\,N\ell\,\frac{dn_p}{dt}. \tag{4.16}$$

Thus, we have a first order differential equation relating
the number of absorbed photons to the incident intensity

$$\frac{dn_p}{dt} = \frac{\alpha_o I_{in}}{N \hbar\omega_o} \left(\frac{3}{3 + n_p}\right)^4 \left(1 + \kappa \frac{3n_p}{3 + n_p}\right) \quad .$$

(4.17)

The equation integrates to the form

$$\frac{1}{81} \int_3^{3 + n_p^t} \frac{x^5 \, dx}{(1 + 3) x - 9\kappa} = \frac{\alpha_o}{N} \frac{E_{in}}{\hbar\omega_o}$$

(4.18)

where E_{in} is the total incident energy in the pulse, i.e.

$$E_{in} = \int_{-\infty}^{\infty} I_{in} \, dt$$

(4.19)

and n_p^t is the total number of photons absorbed per mole-
cule. The left hand side of (4.18) can be integrated in
closed form.

The total energy absorbed by the medium is given by

$$\frac{E_{abs}}{\hbar\omega_o} = n_p^t \, NV$$

(4.20)

where V is the volume of the absorbing medium in the path of the radiation. The transmission T of the sample is defined as

$$T = \frac{E_{out}}{E_{in}} = 1 - \frac{E_{abs}}{E_{in}} . \tag{4.21}$$

Using (4.21) and (4.20) we can express the transmission as

$$T = 1 - \alpha_o \ell \frac{n_p{}^t}{F(n_p{}^t)} . \tag{4.22}$$

The saturation of the absorption of the optically thin sample is dependent on the ratio of the number of photons absorbed per molecule to the effective number of photons incident per molecule given by $F(n_p{}^t)$. Plots of $n_p{}^t/F(n_p{}^t)$ versus $n_p{}^t$ for various values of the cross section ratio κ are shown in Figure 45. The approximate cross section ratios in SF_6 for P(16), P(20) and P(22) radiation have been taken from the estimates of Steinfeld, et al.[49] The cross section ratio increases with increasing line number due to the red shift of the excited state transition with respect to the ground state transition which are listed in Table IV.

For values of κ greater than one the saturation curves
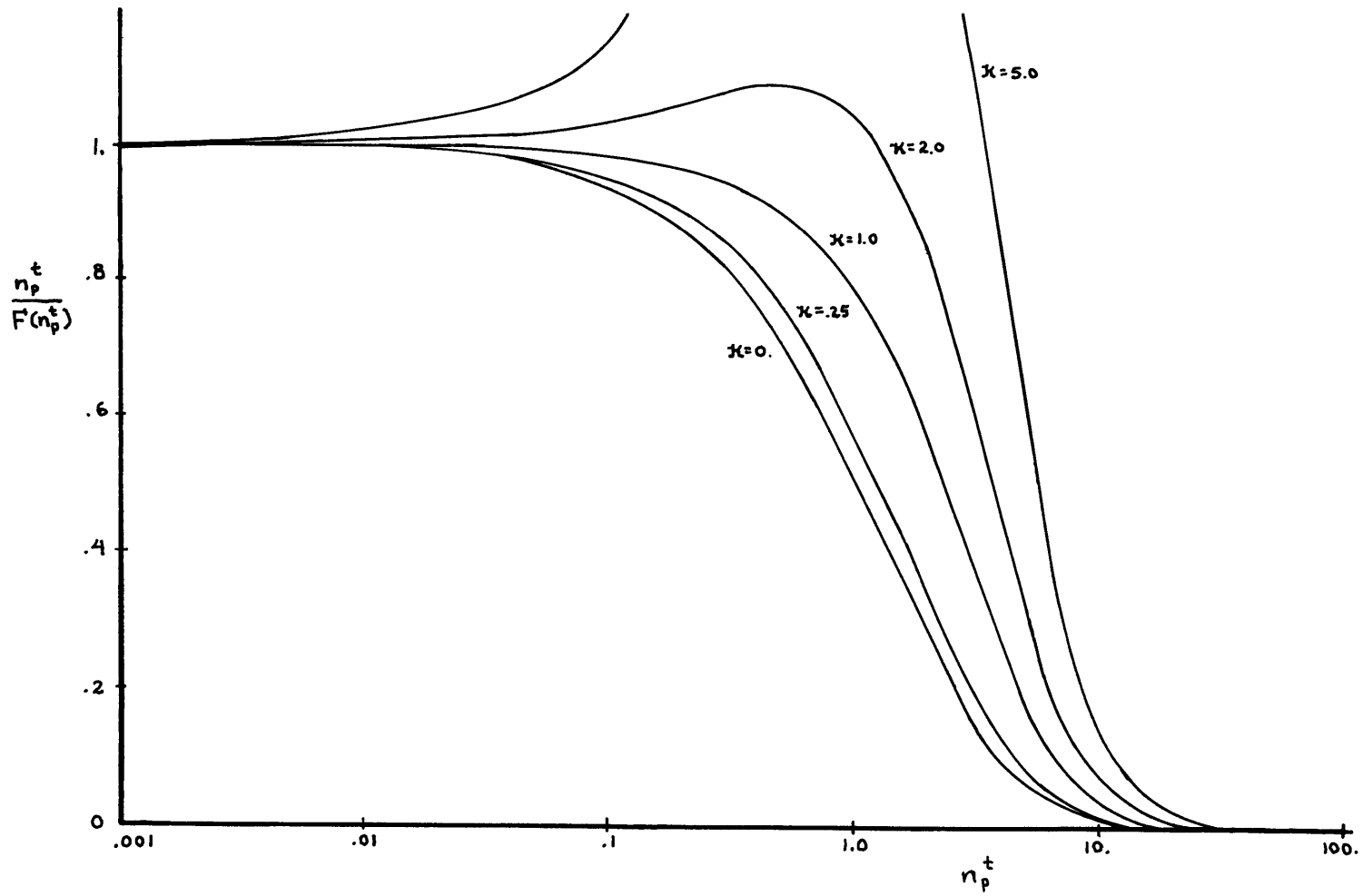
Figure 45: Universal Saturation Curves

Table IV

SF_6 Small Signal Absorption Coefficients and
Cross-Section Ratios on Different CO_2 Transitions

CO_2 Transition	$\alpha_o (cm^{-1} \cdot torr^{-1})$	κ
P(16)	.55	.25
P(20)	.46	1
P(22)	.25	2
P(24)	.19	3

of Figure 45 show an initial increase in absorption with
increasing incident energy (negative saturation) as the mole-
cules in the ground state are pumped to the lower level of
the excited state transition. The excited state transition
must be bleached before the medium saturates. Thus, we ex-
pect the saturation intensity of SF_6 at P(22) to be higher
than that at P(16), as is the case.

Thus far in our analysis we have considered only the role
of the ν_3 mode of SF_6 in the absorption. Following the
approach taken by Brunet   we can extend our modes to account
for the contribution of the other modes of SF_6 to the ab-
sorption of the 10.6 μ band of CO_2.

Brunet succeeded in fitting the saturation curves of
SF_6 excited by a cw CO_2 laser using the expression

$$\alpha + \beta = (\alpha_o + \beta_o) \ \frac{1 + \gamma^{-1} \dfrac{I}{I_s}}{1 + \dfrac{I}{I_s}} \ , \tag{4.23}$$

where $(\alpha_o + \beta_o)$ and $(\alpha + \beta)$ are the unsaturated and
saturated absorption coefficients which have been divided
into a part due to the ground state, α_o, and a part due to
the hot-bands, β_o. The parameter γ used by Brunet is a
measure of the residual absorption of the hot-band transition

in the limit $I \gg I_s$. The saturation intensity is given by

$$I_s = N \frac{\hbar\omega_o \, \eta_o}{\alpha_o \, T_{V-T}} \qquad (4.24)$$

where η_o is the fraction of molecules in the ground vibrational state.

Equation (4.23) is obtainable from an "optical pumping" model developed by Brunet. Photons are absorbed from the ground vibrational state and pump the $\nu_3 = 1$ level. Fast V-V processes, typified by the collisions:

$$SF_6(\nu_3) + SF_6(0) \begin{cases} \rightarrow SF_6(\nu_2) + SF_6(\nu_6) - 42 \text{ cm}^{-1} \\ \rightarrow SF_6(\nu_4) + SF_6(\nu_6) - 16 \text{ cm}^{-1} \\ \rightarrow SF_6(\nu_5) + SF_6(\nu_6) + 76 \text{ cm}^{-1} \end{cases} \qquad (4.25)$$
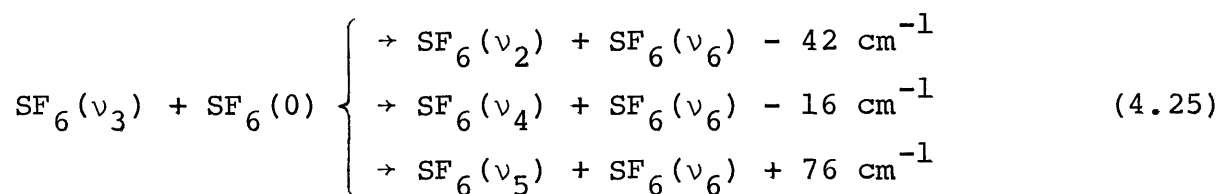
populate the ν_2, ν_4, ν_6 vibrations. Indeed, Knudtson and Flynn[63] have measured the risetime of the ν_4 vibration band as 1.1×10^{-6} sec-torr. Brunet then attributes a total population N_2 and an average absorption coefficient to these hot bands in order to obtain his formula.

Connection to our model can be made by introducing the

fast V-V collisions, of the type

$$SF_6(\nu_6) + SF_6(\nu_6) \rightarrow SF_6(2\nu_6) + SF_6(0) \quad \text{etc.} \qquad (4.26)$$
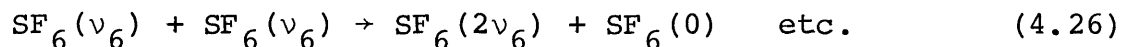
which set up the vibrational temperature within the ν_6 mode. If the population of the ν_6 mode becomes high ($N_2 > N_o$ in Brunet's notation) the fast V-V process will populate the higher vibrational states. The population of each state is given by Equation (4.5) when in Equation (4.10) n_p is replaced by N_2. We assume in the above that there is no transfer from states $k\nu_6$ to any other mode. For $N_2 << N_o$ we expect this to be a good approximation. A very complicated satuation can develop for $N_2 >> N_o$ where several modes are excited to various temperatures. A sweeping assumption can be made at this point, that the absorption of light by levels $SF_6(k\nu_6)$ $k = 1, 2, \ldots$ is all similar, i.e. all the bands $SF_6(k\nu_6) + h\nu \rightarrow SF_6(k\nu_6, \nu_3)$ [$(k\nu_6 + \nu_3)$ - ν_3 in Herzberg's notation] have the same oscillator strength and frequencies. If this is true, Brunet's formula follows.

In a similar manner we can extend our model to include V- other V relaxation processes. In order to give a specific example, we will assume that vibrational thermal equilibrium is maintained within the ν_3 (excited) mode, and in

addition we introduce the process

$$SF_6(\nu_3) + SF_6(0) \overset{\leftarrow}{\to} SF_6(\nu_4) + SF_6(\nu_6). \tag{4.27}$$

In equilibrium the vibrational temperatures of the modes satisfy

$$\gamma_3 = 2\gamma_4 = 2\gamma_6, \tag{4.28}$$

where the vibrational temperatures of the various modes are defined analogously to Equations (4.5)-(4.8). If we now make an assumption even more sweeping than before, i.e. that all $SF_6(k\nu_2,\ \ell\nu_6,\ \nu_3 = 0) + h\nu \to SF_6(k\nu_2,\ \ell\nu_6,\ \nu_3)$ absorption bands have the same frequency and absorption strength, we obtain the same "universal" absorption curves as in our old model, the only difference being that the horizontal scale, $n_p t$ is changed by a factor of 2, i.e., twice as many photons must be absorbed for the same amount of bleaching.

4.3 Rotational Bleaching

The pumping of the vibrational manifold is not the only saturation mechanism. We must also consider the instantaneous response of the rotational levels which interact directly with the incident field.

Under the assumption that both the vibrational and rotation levels remain equilibrated, the rate equations governing the population densities of the energy levels interacting directly with the radiation become[59]

$$\frac{dN_1}{dt} = -\frac{\sigma_o}{\hbar\omega_o} I \left[N_1 - \frac{g_1}{g_2} N_2 \right] - N_1 R - N_{11}^o \beta R$$

$$\frac{dN_2}{dt} = \frac{\sigma_o}{\hbar\omega_o} I \left[N_1 - \frac{g_1}{g_2} N_2 \right] - N_2 R + N_{22}^o \beta R \qquad (4.29)$$

$$\frac{dN_2'}{dt} = -\frac{\sigma_1}{\hbar\omega_o} I \left[N_2' - \frac{g_2}{g_3} N_3 \right] - N_2' R + N_{22} \beta R$$

$$\frac{dN_3}{dt} = \frac{\sigma_1}{\hbar\omega_o} I \left[N_2' - \frac{g_2}{g_3} N_3 \right] - N_3 R + N_{33}^o \beta R \qquad (4.30)$$

where N_{vv}^o is the population density of the levels not

interacting directly with the radiation and is determined from the vibrational distribution dictated by the total number of photons absorbed as in section 4.2. We see that the rate equations (4.29) and (4.30) describe two uncoupled two level absorbers whose population difference equations are

$$\frac{dn_1}{dt} = - \frac{\sigma_o}{\hbar\omega_o} \left[1 + \frac{g_1}{g_2} \right] In_1 - n_1 R + \left[N_{11}^o - \frac{g_1}{g_2} N_{22}^o \right] \beta R \quad (4.31)$$

$$\frac{dn_2}{dt} = - \frac{\sigma_1}{\hbar\omega_o} \left[1 + \frac{g_2}{g_3} \right] In_2 - n_2 R + \left[N_{22}^o - \frac{g_2}{g_3} N_{33}^o \right] \beta R \quad (4.32)$$

where we have defined

$$n_1 \equiv N_1 - \frac{g_1}{g_2} , \qquad n_2 \equiv N_2 - \frac{g_2}{g_3} N_3 . \quad (4.33)$$

The absorption coefficient of the medium is simply

$$\alpha = n_1 \sigma_o + n_2 \sigma_1 . \quad (4.34)$$

In the case where the rotational relaxation rate is fast

compared to the modelocked pulse width, i.e.

$$R \gg \frac{1}{\tau_p} \gg \frac{1}{T_p} \qquad (4.35)$$

the population densities of the levels interacting directly with the radiation are in staedy state with the incident field, so that

$$\frac{dn_1}{dt}, \quad \frac{dn_2}{dt} \simeq 0. \qquad (4.36)$$

Thus, the population differences are given by

$$n_1(t) = \frac{\left(N_{11}^o - \frac{g_1}{g_2} N_{22}^o \right)\beta}{1 + \frac{I(t)}{I_1}} \qquad (4.37)$$

$$n_2(t) = \frac{\left(N_{22}^o - \frac{g_2}{g_3} N_{33}^o \right)\beta}{1 + \frac{I(t)}{I_2}} \qquad (4.38)$$

where we have defined the saturation intensities

$$I_1 \equiv \frac{R \, \hbar\omega_o}{\sigma_o \left(1 + \dfrac{g_1}{g_2}\right)}$$

$$I_2 \equiv \frac{R \, \hbar\omega_o}{\sigma_o \left(1 + \dfrac{g_2}{g_3}\right)} \, . \tag{4.39}$$

Equations (4.37) and (4.38) describe the instantaneous response of the absorber. We now wish to determine the medium response to the entire TEA pulse, both single mode and mode-locking. To do so we model the TEA pulse as shown in Figure 46. The single mode TEA pulse is taken to be a square pulse of duration T_p and intensity I_{SM}. The modelocked TEA pulse consists of a train of equal amplitude rectangular pulses of peak amplitude I_{ML} and duration τ_p separated by the time T_R and lasting for a time T_p. Defining a fast time scale t local to an individual modelocked pulse and a slow time $T = k \, T_R$, where k is an integer counting the pulses in the train, we see from (4.16) that the number of photons absorbed per molecule is governed by the differential equation

$\tau_p = 2.5 ns$

$T_R = 25 ns$

$T_p = 250 ns$
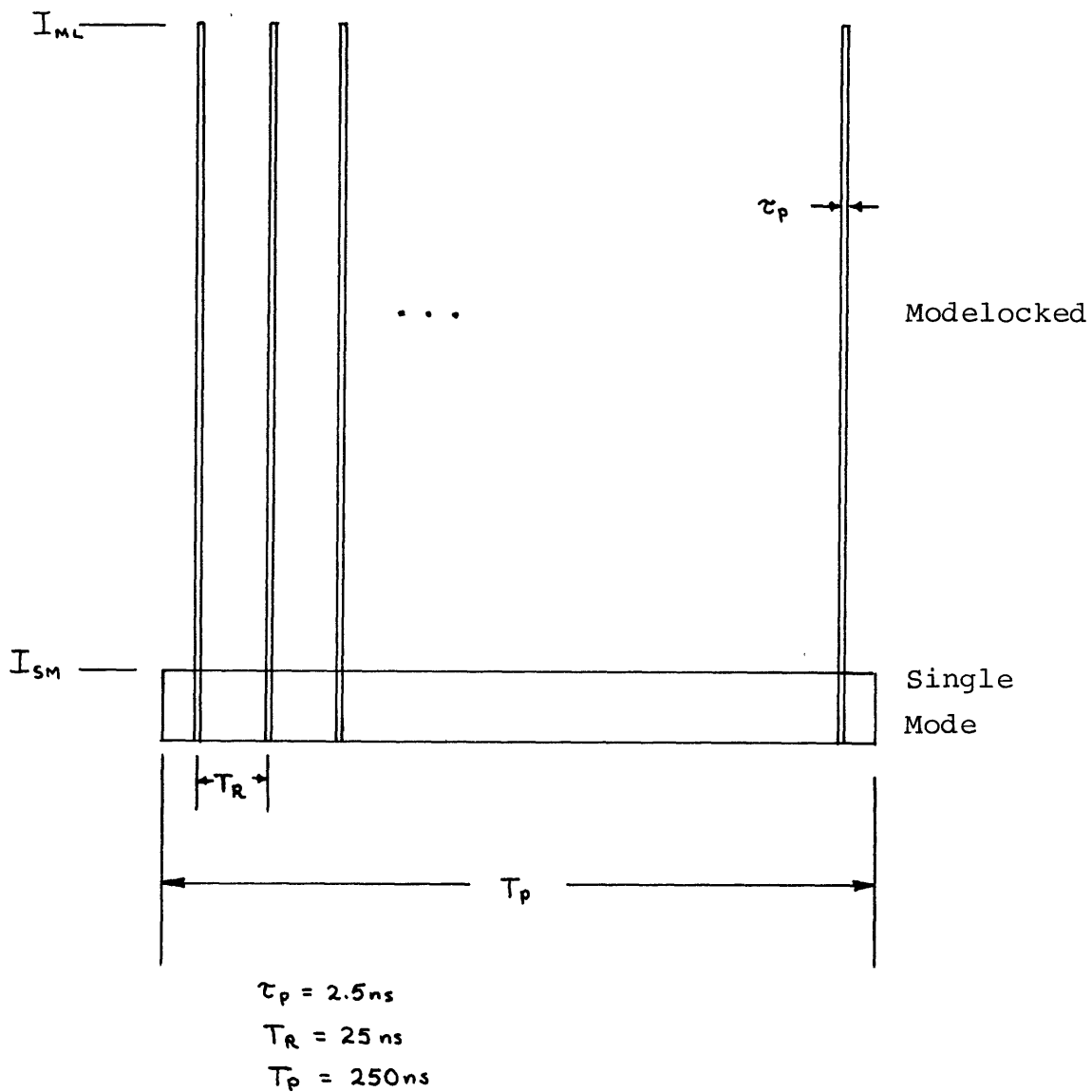
Figure 46: Model of the Incident TEA Pulse

$$\frac{\partial}{\partial t}\left[\frac{\partial n_p}{\partial T}\right] = \frac{\alpha_o}{NT_R}\frac{I(t)}{\hbar\omega_o}\left[n_1(t,\,T) + \kappa n_2(t,\,T)\right].\qquad(4.39)$$

The population differences n_1 and n_2 are found from (4.37) and (4.38) where the population densities $N_{VV}^o(T)$ are now allowed to be functions of the slow time T.

Since we have taken both the single mode and the mode-locked pulses to be rectangular, (4.39) can be integrated directly in t to give

$$\frac{dn_p}{dT} = \frac{\alpha_o\,\tau_p}{NT_R}\frac{I}{\hbar\omega_o}\left[n_1(T) + \kappa n_2(T)\right].\qquad(4.40)$$

The vibrational levels are assumed equilibrated on the slow time scale T, so that substituting (4.37) and (4.38) in (4.40) and making use of (4.11) we obtain

$$\frac{dn_p}{dT} = \frac{\alpha_o'\,t_p}{\hbar\omega_o N\,T_R} I\left(\frac{3}{3+n_p}\right)^3\left|1 + \kappa'\left(\frac{3n_p}{3+n_p}\right)\right|\qquad(4.41)$$

where we have defined

$$\alpha_o{}' = \frac{\alpha_o}{1 + \dfrac{I}{I_1}} \qquad (4.42)$$

and

$$\kappa{}' = \kappa \left(\frac{1 + \dfrac{I}{I_1}}{1 + \dfrac{I}{I_2}} \right) . \qquad (4.43)$$

Equation (4.41) now integrates to the form

$$\frac{1}{81} \int_3^{3 + n_p{}^t} \frac{x^5 \, dx}{(1 + 3\kappa')x - 9\kappa'} = \frac{\alpha_o{}'}{\hbar\omega_o} E_{in} \qquad (4.44)$$

and we have recognized that the total energy incident is given by

$$E_{in} = \frac{\tau_p T_p}{T_R} I. \qquad (4.45)$$

The integral in (4.44) is of the same form as $F(n_p{}^t)$ defined by (4.19).

Equation (4.44) is applicable to both the single mode and the modelocked response. For the single mode response

we set $\tau_p = T_R$ and $I = I_{SM}$. In the case of the modelocked response $\tau_p \ll T_R$ and $I = I_{ML}$.

we set $\tau_p = T_R$ and $I = I_{SM}$. In the case of the modelocked response $\tau_p \ll T_R$ and $I = I_{ML}$.

4.4 Line Broadening

In section 4.2 we argued that the product $\sigma_\nu \beta_\nu$ remains invariant under the influence of pressure and power broadening, so that broadening effects play no role in the saturation due to the pumping of the vibrational manifold. As indicated in (4.39), however, the cross-section alone enters into the expressions for the saturation intensities for rotational bleaching. We now examine the influence of pressure and power broadening on the rotational saturation behavior of SF_6. Pressure broadening is found to be negligible, while power broadening is found to be significant over the range of pressure and power used in the experiments.

Earlier we defined the fraction of the total number of molecules in a given vibrational state which can absorb the incident radiation as

$$\beta_\nu = \frac{N_\nu}{N_\nu + N_{\nu\nu}} .$$

(4.46)

By doing so we determine an effective bandwidth for the absorber

$$\delta f_{eff} = \beta \Delta f$$

(4.47)

where Δf is the total width of the absorption band. For SF_6 Δf is of the order of 10 cm^{-1}.[61] Low pressure measurements of cw SF_6 saturation indicate a value of .003 for β at $P(20)$, resulting in an effective bandwidth $\Delta f_{eff} = .03$ cm^{-1}. Studies of the SF_6 spectrum in the 10.6 μ regime show a density of one line per 10^{-3} cm^{-1}.[61] Thus, δf_{eff} encompasses about thirty lines of the spectrum. Furthermore, δf_{eff} is much wider than the linewidth of an individual transition. As noted by previous authors[52,61] it is therefore likely that a superposition of absorbing transitions is responsible for SF_6 absorption at each P line of the 10.6 μ CO_2 band.

The homogeneous linewidth of an individual SF_6 transition can be estimated from its relaxation time, namely

$$\delta f_H \simeq <\tau>^{-1} = \frac{1}{\pi} (R_{V-V} + R_{R-T}) + \frac{1}{2\pi\tau_{rad}} \qquad (4.48)$$

where R_{V-V} and R_{R-T} are the vibrational and rotational equilibration rates and τ_{rad} is the radiative lifetime of the upper state. When subjected to intense radiation the net relaxation time is further shortened by saturation broadening, giving

$$\delta f_H = \frac{1}{\pi} (R_{V-V} + R_{R-T}) + \frac{1}{2\pi\tau_{rad}} + \frac{IB_{12}}{\pi\delta f_H} . \qquad (4.49)$$

B_{12} is the Einstein absorption coefficient for the ground state transition given by

$$B_{12} = \frac{\alpha_o \Delta f}{\hbar \omega_o N} .$$
(4.50)

The radiative lifetime is related to B_{12} via the expression for the emission coefficient A_{21}

$$\frac{1}{\tau_{rad}} = A_{21} = 8\pi h \frac{f_o^3}{c^2} \frac{g_1}{g_2} B_{12}.$$
(4.51)

The long radiative lifetime dictated by (4.51) enables us to drop the second term of (4.49). Furthermore, our knowledge that R_{R-T} is at least an order of magnitude greater than R_{V-V} enables us to neglect the R_{V-V} term. Solving (4.49) for δf_H now gives

$$\delta f_H = \frac{1}{2\pi} [R_{R-T} + (R_{R-T}^2 + 4\pi \, IB_{12})^{1/2}] .$$
(4.52)

Thus, the homogeneous linewidth is pressure and power dependent and the effective absorber bandwidth becomes

$$\delta f_{eff} = \beta \Delta f \sqrt{1 + (\delta f_H/\beta \Delta f)^2} .$$
(4.53)

At low incident intensities pressure broadening is the dominant mechanism in determining δf_H. Using the value $R_{R-T} = 10^7 \text{ s}^{-1} - \text{torr}^{-1}$ we obtain $\delta f_H \simeq 3 \text{ MHz torr}^{-1}$. Thus, $\delta f_H = \beta \Delta f$ at a pressure of 300 torr. Below 300 torr pressure broadening does not play a significant role in determining δf_{eff}.

At pressures below 300 torr we need only consider the effect of power broadening, i.e.

$$\delta f_H \simeq \sqrt{\frac{I \, B_{12}}{\pi}} . \tag{4.54}$$

The intensity at which saturation broadening becomes significant is determined by

$$I_{sb} = \frac{\pi (\beta \Delta f)^2}{B_{12}} . \tag{4.55}$$

For P(20) we calculate $B_{12} = 2.4 \cdot 10^7 \text{ cm}^2 - \text{erg}^{-1} - \text{s}^{-1}$ using the small signal absorption coefficient given, $\alpha_o = .46 \text{ cm}^{-1} \text{ torr}^{-1}$.[62] (4.55) then gives $I_{sb} \sim 10 \text{ KW/cm}^2$. Assuming for the sake of simplicity that our single mode TEA pulse is a rectangular pulse of duration $T_p = 400 \text{ ns}$, the pulse energy at which saturation broadening becomes

significant is $E_{sb} \sim 4$ mj. Thus, saturation broadening is an important effect over the range of pulse energy used in our experiments.

Our treatment of saturation broadening, limited so far to the ground state transition, can be applied to the excited state transition as well. Since the total absorption bandwidth of the two transitions is approximately equal,[49] the Einstein absorption coefficient of the excited state transition is given by

$$B_{23} = \kappa \, B_{12}. \qquad (4.56)$$

Thus, the excited state transition has a homogeneous linewidth given by (4.52) where B_{23} is substituted for B_{12}. The two transitions are now characterized by different values of σ_ν:

$$\sigma_\nu' = \sigma_\nu \left[1 + \left(\frac{\delta f_{H\nu}}{\beta \Delta f} \right)^2 \right]^{-1/2}. \qquad (4.57)$$

To incorporate line broadening into our saturation analysis, we make the substitution $\sigma_\nu \to \sigma_\nu'$ in equations (4.39). The effect of saturation broadening is to make the medium harder to saturate since, in effect, the relaxation rate R increases with the incident field intensity.

4.5 Comparison of Theory to Experiment

The theoretical transmission curves for the single

mode and modelocked TEA pulse were computed from (4.44)

including the effects of line broadening via (4.57). The

theoretical curves are compared to the experimental results

of section 4.1 in Figures 47 and 48. The fact that the

increase in transmission predicted by the theory is in

reasonably good agreement with that observed, verifies the

underlying premise of the analysis that it is the fast

rotational bleaching which causes the higher transmission

of the modelocked pulse train at a given TEA pulse energy.

We conclude that rotational bleaching is responsible

for the inducement of passive modelocking in the experi-

ments discussed in Chapter III. This conflicts with the

hypothesis of previous authors that the mode coupling is

caused by the dielectric nonlinearity in SF_6,[37,38] rather

than the absorption nonlinearity. Although the dielectric

response can play a role, the effect of the absorption

response must, almost by definition, dominate in a satur-

able absorber. Furthermore, the stability of the mode-

locked pulse requires a fast absorption response in order

to ensure that the net gain between the modelocked pulses

in smaller than at their peak.[66]

The theoretical and experimental curves are seen not
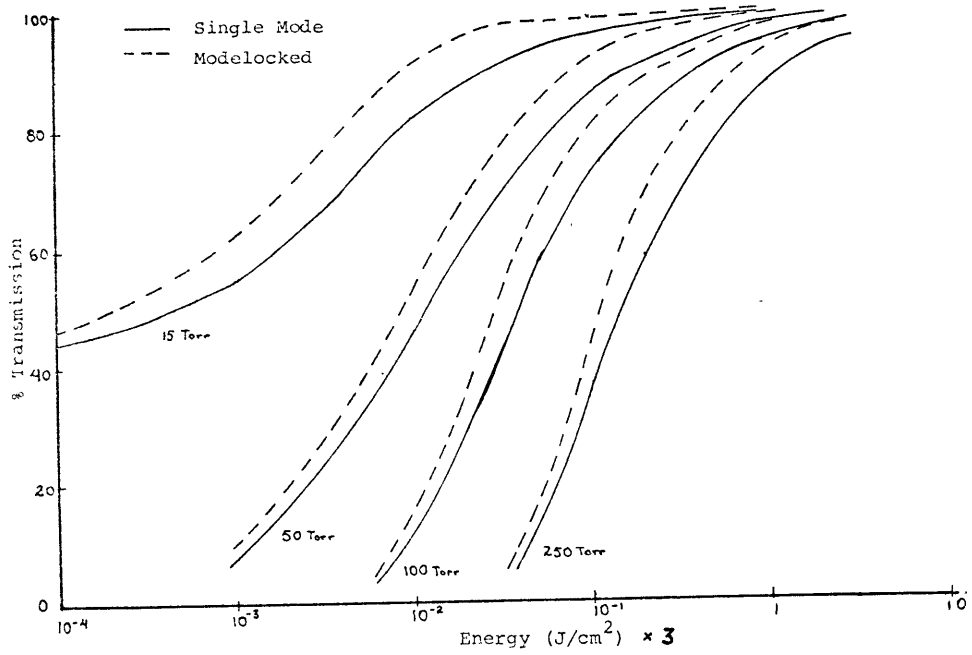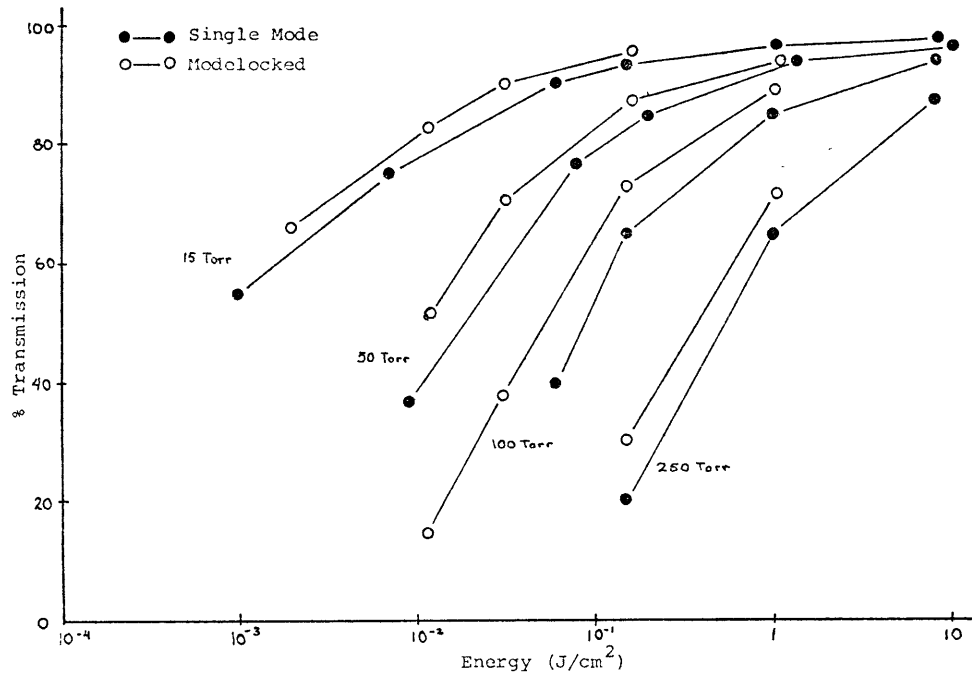
Figure 47: Comparison of Theory to Experiment
on P(16)
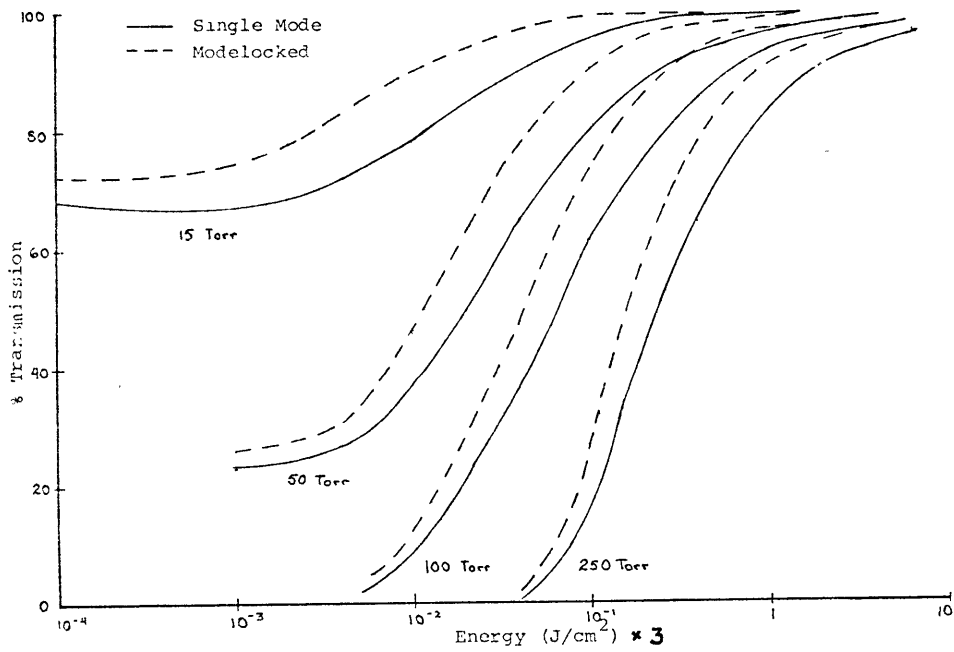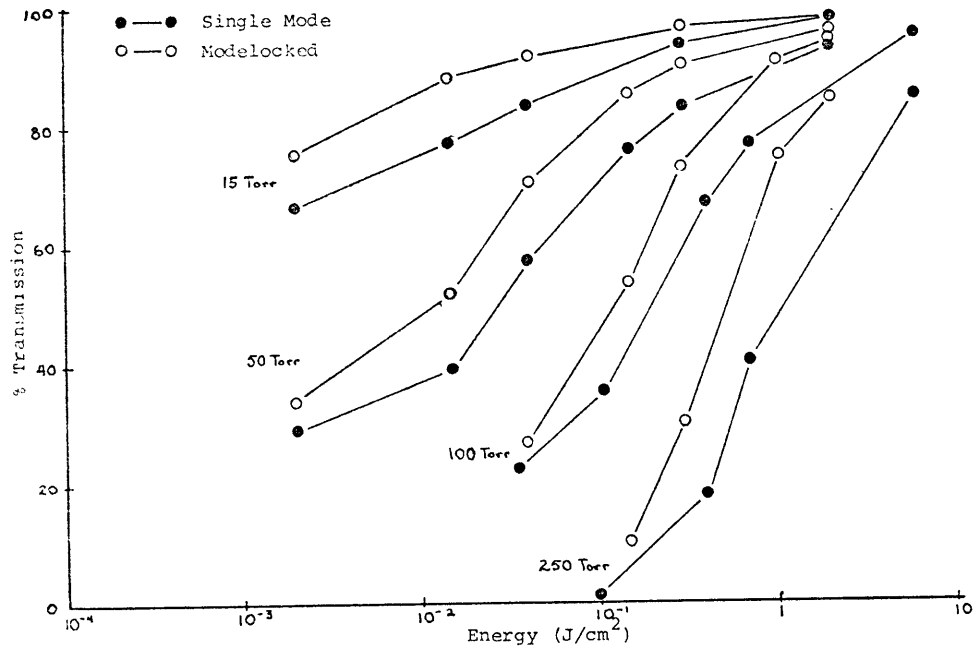
Figure 48: Comparison of Theory to Experiment on P(22)

to agree very well in absolute saturation energy. The discrepancy can be attributed to the fact that equation (4.44) includes only the absorption due to the ν_3 mode. As discussed in section 4.2, the absorption due to the other modes of SF_6 will make the medium harder to saturate, as the experimental curves indicate. The increase of relaxation rates with pressure strengthens the coupling to other modes. Thus, we would expect the disagreement between the simple ν_3 mode theory and experiment to increase with pressure, as is, in fact, the case.

V. Design Criteria for Passively Modelocked Systems

In Chapter II we carried out a detailed investigation
of the steady state and transient behavior of the passively
modelocked system. In our attention to detail, however, we
may have obscured the major results of our analysis. Now
that we have shown in Chapters III and IV that the modelocking
theory is borne out by experiment, we pause here to enumerate
our findings, and their implications for the design of pas-
sively modelocked systems.

Modelocking systems can be divided into two categories:
(1) cw, in which the system must settle into a steady state,
and (2) transient, in which the field builds up and decays
in a finite time, and a true steady state is never attained.
For both the cw and the transient systems the mechanism
which causes evolution of the field in the cavity is the net
gain. The net gain of the cw system increases initially
due to the pumping of the laser medium and then decreases to
zero as the laser medium saturates. The gain variation is
similarly dictated in transient systems, save that the net
gain decreases until it becomes a net loss, and the field
decays in a finite time.

Since the cw system allows "infinite" time for the
field in the cavity to reach steady state, the steady state

is independent of the initial multimode fluctuations in the cavity. In other words, the manner in which the field in the cw system builds up is not important in the determination of the steady state. As shown in Chapter II, however, the system parameters must satisfy a number of constraints in order to ensure that a stable steady state operating point is found.

In the transient system gain only exists for a finite time. Consequently, the output observed is related to the field in the cavity at the modelocking threshold. In order to ensure the deterministic buildup of a single pulse, care must be taken that the field at the modelocking threshold is primarily single mode. On the other hand, because the pulses obtained are always growing or decaying, the existence of modelocking solutions is not subject to the stability constraints required of cw modelocking solutions.

The design criteria for cw and transient systems are considered separately in sections 5.1 and 5.2. In section 5.3 we propose several applications of the criteria to the design of new modelocking systems.

5.1 CW Systems

The criteria for the existence and stability of the steady state modelocking solutions are established in sections 2.2 and 2.6 of Chapter II. Given a set of system parameters one is shown how to find the operating point of the system. The reverse process, in which we are given the desired characteristics of the output pulse and must design a system to produce it, is of more interest to us here. All of the necessary design information is contained in the equations and figures of Chapter II. Rather than lose ourselves in a specific problem, however, we wish to establish some general rules of thumb for the system design.

The criteria gleaned from the analysis in Chapter II, which must be met to ensure a wide operating range of the passively modelocked cw system, can be listed as follows:

1.   A small signal absorber loading which exceeds the
     constant cavity loss

$$q > 1 \tag{5.1}$$

to ensure the availability of sufficient absorber "modulation depth".

2. Saturation powers characterizing the fast (F) and slow (S) relaxation times of the absorber and laser medium which satisfy the inequalities:

$$P_{AF} << P_{LF} \tag{5.2}$$

to ensure that the fast response of the absorber overpowers that of the laser;

$$P_{AF} >> P_{LS} \tag{5.3}$$

to ensure that the slow saturation of the laser is sufficient to stabilize the steady state solutions; and

$$P_{AS} > P_{LS} \tag{5.4}$$

to ensure both that the destabilizing slow saturation of the absorber is negligible, and that condition (5.1) is satisfied at the steady state operating point.

3. A time average power in the cavity which exceeds the modelocking threshold power

$$P > P_o(\ell) = \frac{2\pi^2}{q} \frac{1 + q}{(\omega_L T_R)^2} P_{AF} \tag{5.5}$$

to ensure that the single mode steady state is unstable.

4. A peak power in the cavity which is less than one half
    the absorber saturation power

    $$|v_0|^2 < \frac{P_{AF}}{2} \tag{5.6}$$

    to ensure that the absorber is not fully bleached.

5. A linewidth-transit time product, $\omega_L T_R$, which is large
    enough to enable the obtainment of short pulses, but not
    too large to ensure that operating point intercepts can
    be found.

The above criteria enable us to tell at a "glance" whether a
particular amplitier-absorber-cavity combination can lead to
stable modelocking, and what "knobs" need turning to obtain
the shortest possible pulses with the highest peak power.

We should note here that throughout the analysis we have
assumed the relationship

$$T_{LS} \gg \tau_p \gg T_{AF}$$

between the slow relaxation time of the laser medium, the fast
relaxation time of the absorber and the modelocked pulsewidth.
Cases in which one or the other or both inequalities break-
down have been discussed elsewhere.[25,42]

5.2 Transient Systems

The time variation of the gain in the transient system
provides an additional degree of freedom over the steady state
operation of the cw system. The gain must vary such that
quasi-steady state modelocking solutions of constant perio-
dicity can be found at each transit through the system. Con-
sequently, we establish the following restrictions:

1. A slow rise/easy saturation of the laser medium gain
    near the lasing threshold in order to ensure that lasing
    is primarily confined to a single mode by the time the
    modelocking threshold is reached.

2. The attainment of a sufficient small signal gain to
    ensure that the modelocking threshold is reached, but
    decay/saturation of the gain before the power in the
    cavity fully bleaches the absorber.

3. A small time average gain coefficient, $\alpha \ll 1$, over
    each transit to ensure the adiabatic evolution of the
    quasi-steady state modelocking solutions.

The criteria on all parameters, other than the gain,
for the existence of quasi-steady state solutions over a wide

power range, are identical to those established for the cw
system in section 5.1, with one qualification. The quasi-
steady states need not satisfy the stability criteria. Thus,
the requirement $P_{AF} \gg P_{LS}$ need not be met in transient
systems, provided the small signal gain satisfies conditions
1-3 stated above. From the standpoint of energy extraction
from the system, however, it is clear that condition (5.3)
is desir able to ensure saturation of the laser medium during
the modelocked pulse train.

5.3 Applications of the Design Criteria

The criteria discussed in the previous sections provide the guidelines for two avenues of investigation into the development of new cw and transient passively modelocked systems. First, they provide a handbook by which, given the characteristics of a laser medium and an associated fast absorber, a modelocked system can be designed and optimized. Second, they provide the insight which enables the design of new system configurations with improved stability and reproducibility characteristics. Here we shall proceed a short way along the second avenue to see what lies just ahead.

5.3.1 Multi-Absorber Systems

In the single absorber cw system, constraint (5.5) places an upper bound on the absorber fast saturation power P_{AF} relative to the time average power in the system P, and (5.3) places a lower bound on P_{AF} relative to the laser medium slow saturation power P_{LS}. Care must be taken that an operating regime exists between the two bounds. Furthermore, the lowering of P_{AF} to satisfy (5.5) limits the peak power capability of the system by (5.6).

The difficulty in simultaneously satisfying the various criteria for P_{AF} can be circumvented by the use of two or more absorbers having different saturation powers. Assume, for example, that part of the loading in the cavity consists of a "soft" absorber whose saturation power easily satisfies the threshold condition (5.5), and the remainder consists of a "stiff" absorber whose saturation power ensures that conditions (5.3) and (5.6) are satisfied. The soft absorber enables modelocking to initiate. As the field builds up in the cavity, however, the soft absorber becomes fully bleached, and the stiff absorber must take over the role of narrowing the pulse. Thus, by the time the steady state operating point is reached, the stiff absorber dominates.

The two absorber system does not necessarily require different absorbing media since the saturation power can be varied by a judicious cavity design which adjusts the relative

beam cross-sections in the absorbers. If, however, absorbers

with different saturation intensities were used, it would

not matter if the softer absorber had a relatively long re-

laxation time compared to the steady state pulse, provided

it was still significantly shorter than the cavity transit

time. The soft absorber only governs the initial shaping of

the field where an ultrafast response is not required.

The performance of a two absorber passively modelocked

dye system was recently described by Ippen and Shank:[67]

> "A major improvement in the stability of short-
> pulse generation has been achieved by using a combina-
> tion of two saturable absorbers as the mode-locking
> element. Although DODCI which has a relatively long
> recovery time has been used alone to produce short
> pulses, such operation occurs near laser threshold
> and requires careful adjustment and stabilization of
> all parameters. Addition of the triphenylmethane dye
> malachite green to the DODCI solution permits short-
> pulse operation well above threshold. On the other
> hand, malachite green, which has a recovery time in
> the picosecond range, has not produced stable mode
> locking by itself in this laser. With the absorber
> combination, output pulse characteristics remain con-
> stant for many hours without readjustment."

If we assume that the saturation intensity of the fast

absorber, malachite green, is much greater than that of

DODCI, the observations of Ippen and Shank are entirely

consistent with our discussion. As noted by New and Haus,

DODCI alone can produce short pulses only because of the

response of the gain medium which cuts off the tail of the

234

pulse. We postulate that malachite green does not produce

stable modelocking by itself because the threshold condition,

(5.5), cannot be satisfied without violating the constraints

on the bandwidth-transit time product, $\omega_L T_R$.

5.3.2 Multi-Laser Systems

As discussed in section 2.3, the requirement in transient systems that the field be primarily single mode at the modelocking threshold is extremely restrictive if the laser medium has a wide bandwidth. The upper limit on the rate of increase of the gain per pass was computed to be 10^{-13} for Nd:glass, indicating a pump time of $\sim 10^4$ s ! The addition of a bandwidth limiting etalon to the cavity would make the threshold criterion less stringent, but would preclude the generation of pulses which utilize the full laser medium bandwidth.

A system which employed more than one laser medium, having different bandwidths and saturation powers, however, would allow the threshold condition to be satisfied without curtailing the short pulse capability of the system in the large signal regime. For example, the system could contain both an easily saturated Nd:YAG amplifier and a hard to saturate Nd:glass amplifier. In the low power regime, the comparatively narrowband Nd:YAG laser medium would determine the bandwidth of the system. Consequently, the threshold condition could be satisfied. As power built up in the field, however, the soft Nd:YAG amplifier would saturate quickly, and the bandwidth of the system would broaden to include the full Nd:glass linewidth.

5.3.3 Cascaded Systems

We have proposed a second technique of controlling the buildup of modelocking by using a combination of forced and passive modelocking.[71] Both active and passive techniques of modelocking have drawbacks. However, on several important points the advantages of one technique compensate for the disadvantages of the other.

As observed in section 3.3, forced modelocking is inherently more stable than passive. However, the power handling capability of the modulator is usually lower than that of a saturable absorber, and the absorber has the capability of producing shorter pulses. A system which would realize the stability of forced modelocking, as well as the power handling and short pulse capability of passive modelocking would be one in which the forced modelocked output of a comparatively low power laser is injected off-axis into the saturable absorber of a second, high power laser, to produce "prebleaching" of the absorber during the gain buildup of the second laser. The lengths of the two laser cavities must be set equal to ensure the synchronism of the pulse formed in the second laser with the modulation applied to the absorber by the first.

VI. Conclusion

We have developed the first deterministic theory of
the transient evolution of passive modelocking with a fast
saturable absorber which gives a closed form expression for
the pulse on each transit through the system. The buildup
and decay of the field has been shown to proceed as an
adiabatic succession of quasi-steady state solutions to the
modelocking equation.

The first matching of the experimental pulses to those
predicted by the theory has been performed using a TEA CO_2
laser modelocked by an SF_6 saturable absorber. In applying
the theory, simple two level models are adopted for both the
laser medium and the absorber. The overall laser pulse out-
put predicted shows good qualitative agreement with the out-
put observed in the modelocking regime. Variations in the
output from shot-to-shot are shown to be attributable to
variations in the small signal gain, rather than any statis-
tics of the modelocking buildup. The shapes and relative
amplitudes of the modelocked pulses are shown to be in ex-
cellent agreement with the predictions of the theory. Order
of magnitude agreement is found with the absolute peak power
of the modelocked pulses and the excess gain in the system.

In an attempt to understand the role of SF_6 in mode-

locking, we have also investigated the short pulse saturation properties of SF_6. Measurements of the difference in transmission of SF_6 to long pulse and short pulse 10.6 μ radiation show good agreement with a simple theory of SF_6 saturation which attributes the short pulse response of the medium to rotational bleaching. We are able to conclude, therefore, that the fast rotational bleaching of SF_6 is the mechanism which induces modelocking. The result that the saturation energies predicted by the theory were lower than those measured can be explained by the fact that the model considers only abosrption by the ν_3 mode of SF_6.

The transient modelocking analysis has also shed new light on the steady state behavior of cw modelocked systems. The addition of the periodicity constraint to the eigenvalue relations derived by Haus[24] leads to a simple procedure for finding the operating point of the cw system. The ability to find the steady state operating point provides a powerful new tool in the design of cw passive modelocked systems. Furthermore, the transient analysis is the key to investigating the stability of the steady state solutions. Stability boundaries are delineated in the steady state solution space. Each set of system parameters has been shown to correspond to a <u>unique</u> steady state.

Although we conclude here confident of the wide applicability of the theory of passive modelocking presented, further work is needed to obtain definitive confirmation of

its predictive power. Such confirmation should be attempted by:

(1)   Carrying out detailed experiments on a well understood system to determine the correlation of the operating regimes with those predicted by theory,

(2)   Trying new system configurations, based upon the dictates of the design criteria stemming from the theory, to improve the performance of existing systems, and

(3)   Using the design criteria to search for successful operating regimes of modelocked systems employing new laser and absorber materials.

In any event, dear reader, whatever the future may bring-- our work here is done!

Appendix A

Periodic Solutions to the Steady State

Modelocking Equation

The solutions to the modelocking equation (2.23) are characterized by a quartic potential (2.26). As enumerated in Abramowitz and Stegun[70], twelve periodic solutions exist to an equation of this form. By restricting our attention to physically meaningful solutions, namely stable bounded solutions characterized by positive real values of power, we can narrow the field of solutions to two.

In order to simplify the algebra we first normalize the equation as follows:

$$\left(a^2 \frac{d^2}{dx^2} + 2y^2 - b\right) y = 0 \qquad (A.1)$$

where

$$y \equiv v/v_o$$

$$x \equiv t/\tau_p$$

$$a \equiv \frac{1}{\omega_L \, \tau_p \, v_o} \sqrt{\frac{2P_A(1 + q)}{q}}$$

$$b \equiv \frac{1 + q - g}{q} \, \frac{2P_A}{v_o^2} \, .$$

Equation (A.1) can be integrated to the form

$$a^2 (dy/dx)^2 + y^4 - by^2 + c = 0 \qquad (A.2)$$

where c is the constant of integration. Solving for x(y) we obtain

$$x = \int_{y_1}^{y_2} \frac{dy}{\sqrt{P(y)}} \qquad (A.3)$$

where y_1 and y_2 are the roots of the polynomial

$$P(y) = - y^4 + by^2 - c \qquad (A.4)$$

which determine the turning points of x(y).

For the two cases of interest here the solution (A.3) can be inverted to obtain $y(x)$ in terms of the Jacobian elliptic functions of x and modulus γ:

$$y = \begin{cases} dn(x, \gamma) & 0 \le \gamma < 1 & \text{(A.5a)} \\ \\ cn(x, 1/\gamma) & 1 < \gamma \le \sqrt{2}. & \text{(A.5b)} \end{cases}$$

The coefficients of the equation are constrained to be

$$a = \begin{cases} 1 & \text{(A.6a)} \\ \\ \gamma & \text{(A.6b)} \end{cases}$$

in the respective ranges of γ indicated in (A.5) and

$$b = 2 - \gamma^2 \tag{A.7}$$

$$c = 1 - \gamma^2 \tag{A.8}$$

over the full range $0 \le \gamma \le \sqrt{2}$.

The periodicity of the two solutions is as follows

$$dn(x + 2K) = dn(x) \tag{A.9a}$$

$$cn(x + 2K) = - cn(x) \qquad \text{(A.9b)}$$

where $K(\gamma)$ is the complete elliptic integral of the first kind. The first solution is periodic in $2K$ and is positive definite while the second is periodic in $4K$ and alternates sign over period $2K$. Hence, we call (A.5a) the symmetric (S) solution and (A.5b) the antisymmetric (AS) solution.

The strong saturation equation (2.121) differs from (2.23) in that it has a potential which is cubic in v^2. We rewrite the equation in the form

$$\left(a_s^2 \frac{d^2}{dx^2} - 3y^4 + 2b_s y^2 - c_s \right) y = 0 \qquad \text{(A.10)}$$

where the coefficients are now defined as

$$a_s = \sqrt{\frac{3(1 + q)}{q}} \; \frac{P_A}{v_o^2 \, \omega_L \, \tau_p}$$

$$b_s = \frac{3 P_A}{2 v_o^2}$$

$$c_s = \frac{3(1 + q - g)}{q} \frac{P_A^2}{v_o^4} .$$

Integrating (A.10) we obtain

$$a_s^2 (dy/dx)^2 - y^6 + b_s y^4 - c_s y^2 + d_s = 0 \qquad \text{(A.11)}$$

where d is the constant of integration. The expression
for $x(y)$ is given by (A.3) where y_1 and y_2 are the
first two roots of the polynomial

$$P(y) = y^6 - b_s y^4 + c_s y^2 - d_s \qquad \text{(A.12)}$$

which determine the turning points of $x(y)$.

The inversion of (A.3) in the strong saturation case now
gives the solutions

$$y = \frac{dn(x, \ \gamma)}{\sqrt{1 - \beta^2 \ sn^2(x, \ \gamma)}} \qquad 0 < \beta < \gamma < 1 \qquad \text{(A.13a)}$$

$$y = \frac{cn(x, \ 1/\gamma)}{\sqrt{1 - (\beta/\gamma)^2 \ sn^2(x, \ 1/\gamma)}} \qquad 1 < \gamma < \sqrt{2} \qquad \text{(A.13b)}$$

$$0 < \beta < \gamma.$$

Restricting our attention to (A.13a) for the sake of brevity we find the coefficients of (A.10) to be

$$a_s = \sqrt{\frac{\gamma^2 - \beta^2}{\beta^2 (1 - \gamma^2)}} \qquad (A.14)$$

$$b_s = \frac{G_{\beta\gamma}}{a^2} \qquad (A.15)$$

$$c_s = \frac{G_{\gamma\beta}}{a^2} \qquad (A.16)$$

where

$$G_{\beta\gamma} = \frac{2\beta^4 + 2\gamma^4\beta^2 - (\beta^6 + \beta^4\gamma^2 + \beta^2\gamma^2 + \gamma^4)}{(\gamma^2 - \beta^2)^2}$$

and $G_{\gamma\beta}$ is obtained by interchanging γ and β in $G_{\beta\gamma}$. The constant of integration in (A.11) is related to γ and β via the roots of the polynomial (A.12) as shown in Figure 22, i.e.

$$\gamma^2 = \left(\frac{v_o^2 - v_-^2}{v_+^2 - v_-^2}\right) \frac{v_+^2}{v_o^2} \qquad (A.17)$$

$$\beta^2 = \frac{v_o^2}{v_+^2} .$$

Appendix B

Relaxation Rates in the CO_2 Molecule

Justification of the simple two-level saturation model adopted in Chapter 3 requires a knowledge of the energy transfer mechanisms in the TEA CO_2 amplifier. We are able to group the relevant relaxation rates of the medium into those which are fast and those which are slow compared to the modelocked pulse width. The only fast saturation mechanism is the cross relaxation among the rotational levels.

The TEA laser medium is a gaseous mixture of CO_2, N_2, and He. The total number density of molecules in the mixture is given by

$$N = \psi_C N + \psi_N N + \psi_H N \qquad (B.1)$$

where ψ_C, N, H is the mole fraction of CO_2, N_2, and He respectively. The vibrational energy levels of CO_2 and N_2 pertinent to amplification are shown in Figure 49 . The single vibrational mode of the diatomic nitrogen molecule has its first vibrational energy level in the electronic ground state lying at 2330 cm^{-1}, while the linear triatomic CO_2 molecule has three independent vibrational modes designated as follows:
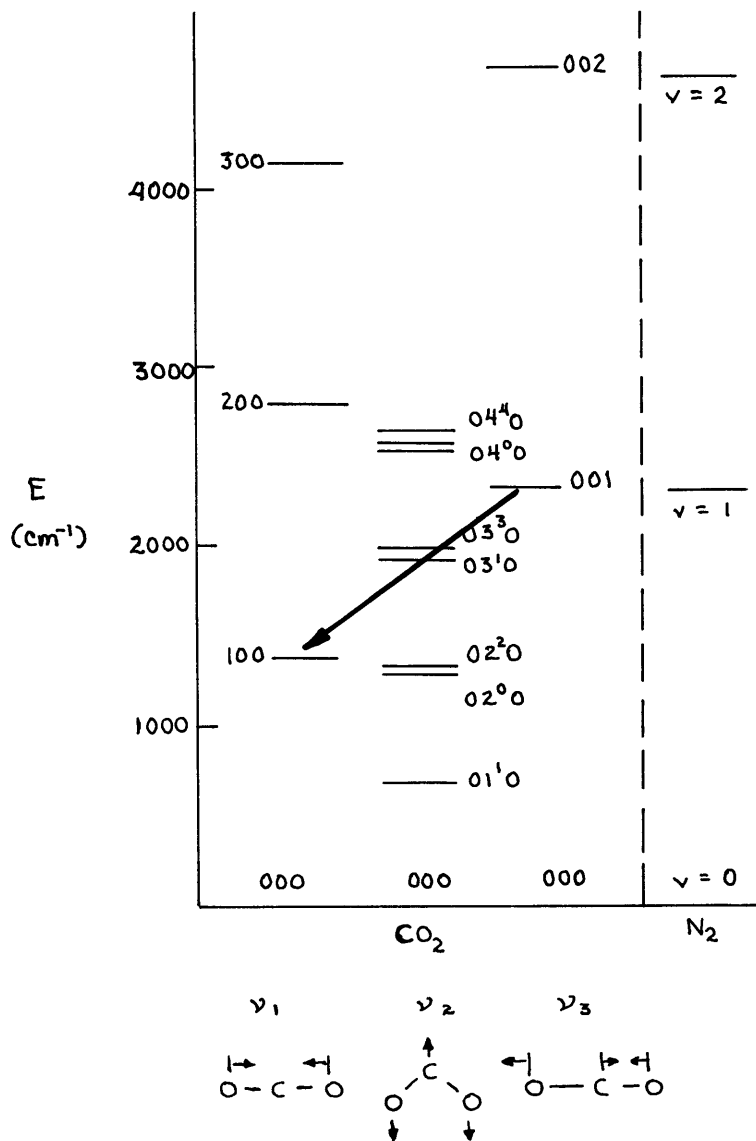
Figure 49: Energy Level Diagram of CO_2 and N_2

$\nu 1$ = symmetric stretch mode $[\hbar\omega_1 = (1388\ cm^{-1})\hbar c]$,

$\nu 2$ = doubly degenerate bending mode $[\hbar\omega_2 = (667\ cm^{-1})\hbar c]$, and

$\nu 3$ = asymmetric stretch mode $[\hbar\omega_3 = (2349\ cm^{-1})\hbar c]$.

The carbon dioxide molecule can oscillate in any combination of these normal modes, for example, with i quanta of excitation in $\nu 1$, j in the degenerate $\nu 2$ mode, and k quanta in mode $\nu 3$. Each vibrational energy level has a corresponding set of rotational energy levels.

The dominant energy transfer processes in the amplifying medium due to binary collisions of the molecules are summarized as follows:

1. V-T in the ν_2 mode:

The process by which bending mode vibrational energy is converted into kinetic energy of the gas.

$$CO_2[i,\ j,\ k] + M \overset{Z_{VT}}{\rightleftarrows} CO_2[i,\ j - 1,\ k] + M + \hbar\omega_2$$
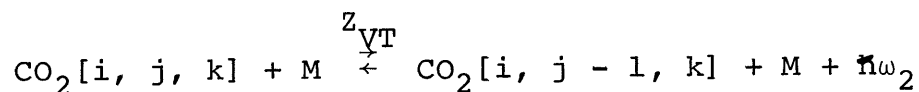
where Z_{VT} is the characteristic rate of the process and M is an arbitrary collision partner, i.e. CO_2, N_2, or He for the system under consideration. The released energy is taken up by the translational kinetic energy of the gas.

2. Intermolecular V-V between ν_3 and ν_N:

The resonant collisional transfer of vibrational energy between N_2 and CO_2 molecules

$$CO_2[i, j, k] + N_2[v] \overset{Z_{3N}}{\rightleftarrows} CO_2[i, j, k - 1]$$

$$+ N_2[v + 1] + 18 \text{ cm}^{-1}.$$
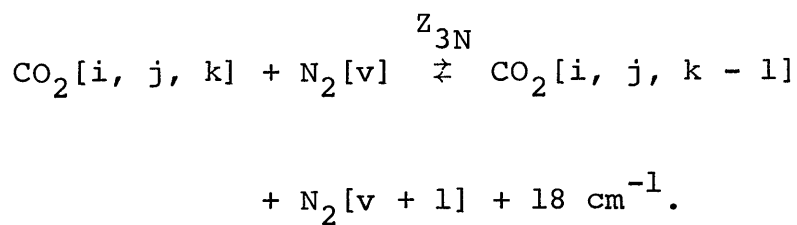
3. Intramolecular V-V:

The dominant transfer processes among the three vibrational modes of CO_2 are:

$$CO_2[i, j, k + 1] + M \overset{Z_{32}}{\rightleftarrows} CO_2[i, j + 3, k]$$

$$+ M + \hbar(3\omega_2 - \omega_3)$$

$$CO_2[i + 1, j, k] + M \overset{Z_{12}}{\rightleftarrows} CO_2[i, j + 2, k]$$

$$+ M + \hbar(\omega_1 - 2\omega_2).$$
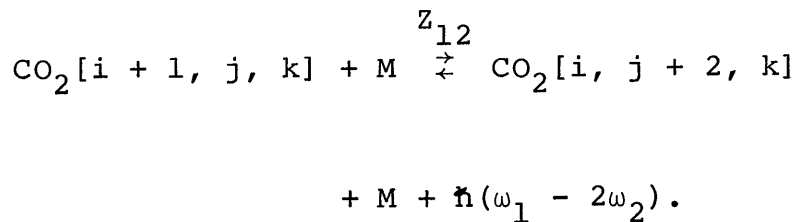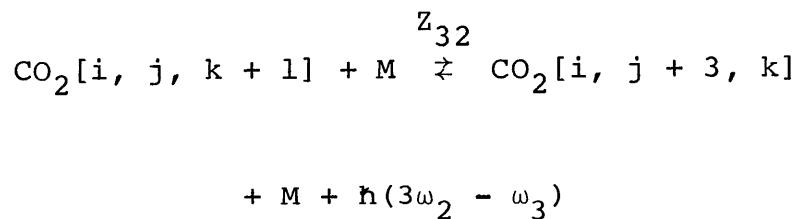
4. Intramode V-V:

The energy equilibration within a given vibrational mode, for example in ν_3

$$CO_2[i, j, k + 1] + CO_2[i', j', k'] \overset{Z_{33}}{\rightleftarrows} CO_2[i, j, k]$$

$$+ CO_2[i', j', k' + 1]$$
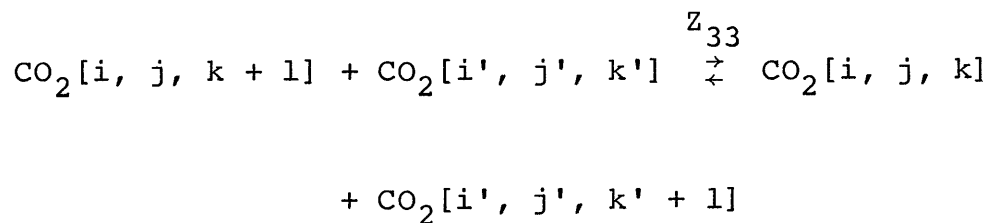
allows the population of the levels in that mode to be characterized by a Boltzmann Temperature.

5. R-T:

A CO_2 molecule in a particular vibrational state specified by the quantum numbers [i, j, k] can also experience cross relaxation among its rotational levels via the process

$$CO_2[J] + M \overset{R}{\rightleftarrows} CO_2[J'] + M.$$
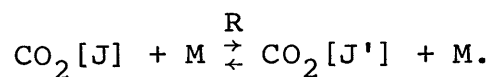
The characteristic relaxation rates of the energy transfer processes are listed in Table V . In general each of the rates depends on the gas mixture. However, the V-T rate is

known to be He dominated[72] and it is reasonable to assume that the intramolecular and intramode V-V rates are CO_2 dominated, so that the rates quoted for processes 1., 3., 4. are for the pure gases. The intermolecular V-V rate for CO_2 - N_2 resonance transfer is dependent on the combined CO_2 - N_2 pressure.

For the gas mix $(CO_2:N_2:He = 2:1:6)$ and pressure range (200 - 600 Torr) used in our experiments we can compare the relaxation rates to the characteristic time scales of the modelocked TEA laser pulse given below

$$T_p \sim 250 \text{ ns.}$$
$$T_R = 24 \text{ ns.}$$
$$1.5 \text{ ns.} < \tau_p < 10 \text{ ns.}$$

From the rates given in Table B-1 we conclude

$$z_{3N} \lesssim \frac{1}{T_p} \ll z_{12}$$

$$\frac{1}{T_R} \sim z_{12}$$

$$z_{12} < \frac{1}{\tau_p} \lesssim z_{33} < R.$$

Table V

Characteristic Relaxation Rates of Energy
Transfer Processes in CO_2 - N_2 - He

	Process	Rate	Reference
1.	V-T	$Z_{VT} = 4.10^3 \ s^{-1} \ torr^{-1}$	72
2.	Intermolecular V-V	$Z_{3N} = 1.9 \times 10^4 \ s^{-1} \ torr^{-1}$	72
3.	Intramolecular V-V	$Z_{32} = 40 \ s^{-1} \ torr^{-1}$	72
		$Z_{12} = 3 \cdot 10^5 \ s^{-1} \ torr^{-1}$	54
4.	Intramode V-V	$Z_{33} = 5.3 \times 10^6 \ s^{-1} \ torr^{-1}$	72
5.	R-T	$R = 1.5 \cdot 10^7 \ s^{-1} \ torr^{-1}$	50

The above comparison, which show that the characteristic pulse widths roughly fall between the characteristic medium times, form the basis for our treatment of the laser saturation in Chapter 3. Both Z_{VT} and Z_{32} are slower than Z_{3N}, which is slow compared to the TEA pulsewidth, and, hence, can be ignored.

References

1. C. V. Shank, E. P. Ippen, "Subpicosecond Kilowatt Pulses from a Mode-Locked cw Dye Laser," Appl. Phys. Lett., 24, no. 8, 15 Aug. 1974, p. 373.

2. C. L. Tang, H. Statz, G. deMars, "Regular Spiking and Single-Mode Operation of Ruby Laser," Appl. Phys. Lett., 2, no. 11, 1 June 1963, p. 222.

3. P. W. Smith, "The Self-Pulsing Laser Oscillator," IEEE JQE, QE-3, no. 11, Nov. 1967, p. 627.

4. D. L. Lyon, E. V. George, H. A. Haus, "Observation of Spontaneous Modelocking in a High Pressure CO_2 Laser," Appl. Phys. Lett., 17, no. 11, 1 Dec. 1970, p. 474.

5. O. R. Wood, S. E. Schwarz, "Passive Mode Locking of a CO_2 Laser," Appl. Phys. Lett., 12, no. 8, 15 April 1968, p. 263.

6. E. P. Ippen, C. V. Shank, A. Dienes, "Passive Mode-locking of the cw Dye Laser," Appl. Phys. Lett., 21, no. 8, 15 Oct. 1972, p. 348.

7. B. I. Davis, D. V. Keller, "Undamped Regular Spiking of High Energy Ruby Laser," Appl. Phys. Lett., 5, no. 4, 15 Aug. 1964, p. 80.

8. A. Nurmikko, T. A. DeTemple, S. E. Schwarz, "Single-Mode Operation and Mode Locking of High-Pressure CO_2 Lasers by Means of Saturable Absorbers," Appl. Phys. Lett., 18, no. 4, 15 Feb. 1971, p. 130.

9. A. R. Clobes, M. J. Brienza, "Passive Modelocking of a Pulsed Nd:YAG Laser," Appl. Phys. Lett., 14, no. 9, 1 May 1969, p. 287.

10. A. Schmackpfeffer, H. Weber, "Mode-Locking and Mode-Competition by Saturable Absorbers in a Ruby Laser," Phys. Lett., 24A, no. 3, 30 Jan. 1967, p. 190.

11. A. F. Gibson, M. F. Kimmitt, C. A. Rosito, "Passive Mode Locking of a High-Pressure CO_2 Laser with a CO_2 Saturable Absorber," Appl. Phys. Lett., 18, no. 12, 15 June 1971, p. 546.

12. J. Comly, E. Garmire, J. P. Laussade, A. Yariv, "Observation of Mode Locking and Ultrashort Optical Pulses Induced by Antisotropic Molecular Liquids," Appl. Phys. Lett., 13, no. 5, 1 Sept. 1968, p. 176.

13. A. F. Gibson, M. F. Kimmitt, B. Norris, "Generation of Bandwidth-Limited Pulses for a TEA CO_2 Laser Using p-type Germanium," Appl. Phys. Lett., 24, no. 17, 1 April 1974, p. 27.

14. M. Di Domenico, J. E. Geusic, H. M. Marcos, R. G. Smith, "Generation of Ultrashort Optical Pulses by Mode Locking the YAlG:Nd Laser," Appl. Phys. Lett., 8, no. 7, 1 April 1966, p. 180.   .

15. D. J. Kuizenga, A. E. Siegman, "FM and AM Mode Locking of the Homogeneous Laser--Part II: Experimental Results in a Nd:YAG Laser with Internal FM Modulation," IEEE JQE, QE-6, no. 11, Nov. 1970, p. 709.

16. J. Hirano, T. Kimura, "Multiple Modelocking of Lasers," IEEE JQE, QE-5, no. 5, May 1969, p. 219.

17. O. R. Wood, R. L. Abrams, T. J. Bridges, "Mode Locking of a Transversely Excited Atmospheric Pressure CO_2 Laser," Appl. Phys. Lett., 17, no. 9, 1 Nov. 1970, p. 376.

18. P. W. Smith, T. J. Bridges, E. G. Burkhardt, O. R. Wood, "Modelocked High-Pressure Waveguide CO_2 Laser," Appl. Phys. Lett., 21, no. 10, 15 Nov. 1972, p. 470.

19. M. M. Mann, R. G. Eguchi, W. B. Lacina, M. L. Bhaumik, W. H. Steier, "Mode Locking of the CO_2 Laser by Intra-cavity Phase Modulation," Appl. Phys. Lett., 17, no. 9, 1 Nov. 1970, p. 393.

20. A. Dienes, E. P. Ippen, C. V. Shank, "A Mode-Locked cw Dye Laser," Appl. Phys. Lett., 19, no. 8, 15 Oct. 1971, p. 258.

21. P. W. Smith, "Mode-Locking of Lasers," IEEE Proc., 58, no. 9, Sept. 1970, p. 1342.

22. A. J. DeMaria, W. H. Glenn, N. J. Brienza, M. E. Mack, "Picosecond Laser Pulses," IEEE Proc., 57, no. 1, Jan. 1969, p. 2.

23. D. von der Linde, "Mode-Locked Lasers and Ultrashort Light Pulses," Appl. Phys., 2, 1973, p. 281.

24. H. A. Haus, "Theory of Mode Locking with a Fast Saturable Absorber," J. Appl. Phys., 46, no. 7, July 1975, p. 3049.

25. H. A. Haus, "Theory of Mode Locking with a Slow Saturable Absorber," IEEE JQE, QE-11, no. 9, Sept. 1975, p. 736.

26. J. A. Fleck, "Mode-Locked Pulse Generation in Passively Switched Lasers," Appl. Phys. Lett., 12, no. 5, 1 March 1968, p. 178.

27. B. K. Garside, T. K. Lim, "Laser Mode Locking Using Saturable Absorbers," J. Appl. Phys., 44, no. 5, May 1973, p. 2335.

28. G. H. C. New, "Pulse Evolution in Mode-Locked Quasi-Continuous Lasers," IEEE JQE, QE-10, no. 2, Feb. 1974, p. 115.

29. A. Caruso, R. Gratton, W. Seka, "Mode-Locked Ring-Laser and Ring-Amplifier Characteristics," IEEE JQE, QE-9, no. 11, Nov. 1973, p. 1039.

30. E. M. Garmire, A. Yariv, "Laser Mode-Locking with Saturable Absorbers," IEEE JQE, QE-3, no. 6, June 1967, p. 222.

31. B. Hausherr, E. Mathieu, H. Weber, "Influence of Saturable Absorber Transmission and Optical Pumping on the Reproducibility of Passive Mode Locking," IEEE JQE, QE-9, no. 4, April 1973, p. 445.

32. J. R. Fontana, "Theory of Spontaneous Mode Locking in Lasers Using a Circuit Model," IEEE JQE, QE-8, no. 8, Aug. 1972, p. 699.

33. V. S. Letokhov, "Dynamics of Generation of a Pulsed Mode-Locking Laser," Sov. Phys. JETP, 27, no. 5, Nov. 1968, p. 746.

34. P. G. Kryukov, V. S. Letokhov, "Fluctuation Mechanism of Ultrashort Pulse Generation by Laser with Saturable Absorber," IEEE JQE, QE-8, no. 10, Oct. 1972, p. 766.

35. W. H. Glenn, "The Fluctuation Model of a Passively Mode-Locked Laser," IEEE JQE, QE-11, no. 11, Jan. 1975, p. 8.

36. R. Wilbrandt, H. Weber, "Fluctuations in Mode-Locking Threshold Due to Statistics of Spontaneous Emission," IEEE JQE, QE-11, no. 5, May 1975, p. 186.

37. S. E. Schwarz, "Theory of an Optica Pulse Generator," IEEE JQE, QE-4, no. 9, Sept. 1968, p. 509.

38. C. P. Christensen, S. E. Schwarz, "Nonlinear-Optical Device Characteristics of Gaseous Saturable Absorbers," IEEE JQE, QE-10, no. 3, March 1974, p. 338.

39. B. J. Feldman, J. F. Figueira, "Generation of Sub-nanosecond CO_2 Laser Pulses at 10.6 μm by Pulse Compression Techniques," Appl. Phys. Lett., 25, no. 5, 1 Sept. 1974, p. 301.

40. C. L. Sam, "An Experimental Study of the Linear Growth Region of Ultrashort-Pulse Generation in a Mode-Locked Nd:glass Laser," Appl. Phys. Lett., 24, no. 12, 15 June 1974, p. 631.

41. R. H. Pantell, H. E. Puthoff, Fundamentals of Quantum Electronics, John Wiley, 1969, p. 36.

42. P. L. Hagelstein, C. P. Ausschnitt, "Shape and Stability Dependence of Passively Modelocked Pulses on Absorber Relaxation Time," J. Appl. Phys., to be published, Jan. 1976.

43. E. T. Whittaker, G. N. Watson, A Course of Modern Analysis, Cambridge University Press, Fourth Edition, 1969, Chapter 22.

44. D. L. Lyon, "Collisional Relaxation Mechanisms Governing Operation of High-Pressure CO_2 Lasers," Ph. D. Thesis, MIT Dept. of Elec. Eng., August 1972.

45. R. M. Kulsrud, "Adiabatic Invariant of the Harmonic Oscillator," Phys. Rev., 106, no. 2, April 1957, p. 205.

46. W. H. Glenn, M. J. Brienza, "Time Evolution of Pico-second Optical Pulses," Appl. Phys. Lett., 10, no. 8, 15 April 1967, p. 221.

47. C. B. Mills, "CO_2 Gas Laser Studies," LASL Rept., LA-5151-MS, Jan. 1973.

48. O. R. Wood, P. L. Gordon, S. E. Schwarz, "Saturation of Infrared Absorption in Gaseous Molecular Systems," IEEE JQE, QE-5, no. 10, Oct. 1969, p. 502.

49. J. I. Steinfeld, J. Burak, D. G. Sutton, A. V. Nowak, "Infrared Double Resonance in Sulfur Hexafluoride," J. Chem. Phys., 52, no. 10, 15 May 1970, p. 5421.

50. R. L. Abrams, P. K. Cheo, "Collisional Relaxation of CO_2 Rotational Levels by N_2 and He," Appl. Phys. Lett., 15, no. 6, 15 Sept. 1969, p. 177.

51. E. T. Gerry, D. A. Leonard, "Measurement of 10.6 μ CO_2 Laser Transition Probability and Optical Broadening Cross-Sections," Appl. Phys. Lett., 8, May 1966, p. 227.

52. C. K. N. Patel, R. E. Slusher, "Photon Echoes in Gases," Phys. Rev. Lett., 20, May 1968, p. 1087.

53. R. J. Harrach, T. H. Einwohner, "Four-Temperature Kinetic Model for a CO_2 Laser Amplifier," LLL Rept., UCRL-51399, 30 May 1973.

54. B. K. Garside, J. Reid, E. A. Ballik, "TE CO_2 Laser Pulse Delay and Molecular Relaxation Rates," IEEE JQE, QE-11, no. 8, Aug. 1975, p. 583.

55. M. Abramowitz, I. A. Stegun, Handbook of Mathematical Functions, NBS Appl. Math, Series 55, 1964, p. 722.

56. D. J. Kuizenga, A. E. Siegman, "FM and AM Mode Locking of the Homogeneous Laser--Part I: Theory," IEEE JQE, QE-6, no. 11, Nov. 1970, p. 694.

57. H. A. Haus, "A Theory of Forced Mode Locking," IEEE JQE, QE-11, no. 7, July 1975, p. 323.

58. O. R. Wood, S. E. Schwarz, "Passive Q Switching of a CO_2 Laser," Appl. Phys. Lett., 11, Aug. 1967, p. 88.

59. U. P. Oppenheim, Y. J. Kaufman, "Molecular Saturation and the Criterion for Passive Q Switching," IEEE JQE, QE-10, no. 7, July 1974, p. 533.

60. I. Burak, J. I. Steinfeld, D. G. Sutton, "Infrared Saturation in Sulfur Hexafluoride," J. Quant. Spect. Radiat. Trans., 9, Pergamon Press, 1969, p. 959.

61. J. L. Lyman, R. J. Jensen, T. Rink, C. P. Robinson, S. D. Rockwood, "Isotopic Enrichment of SF_6 in S^{34} by Multiple Absorption of CO_2 Laser Radiation," Appl. Phys. Lett., 27, no. 2, 15 July 1975, p. 87.

62. H. Brunet, "Saturation of Infrared Absorption in SF_6," IEEE JQE, QE-6, Nov. 1970, p. 678.

63. W. D. Breshears, L. S. Blair, "Vibrational Relaxation in Polyatomic Molecules: SF_6^*," J. Chem. Phys., 59, no. 11, 1 Dec. 1969, p. 5824.

64. J. T. Knudtson, G. W. Flynn, "Laser Flourescence Study of the Equilibrium of Excited Vibrational States of SF_6 During SF_6-Rare Gas Collisions," J. Chem. Phys., 58, no. 4, 15 Feb. 1973, p. 1467.

65. J. J. Armstrong, O. L. Gaddy, "Saturation Behavior of SF_6 at High Pressure and Laser Intensity," IEEE JQE, QE-8, no. 10, Oct. 1972, p. 797.

66. A. Szöke, to be published.

67. G. Herzberg, Molecular Spectra and Molecular Structure: II. Infrared and Raman Spectra of Polyatomic Molecules, D. Van Nostrand, 1945, p. 512.

68. C. P. Ausschnitt, H. A. Haus, "Passive FM Modelocking with a Nonlinear Refractive Index Medium," RLE Prog. Rept. No. 115, Jan. 1975, p. 59.

69. E. P. Ippen, C. V. Shank, "Dynamic Spectroscopy and Subpicosecond Pulse Compression," Appl. Phys. Lett., 27, no. 9, 1 Nov. 1975, p. 488.

70. M. Abramowitz, I. A. Stegun, Handbook of Mathematical Functions, NBS Appl. Math. Series 55, 1964, p. 596.

71. C. P. Ausschnitt, "Cascaded Modelocked Laser Systems," MIT Invention Record, Nov. 1974.

72. R. L. Taylor, S. Bitterman, "Survey of Vibrational Relaxation Data for Processes Important in the CO_2 - N_2 System," Rev. Mod. Phys., 83, Sept. 1951, p. 1159.

73. C. V. Shank, private communication

BIOGRAPHICAL NOTE

Christopher Perry Ausschnitt was born in New York City on December 27, 1947. He attended P.S. 40, J.H.S. 104 and Stuyvesant High School in New York. In September 1961 he was the winner of a state-wide creative writing award, and has pursued an interest in writing ever since. He graduated from Stuyesant High in June 1964.

In September 1964 Kit entered Princeton University, where he majored in electrical engineering. During his junior and senior years he served as Editor-in-Chief of the Princeton Engineer, and Secretary of the Undergraduate Engineering Council. He was awarded the Princeton Engineering Association Scholarship of 1966-67.

Graduating from Princeton with honors in June 1968, Kit began work in the Advanced Microwave Technology Group of the RCA Missile and Surface Radar Division in Moorestown, New Jersey. Over a three year period his projects included the design of novel antenna radiating elements, a study of short pulse scattering and the design and fabrication of microwave integrated circuits. In June 1970 he received the M. S. degree from the University of Pennsylvania, having attended part-time under the auspices of the RCA Graduate Study Program.

Awarded an RCA Sarnoff Fellowship to continue his education at a university of his choice in January 1971, Kit entered the Massachusetts Institute of Technology that September.

From January 1973 to January 1976 he was a member of the Gas Laser Group headed by Professor H. A. Haus. During the last two and one-half years of his doctoral studies financial support was provided by the Research Laboratory of Electronics, and by a Sloan Fellowship in the summer of 1975. The work performed in this period is presented here.

Kit's future plans have been summarized by him as follows:

> "When I get my ScD.
> I plan to sit up in a tree.
> Aloft, alone, in a virgin sky,
> just forty concubines and I.
> They my desire to satiate,
> while to the hands of passers-by,
>   lower I
> a collection plate."

If that doesn't work out, he will join the technical staff of Bell Laboratories in Holmdel, New Jersey.